Supplementary Information

Biomimetic supported catalyst inspired by stalked crinoid

Can Liao,[a] [b] Shunjie Liu*,[a] [b] Qingxian Kuang,[a] [b] Ruoyu Zhang,[a] [b] Chunwei Zhuo,[a] Zhaoyan Sun,[a] [b] Xuesi Chen, [a] [b] Xianhong Wang*,[a] [b]

[a] *State Key Laboratory of Polymer Science and Technology, Changchun Institute of Applied Chemistry, Chinese Academy of Sciences; No.5625, Renmin Street, Changchun, Jilin, 130022, P. R. China*

[b] *School of Applied Chemistry and Engineering, University of Science and Technology of China; No.96, JinZhai Road, Hefei, Anhui, 230026, P. R. China*

E-mail: sjliu@ciac.ac.cn, xhwang@ciac.ac.cn

Contents

General chemicals and characterizations

All manipulations involving air- and/or water-sensitive compounds were carried out in a glove box or using standard Schlenk techniques under an inert atmosphere of dry nitrogen.

4-bromobenzaldehyde, 4-hydroxybenzaldehyde, propionic acid, triethylamine, methacryloyl chloride, 1-dodecanethiol, methyl trioctyl ammonium chloride, carbon disulfide, acetone, chloroform, 2-propanol, 1-Hydroxybenzotriazole (HOBt), n-(3-dimethylaminopropyl)-n'-ethylcarbodiimide hydrochloride (EDC), 4-pentyn-1-ol, propargyl bromide, 7-octyn-1-ol, 11-dodecyn-1-ol, (3-chloropropyl)trimethoxy silane, sodium azide, methyl methacrylate (MMA), 2-(dimethylamino)-ethyl methacrylate (DMAEMA), cuprous bromide (CuBr), N, N, N', N', N''-pentamethyldiethylenetriamine (PMDETA), pyridine, *p*-toluenesulfonyl chloride, diethylaluminium chloride (AlEt$_2$Cl, 2 M in hexane), sodium hydroxide (NaOH), sodium carbonate (Na$_2$CO$_3$), sodium chloride (NaCl), magnesium sulfate (MgSO$_4$), sodium hydride (NaH), potassium iodide (KI), methanol, tetrahydrofuran, acetonitrile, hexane were commercially available and could be used without further purification unless otherwise specified. Anhydrous methylene chloride (CH$_2$Cl$_2$), N'N-dimethylformamide (DMF), toluene, propylene oxide (PO) were distilled from calcium hydride under nitrogen atmosphere. Pyrrole (99%, Energy Chemical) was distilled under vacuum before use. Azodiisobutyronitrile (AIBN, 98%, Energy Chemical) and Bis(triphenylphosphine)iminium chloride (PPNCl, 99%, Energy Chemical) were recrystallized before use. Nano-silica (15 nm, 99.5%) was purchased from Aladdin. Sebacic acid (SA), adipic acid (AA), succinic acid (SuA), oxalic acid (OA), polyethylene glycol (PEG, M_n = 300 g/mol), bisphenol A (BPA), trimesic acid (TMA) and 1,2,4,5-benzenetetracarboxylic acid (BTC) were purchased from Energy Chemical and dried under vacuum for 24 hours and stored in glovebox. Carbon dioxide gas (99.999%) was purchased and used without further purification.

Solution NMR: ^{1}H NMR spectra and ^{13}C NMR spectra were recorded on a Bruker ARX-400 and ARX-500 spectrometer at ambient temperature in deuterated chloroform (CDCl$_3$)

or dimethylsulfoxide (DMSO) with tetramethylsilane (TMS) as the internal reference. Chemical shifts were reported in ppm from the internal standard, tetramethylsilane (0 ppm) for ^{1}H NMR. Solvent proton shifts (ppm): CDCl$_3$, 7.26 (s); DMSO-d$_6$, 2.50 (s). Solvent carbon shifts (ppm): CDCl$_3$, 77.16 (t); DMSO-d$_6$, 39.52 (m).

Solid-state NMR: The ^{29}Si CPMAS NMR spectra were recorded on a Bruker Avance 400 MHz spectrometer operating with a 9 T wide-bore magnet with MAS rate of 12 kHz and 300 scans. The ^{13}C CPMAS NMR spectra were collected using Bruker Avance 400 MHz spectrometer with a 9 T wide-bore magnet. MAS rates of 8 kHz, 1000, 500, 3478, 2000, 4000 scans were taken for SiO$_2$-N$_3$, **sBFPC-1**, **sPC-1**, **sSC-1**, **sBFPC'-1** respectively.

Solvent relaxation NMR: All single-pulse experiments and ^{1}H NMR relaxation (T_2) measurements were carried out using a PQ001 NMR analyzer (Suzhou Niumag Analytical Instrument Corporation, China). The measurement temperature was maintained at 32 °C with the aid of an external temperature control unit connected to the sample chamber. Each sample was dispersed in ethanol by sonication to create particle suspensions at a concentration of 10 mg/mL. The Carr−Purcell−Meiboom−Gill (CPMG) pulse sequence was used to generate and collect the magnetization and the corresponding echo, allowing for the determination of the solvent relaxation time for the suspended sample. This method simply involved collecting the magnetization echo intensity following a 90° pulse and ceasing the collection after the 180° pulse.

Scanning electron microscopy (SEM): SEM images were obtained through the Zeiss lens in Merlin (Resolution: 0.6~1.0 nm (15 KV), 1.0~2.0 nm (1 KV); Acceleration voltage: 0.02~30 KV; Beam strength: 1 pA-100 Na; Detector: Everhart-Thornley secondary electron detector of the photocoupled photomultiplier tube).

Cryo-TEM: Cryo-TEM images were obtained using a JEOL JEM-3200FSC transmission electron microscope (TEM) operating at 200 kV. Cryo-TEM grids (quantifoil R 2/2 with 300 mesh copper) were plasma-treated for 30 seconds. 5 μL of sample (2 mg powder / mL DMSO) was pipetted onto a freshly glow-discharged grid. The sample solution was incubated on the TEM grid for 20 seconds, blotted for 5 seconds, and then plunged into liquid ethane that had been pre-cooled with liquid nitrogen.

ESI-MS: The samples for electrospray ionization mass spectrometry (ESI-MS) were

prepared in a solution of $CDCl_3$ and analyzed using the Waters Quattro Premier XE mass spectrometer.

MALDI-TOF-MS: Matrix-assisted laser desorption/ionization time-of-flight mass spectrometry (MALDI-TOF-MS) was carried out on a Bruker auto flex III Mass spectrometer. The samples were dissolved in $CDCl_3$ at a concentration of 1~10 mg mL^{-1}. The matrix was Trans-2-[3-(4-tert-butylphenyl)-2-methyl-2-propenylidene] malononitrile (DCTB).

Gel permeation chromatography (GPC): The molecular weight and its distribution of the CO_2-polyols products were determined by gel permeation chromatography at 25 °C against polystyrene standard on Waters 410 GPC instrument with THF as eluent, where the flow rate was set at 1.0 mL min^{-1}.

Thermogravimetric analyzer (TGA): The TGA characterizations were carried out on the Mettler TGA2 at a heating rate 10 °C/min under N_2 atmosphere from ambient temperature to 100 °C and keep for 10 minutes. Then heat to 800 °C at a heating rate 10 °C/min.

Attenuated total reflection Fourier transform infrared (ATR-FT-IR): ATR-FT-IR spectra were recorded on INVENIO-R Fourier transform infrared spectrometer. The spectral resolution is 2 cm^{-1} from 4000 cm^{-1} to 400 cm^{-1}.

Ultraviolet and visible spectrum (UV): UV-vis spectra were recorded on a HITACHI U-4100 spectrophotometer with a high-temperature and high-pressure resistant cuvettes.

X-ray photoelectron spectrometer (XPS): The XPS data were collected on a Thermo ESCALAB 250Xi spectrometer equipped with a monochromatic Al K radiation source (1486.6 eV; pass energy, 30.0 eV). The data were calibrated with C 1s 284.8 eV.

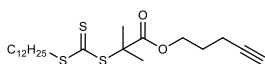**Previous strategies for supported catalysis**
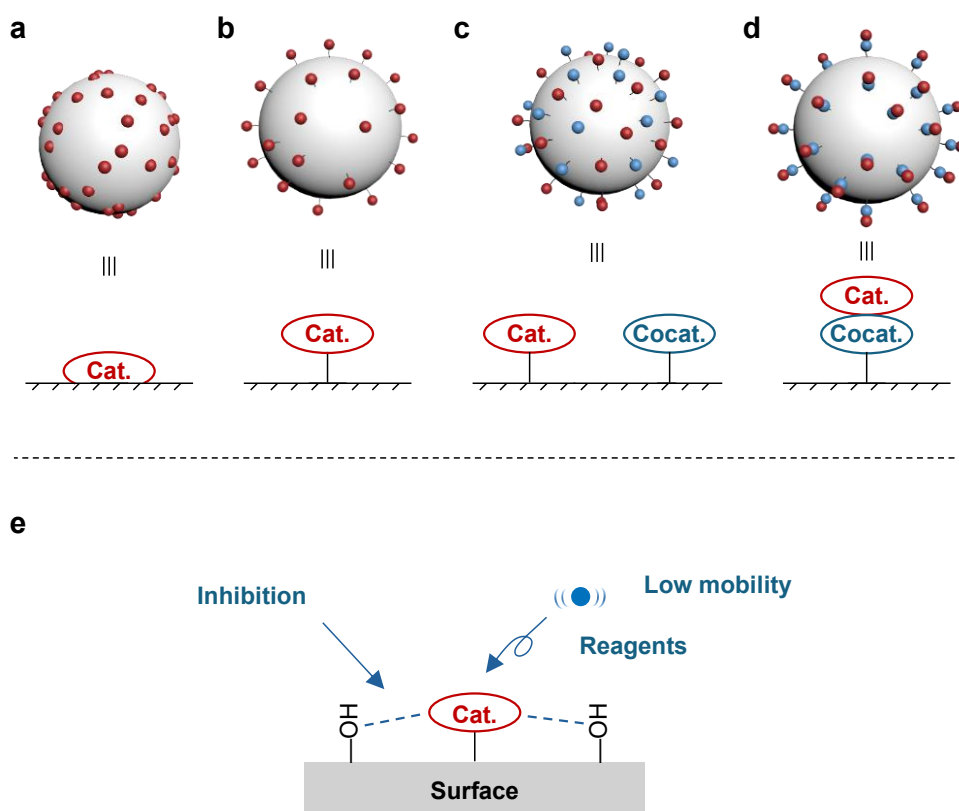
Supplementary Scheme 1. Cartoon models of previous heterogenization strategies: a) supported by coordination bonding, b) supported by covalent bonding, c) supporting catalyst and cocatalyst using their own anchors and d) connecting catalyst and cocatalyst prior to supporting. e) Schematic illustration of detrimental effects of surface on metal complex.
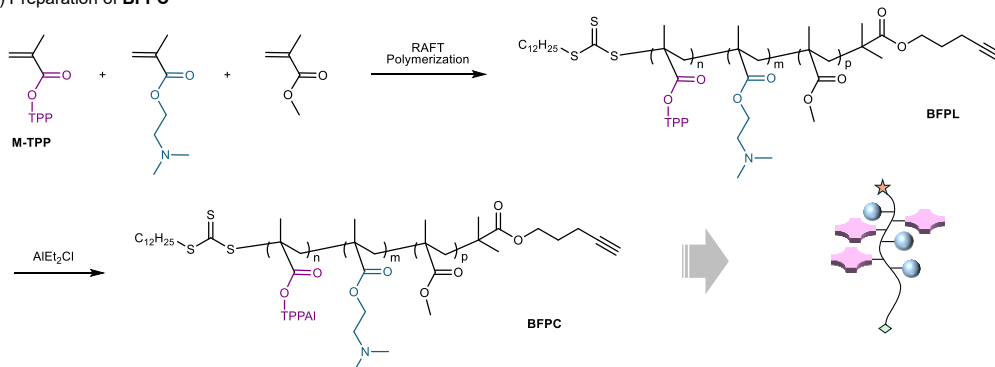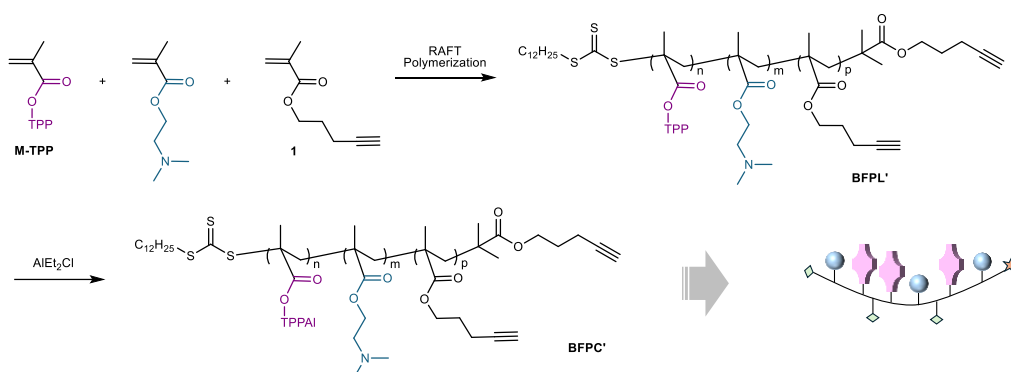
General synthetic routes
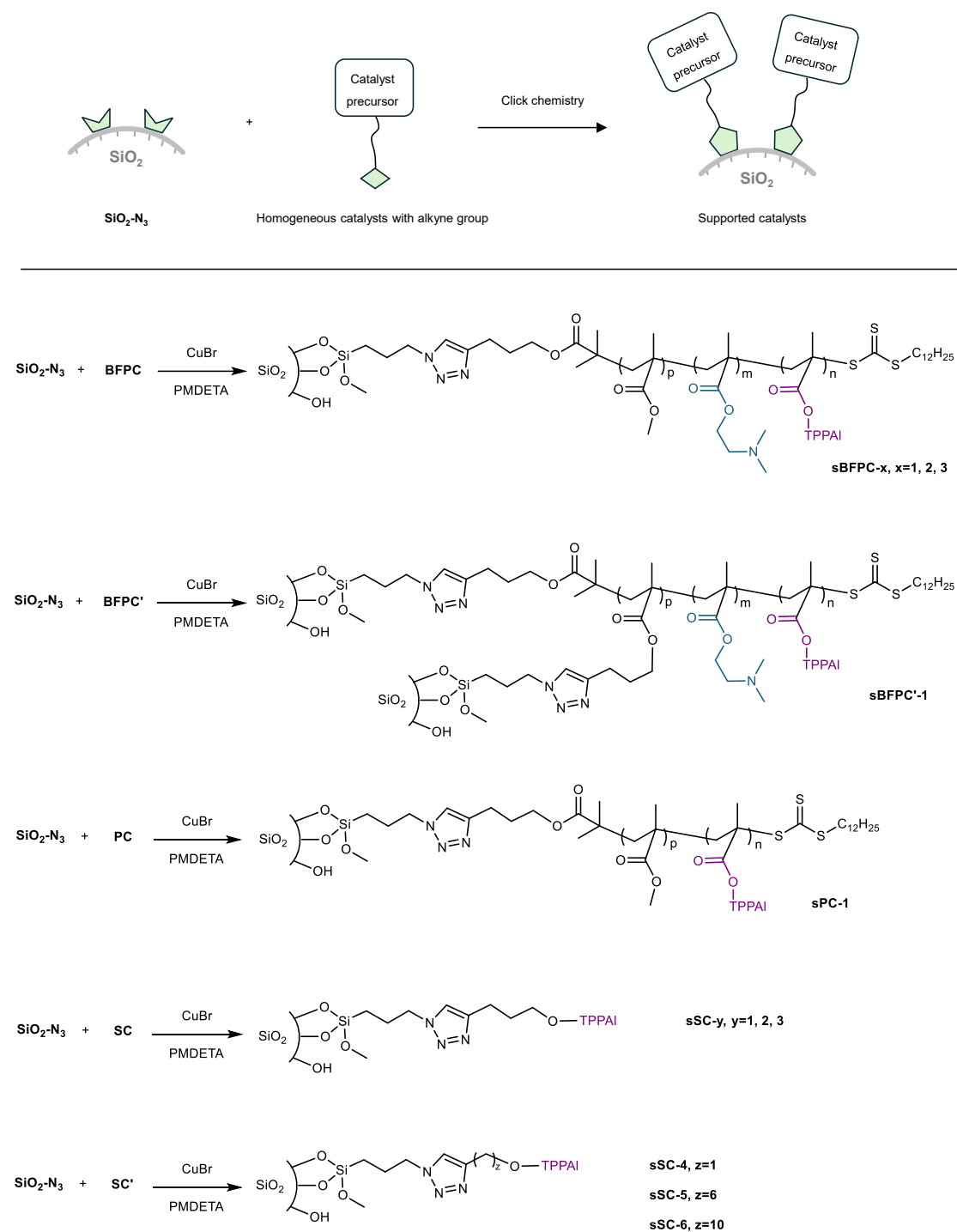
Supplementary Scheme 2. Immobilization of homogeneous catalysts onto the surface of **SiO₂-N₃**.
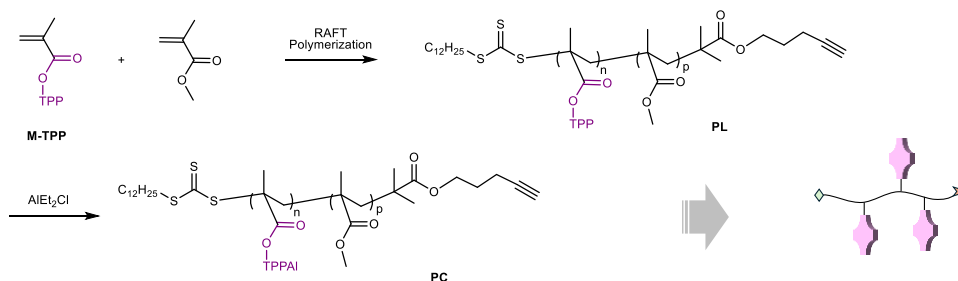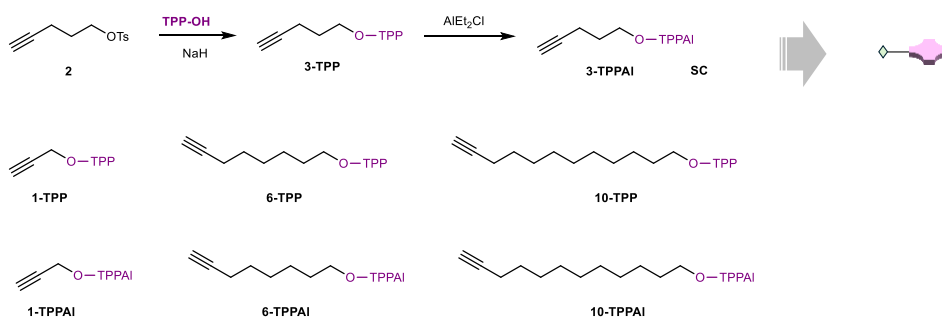
Supplementary Scheme 3. Synthetic routes of the homogeneous ligands and catalysts with alkyne group. Preparation of a) **BFPL** and **BFPC**, b) **BFPL'** and **BFPC'**, c) **PL** and **PC** and d) **SC**.
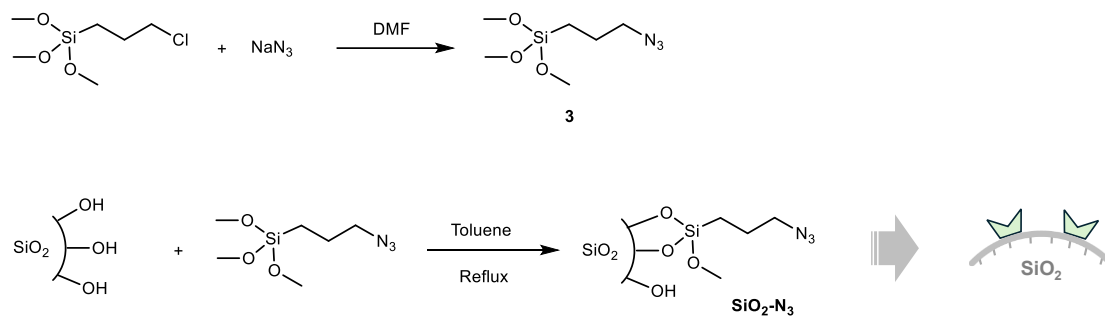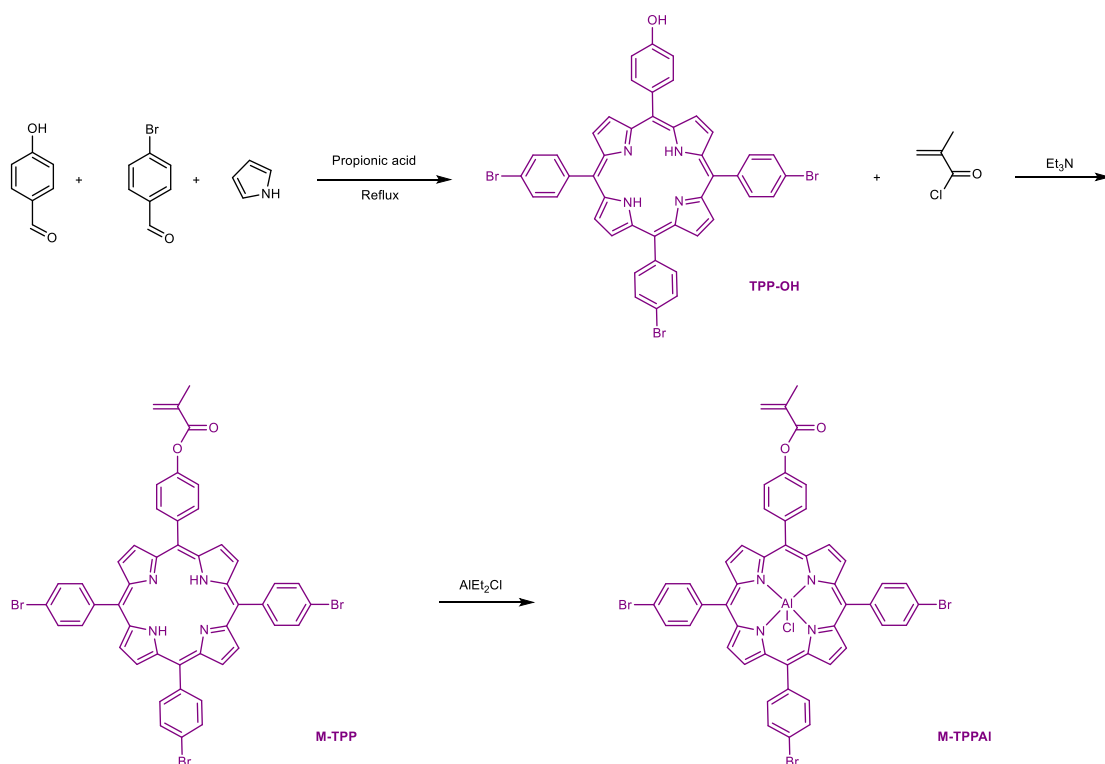
Supplementary Scheme 4. Synthetic route of azide-functionalized SiO₂ (SiO_2-N_3).

Supplementary Scheme 5. Synthetic route of **TPP-OH,** monomer porphyrin (**M-TPP**) and monomer Al porphyrin (**M-TPPAl**).
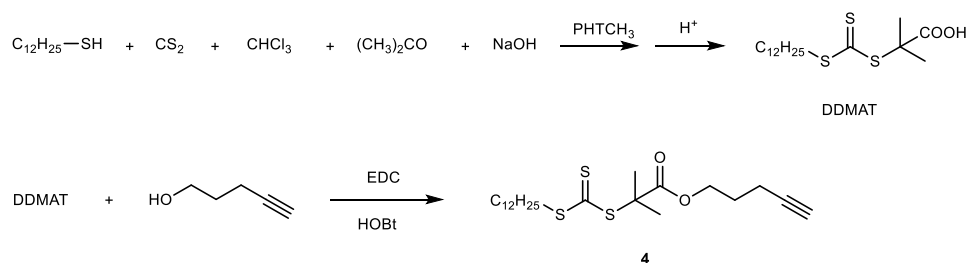
Supplementary Scheme 6. Synthetic route of RAFT agent (**4**) used in this work.

Synthesis of TPP-OH

TPP-OH

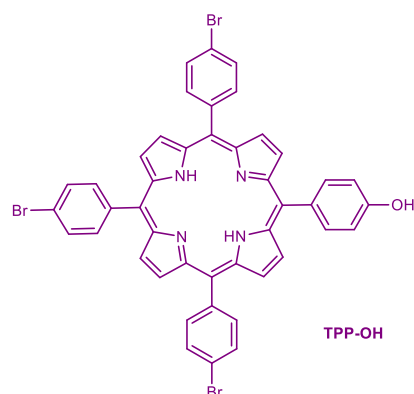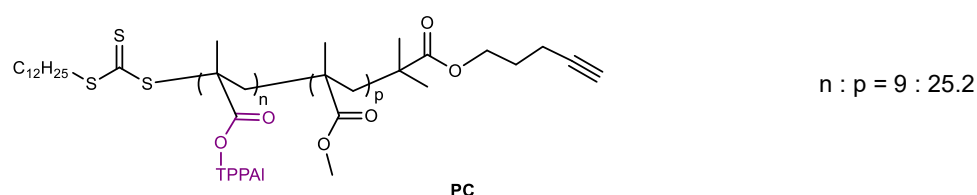4-(10,15,20-tris(4-bromophenyl)porphyrin-5-yl)phenol (**TPP-OH**) was prepared according to the literature procedures[1]. In a three-neck flask, 4-bromobenzaldehyde (20.68 g, 112 mmol) and 4-hydroxybenzaldehyde (4.55 g, 37 mmol) were dissolved in propionic acid (500 mL) and heated to 135 °C for 0.5 h. Then, pyrrole (10.00 g, 149 mmol) was added dropwise to the mixture under nitrogen. After refluxing for 2 h at 165 °C, the mixture was cooled to room temperature. The cooled mixture was then transferred to 1.5 L methanol and stored overnight at 0 °C. Following filtration, the purple solid was washed with methanol and hot water. The crude product was further purified using silica gel column with dichloromethane as eluent. Yield 6%. ^{1}H NMR (500 MHz, CDCl$_3$, δ, ppm): 8.94-8.68 (m, 8H), 8.21-8.01 (m, 8H), 7.92 (d, J = 7.5 Hz, 6H), 7.15 (d, J = 8.3 Hz, 2H), 5.15 (s, 1H), -2.81 (s, 2H).
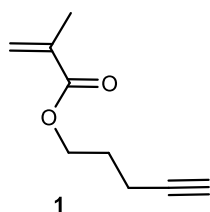
Synthesis of M-TPP
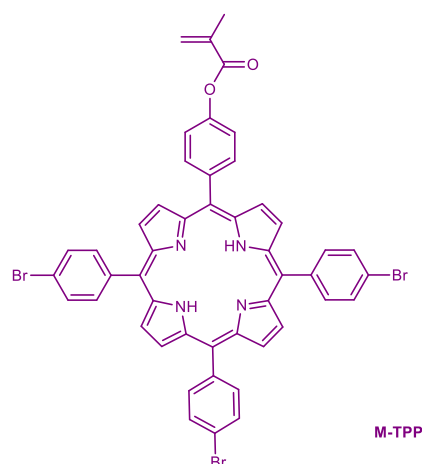
M-TPP

The product was prepared according to the literature procedures[1]. Briefly, **TPP-OH** (1.0 g,

1.1 mmol) and triethylamine (0.15 g, 1.5 mmol) were dissolved in the anhydrous CH_2Cl_2 under nitrogen. Methacryloyl chloride (0.14g, 1.3 mmol) was then added dropwise to the solution at 0 °C, and the mixture was stirred overnight at 30 °C. The solution was subsequently washed with brine. The crude product was purified using silica gel column with CH_2Cl_2 as eluent and recrystallized from a mixture of CH_2Cl_2 and hexane. The yield was 80%.. ^{1}H NMR (500 MHz, CDCl₃, δ, ppm): 8.94-8.68 (m, 8H), 8.21 (d, J = 7.5 Hz, 2H), 8.06 (d, J = 8.4 Hz, 6H), 7.90 (d, J = 7.5 Hz, 6H), 7.55 (d, J = 8.3 Hz, 2H), 6.55 (s, 1H), 5.91 (s, 1H), 2.22 (s, 3H), -2.85 (s, 2H).

Synthesis of BFPC, BFPC' and PC

n : m : p = 6 : 14.4 : 11.4

BFPC

n : m : p = 6 : 12 : 12.6

BFPC'

n : p = 9 : 25.2

PC

Polymeric porphyrin was prepared according to the literature[1]. Generally, **M-TPP** (1 g, 1.07 mmol), MMA (0.214 g, 2.14 mmol), DMAEMA (0.336 g, 2.14 mmol) (no need for **PC**), **4** (46 mg, 0.107 mmol), AIBN (9 mg, 0.05 mmol) were dissolved in THF (20 mL). After degassing, the mixture was heated to 65 °C for 48 h. Once cooled to room temperature, the mixture was centrifuged in cold diethyl ether and washed with cold diethyl ether three times. The ligands were dried under vacuum at 80 °C. Subsequently, within a glove box, the ligands were metallized with $AlEt_2Cl$ to yield the corresponding Al porphyrins.
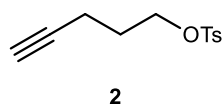
Synthesis of pent-4-yn-1-yl methacrylate (1)

The preparation of **1** is similar to that of **M-TPP**, except that the raw material was replaced by 4-pentyn-1-ol. Yield 95%. ^{1}H NMR (500 MHz, CDCl$_3$, δ, ppm): 6.11 (s, 1H), 5.57 (s, 1H), 4.25 (t, J = 6.1 Hz, 2H), 2.32 (td, J = 7.2, 2.8 Hz, 2H), 1.97 (t, J = 2.8 Hz, 2H), 1.95 (s, 3H), 1.91 (m, 2H).

## Synthesis of pent-4-yn-1-yl 4-methylbenzenesulfonatein (2)

4-pentyn-1-ol (2.5 g, 30 mmol) and pyridine (3.38 g, 43 mmol) were dissolved in DCM (20 mL) at 0 °C. *p*-Toluenesulfonyl chloride (8.4 g, 44 mmol) was added in three portions. The mixture was stirred at room temperature until completion, as monitored by thin-layer chromatography (TLC). The mixture was partitioned between DCM and water, and the organic layer was separated and washed with water three times. Subsequently, the organic layer was dried over anhydrous Na$_2$SO$_4$ and evaporated. The crude product was purified using silica gel column with CH$_2$Cl$_2$/hexane (1/2, V/V) as eluent to obtain oily colorless liquid. Yield: 95%. Synthesis of other p-toluenesulfonic acid substituted products follows a similar procedure, with the raw materials replaced by 7-octyn-1-ol and 11-dodecyn-1-ol. ^{1}H NMR (500 MHz, CDCl$_3$, δ, ppm): 7.79 (d, J = 7.9 Hz, 2H), 7.35 (d, J = 7.9 Hz, 2H), 4.14 (t, J = 5.5 Hz, 2H), 2.45 (s, 3H), 2.26 (td, J = 6.9, 2.5 Hz, 2H), 1.95 (t, J = 2.5 Hz, 1H), 1.86 (m, 2H).

Synthesis of single site porphyrin ligand
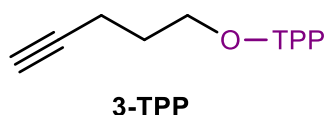
3-TPP

A single-site porphyrin ligand (**3-TPPAl**) was synthesized by reacting **TPP-OH** (500 mg, 0.58 mmol) with an excess of pent-4-yn-1-yl 4-methylbenzenesulfonatein (143 mg, 0.60 mmol) in DMF in the presence of NaH and KI at 50 °C for 5 h under nitrogen. Then, DMF was removed via vacuum distillation at 55 °C. The mixture was then cooled to room temperature, dissolved in dichloromethane and washed three times with deionized water. The CH_2Cl_2 was removed by rotary evaporators. After drying, the crude product was further purified on silica gel column with CH_2Cl_2/hexane (1/1 v/v) as eluent. Yield: 95%. Synthesis of other single-site porphyrin ligands follows a similar procedure. ^{1}H NMR (500 MHz, CDCl₃, δ, ppm): 8.95-8.77 (m, 8H), 8.16-8.02 (m, 8H), 7.90 (d, J = 8.3 Hz, 6H), 7.29 (d, J = 8.3 Hz, 2H), 4.38 (d, J = 6.1 Hz, 2H), 2.60 (td, J = 7.2, 2.7 Hz, 2H), 2.21 (m, 2H), 2.08 (t, J = 2.7 Hz, 1H), -2.80 (s, 2H).

General method of metallization of porphyrin ligands
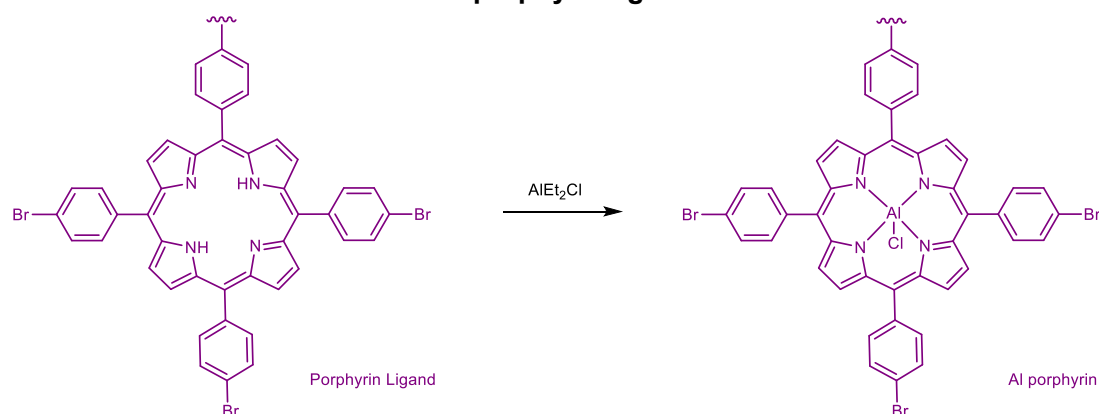
In an argon glove box, porphyrin ligand (1 mmol) was dissolved in CH_2Cl_2 followed by the addition of $AlEt_2Cl$ (1.1 mmol, 2.0 mol/L in hexane). After 2 h, CH_2Cl_2 was removed by vacuum distillation. The crude product was further purified on neutral alumina with CH_2Cl_2/CH_3OH (10/1 v/v). Yield: 95%.

## Synthesis of (3-azidopropyl)trimethoxy silane (3)

3
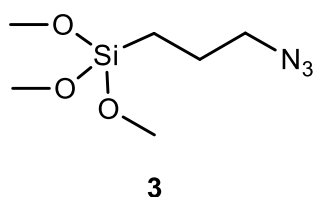
(3-azidopropyl)trimethoxy silane (**3**) was prepared according to the literature[2]. Generally, (3-chloropropyl)trimethoxy silane (10 g, 50.3 mmol), sodium azide (4.9 g, 75.5 mmol), sodium iodide (0.1 g) and dry DMF (150 mL) were mixed in a round-bottom flask under nitrogen. The mixture was stirred at 100 °C for 24 h. After cooling to room temperature, the mixture was poured into the mixture of ethyl ether and water. The organic layer was washed with brine and water. After drying with $MgSO_4$, the organic layer was concentrated to yield the product. Yield: 90%. ^1H NMR (500 MHz, $CDCl_3$, δ, ppm): 3.56 (s, 9H), 3.25 (t, J = 6.1 Hz, 2H), 1.70 (m, 2H), 0.68 (t, J = 8.0 Hz, 2H).

Synthesis of SiO_2-N_3

SiO_2-N_3
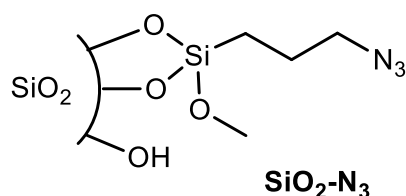
The process of functionalization of silica was referred to the literature[2]. Generally, 1.0 g of freshly dried nano-silica (350 °C, 12 h) was added to anhydrous toluene (50 mL) under nitrogen and sonicated for 10 min. 0.1 mL of (3-azidopropyl)trimethoxy silane was added and the suspension was sonicated for an additional 10 min. Then the mixture was heated to 110 °C for 12 h. After cooling to room temperature, the functionalized silica was separated by centrifugation and washed successively with toluene, acetonitrile and ethanol, before being dried under vacuum at 80 °C.

Synthesis of DDMAT
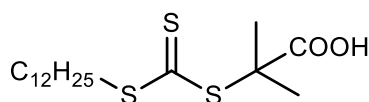
DDMAT

The RAFT agent S-1-Dodecyl-S'-(α,α'-dimethyl-α"-acetic acid) (**DDMAT**) was prepared according to the literature changelessly[3]. Generally, 1-dodecanethiol (20.2 g, 0.1 mol), acetone (48.1 g, 0.83 mol) and methyl trioctyl ammonium chloride (1.6 g, 4 mmol) were mixed under nitrogen. Then NaOH solution (50%) (8.4 g, 0.1 mol) was slowly added and stirred for 20 min. Carbon disulfide (7.6 g, 0.1 mol) in acetone (10.1 g, 0.17 mol) was added and stirred for 30 min. Following this, $CHCl_3$ (17.8 g, 0.15 mol) was added in one portion, followed by dropwise addition of NaOH solution (50%) (40 g, 0.5 mol). The mixture was stirred overnight. 300 mL of water was added, followed by 30 mL of concentrated HCl to acidify the aqueous solution. Acetone was evaporated by purging with nitrogen, and the solid was filtered off. The solid was then stirred in 2-propanol (400 mL). After filtering off the undissolved solid, the 2-propanol solution was concentrated to dryness. The resulting solid was recrystallized from hexanes, yielding a yellow crystalline product. ^{1}H NMR (500 MHz, $CDCl_3$, $δ$, ppm): 3.29 (t, J = 7.4 Hz, 2H), 1.73 (s, 6H), 1.65 (m, 2H), 1.48-1.17 (m, 18H), 0.89 (t, J = 6.6 Hz, 3H).

Synthesis of RAFT agent (4)
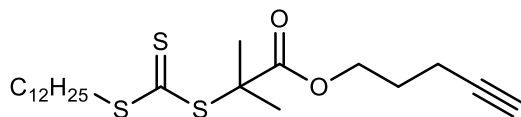
4

DDMAT (1.0 g, 2.75 mmol) was dissolved in methylene chloride (10 mL) in a 100 mL round-bottom flask and cooled to 0 °C. 1-Hydroxybenzotriazole (0.41 g, 3.0 mmol) and EDC (0.58 mg, 3.0 mmol) were added, and the solution was stirred at 0 °C for 30 min. Then a solution of 4-pentyn-1-ol (0.23 g, 2.75 mol) in methylene chloride (5 mL) was added dropwise, and the reaction mixture was allowed to warm to room temperature and stir for 48 h. The reaction mixture was poured into a 10% aqueous sodium carbonate

solution and stirred for 30 min. The mixture was extracted with methylene chloride (50 mL × 2), and the organic layer was washed with a 10% sodium carbonate solution (100 mL), water (100 mL), and a saturated NaCl solution (100 mL), successively. The organic layer was dried over $MgSO_4$, filtered, and concentrated under reduced pressure. The crude product was purified on silica gel column with CH_2Cl_2 as eluent to obtain oily yellow liquid. Yield: 40%. ^1H NMR (500 MHz, $CDCl_3$, δ, ppm): 4.19 (t, J = 5.9 Hz, 2H), 3.27 (t, J = 7.5 Hz, 2H), 2.26 (td, J = 6.9, 2.5 Hz, 2H), 1.95 (t, J = 2.5 Hz, 1H), 1.86 (m, 2H), 1.71-1.63 (m, 8H), 1.48-1.17 (m, 18H), 0.89 (t, J = 6.6 Hz, 3H).

Synthesis of immobilized catalysts

Generally, **SiO₂-N₃** (0.5 g), homogeneous catalyst (0.05 g), CuBr (0.01 g, 0.07 mmol), PMDETA (0.025 g, 0.14 mmol) were added into a round-bottom flask. Then 10 mL DMF (10 mL) was injected under nitrogen. The mixture was dispersed by sonication and stirred for 24 h. The immobilized catalyst was separated by centrifugation, washed with CH_2Cl_2/CH_3OH (V/V, 10/1) and then dried under vacuum at 80 °C.

Characterization of precursors and catalysts
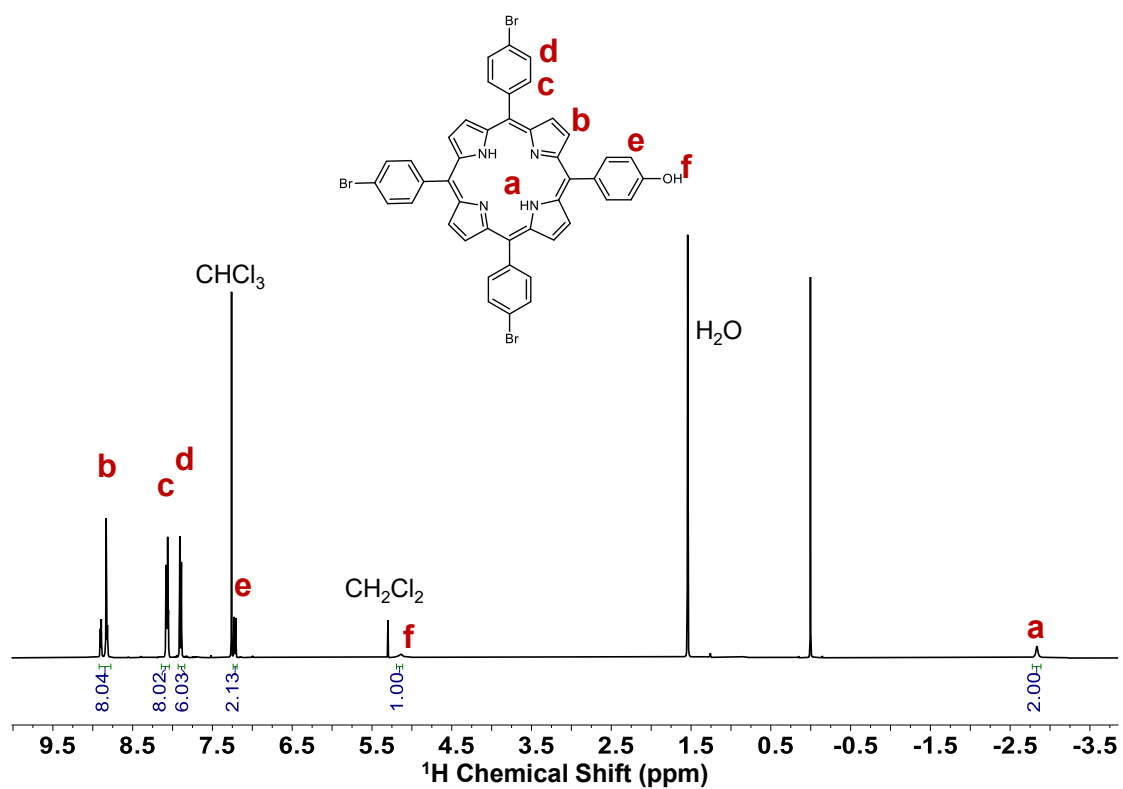
Supplementary Figure 1. ^{1}H NMR spectrum of **TPP-OH** in CDCl$_3$ at 25 °C.
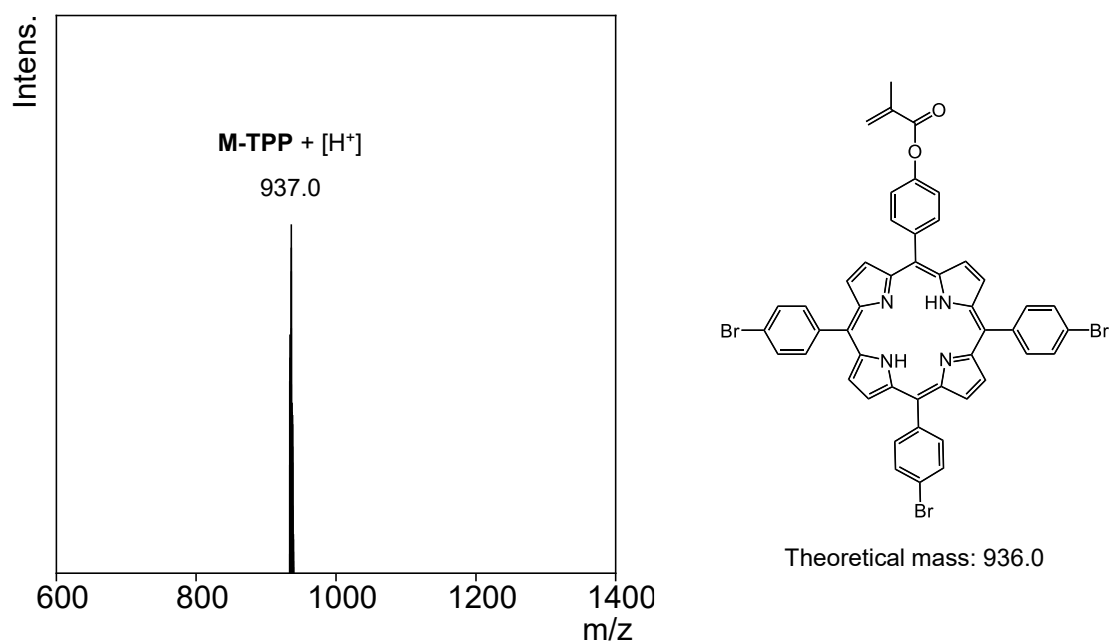

Theoretical mass: 866.0
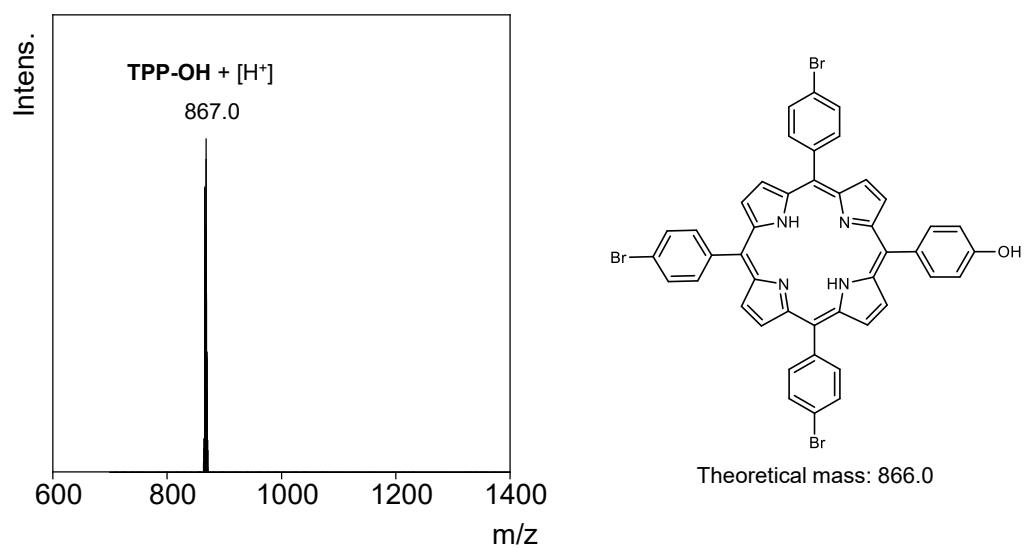
Supplementary Figure 2. MALDI-TOF-MS spectrum of **TPP-OH**.
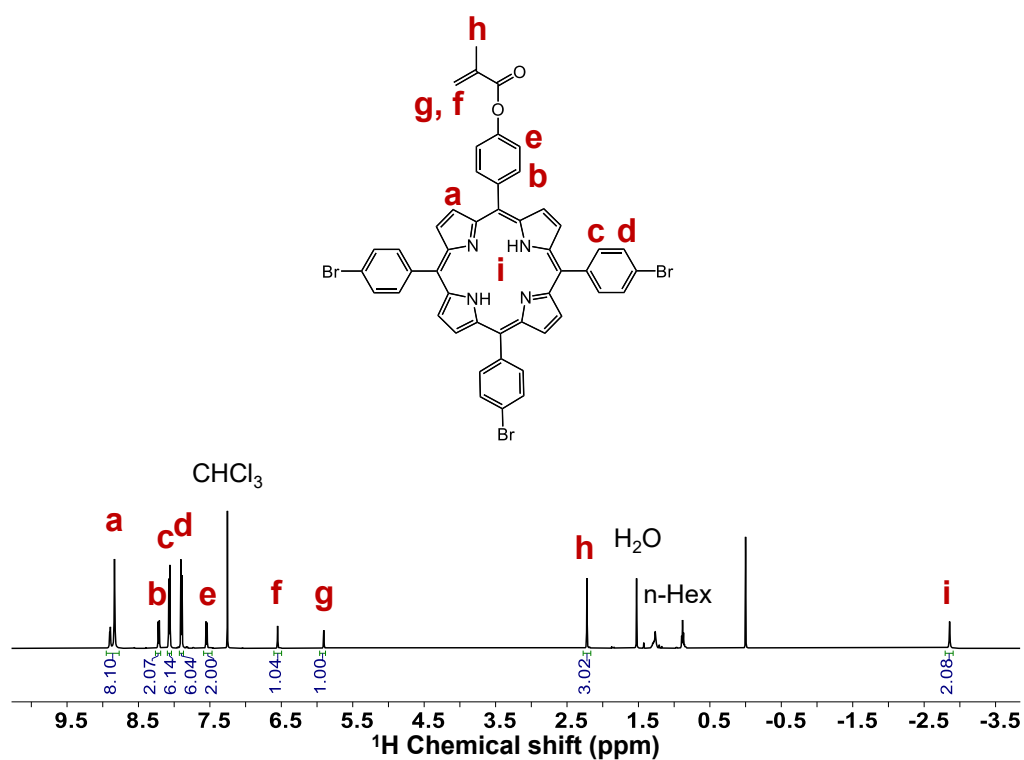
Supplementary Figure 3. ^{1}H NMR spectrum of **M-TPP** in CDCl$_3$ at 25 °C.

Theoretical mass: 936.0

Supplementary Figure 4. MALDI-TOF-MS spectrum of **M-TPP**.
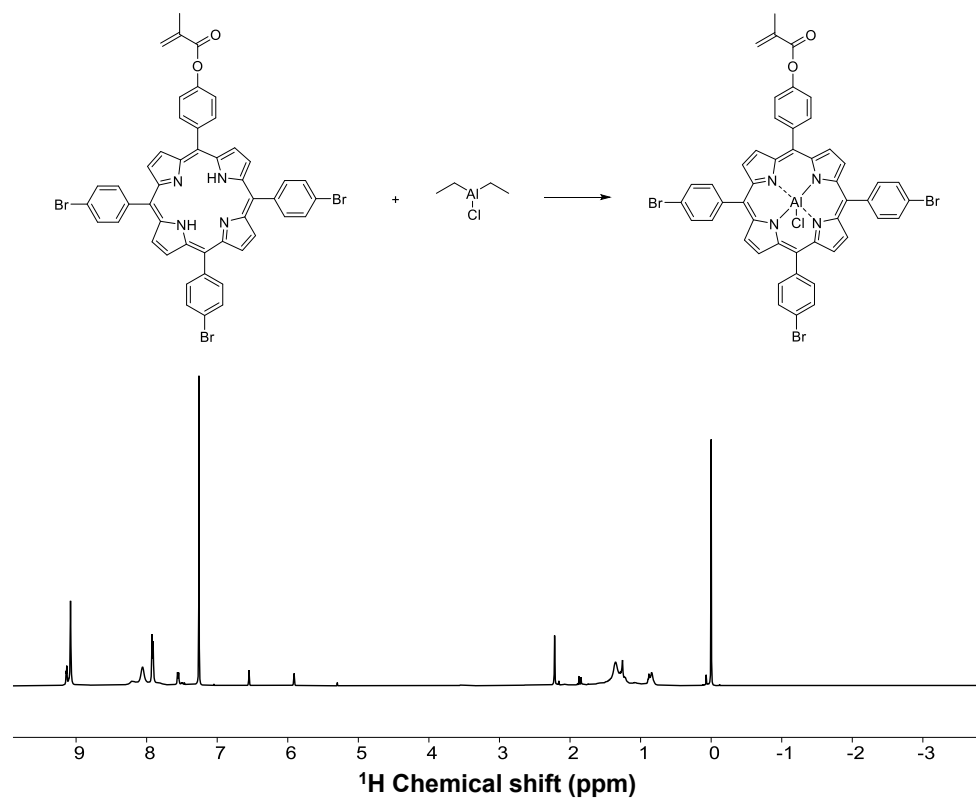
Supplementary Figure 5. ¹H NMR spectrum of **M-TPPAl** in CDCl₃ at 25 °C. The ring hydrogen peak (-2.8 ppm) disappeared after metallization.
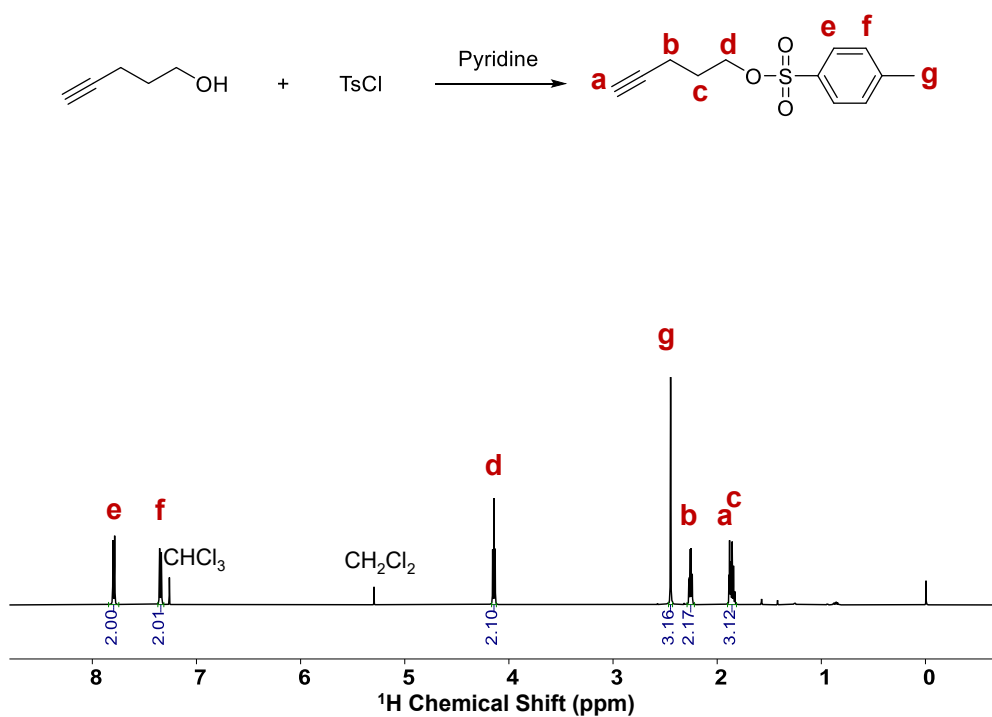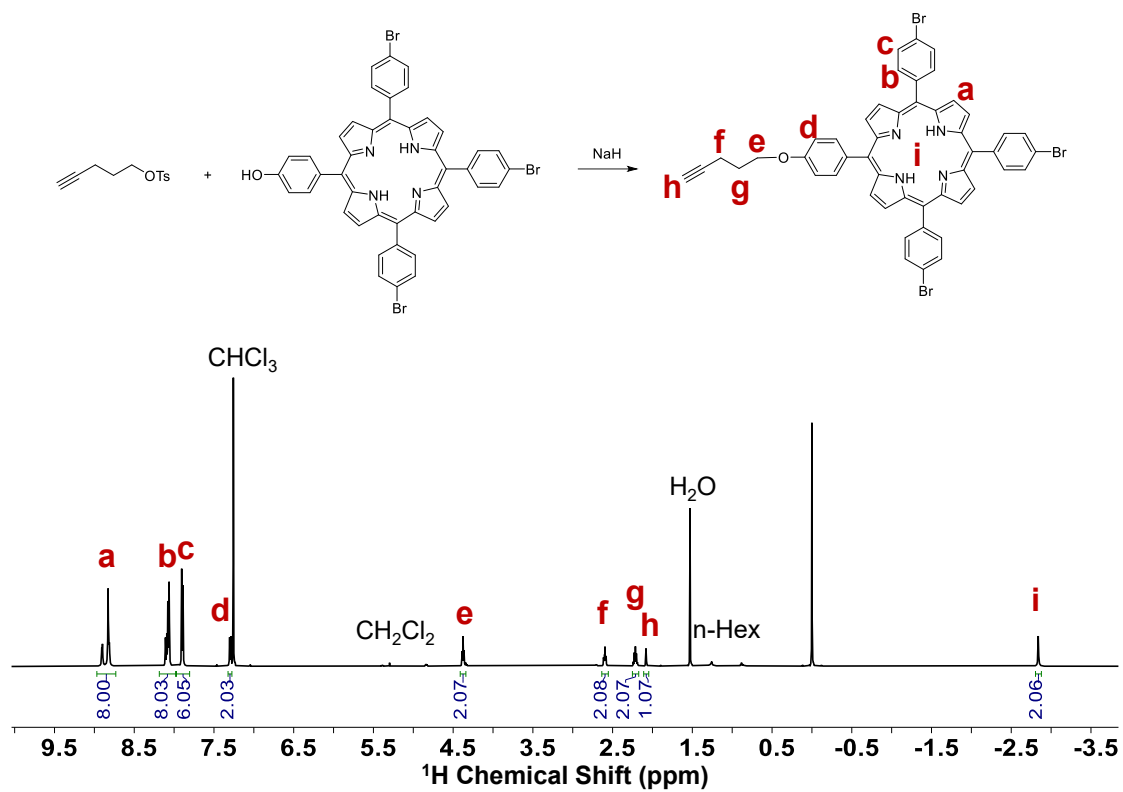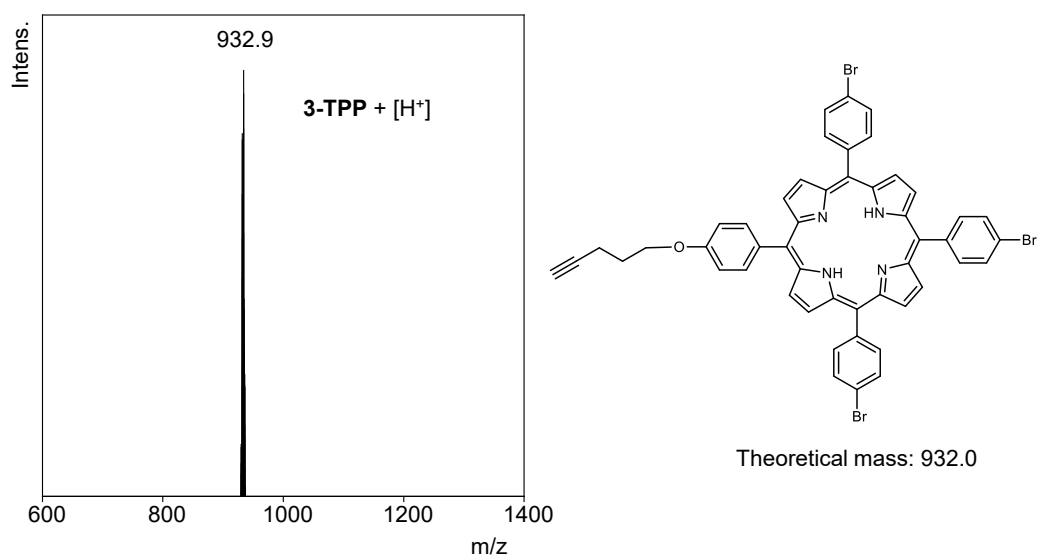

Supplementary Figure 6. ¹H NMR spectrum of **2** CDCl₃ at 25 °C.

Supplementary Figure 7. ¹H NMR spectrum of **3-TPP** in CDCl$_3$ at 25 °C.

Supplementary Figure 8. MALDI-TOF-MS spectrum of **3-TPP**.

Supplementary Figure 9. ^{1}H NMR spectrum of **3-TPPAl** in d^6-DMSO at 25 °C. The ring hydrogen peak (-2.8 ppm) disappeared after metallization.

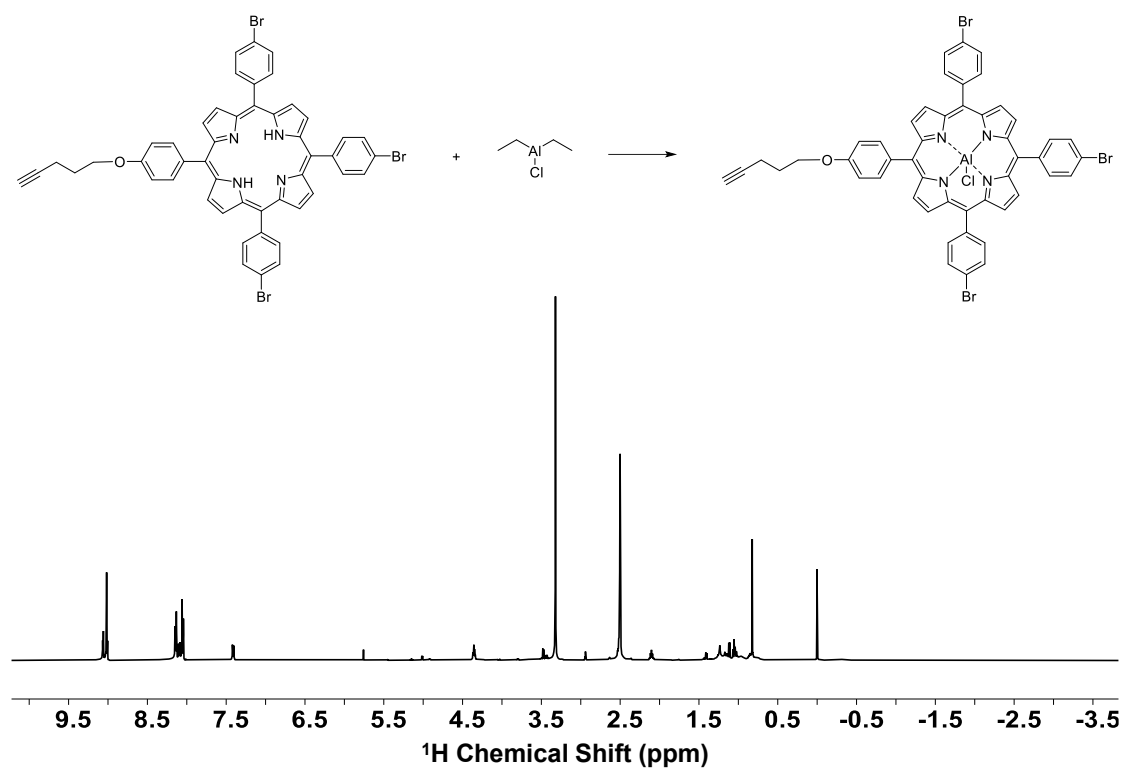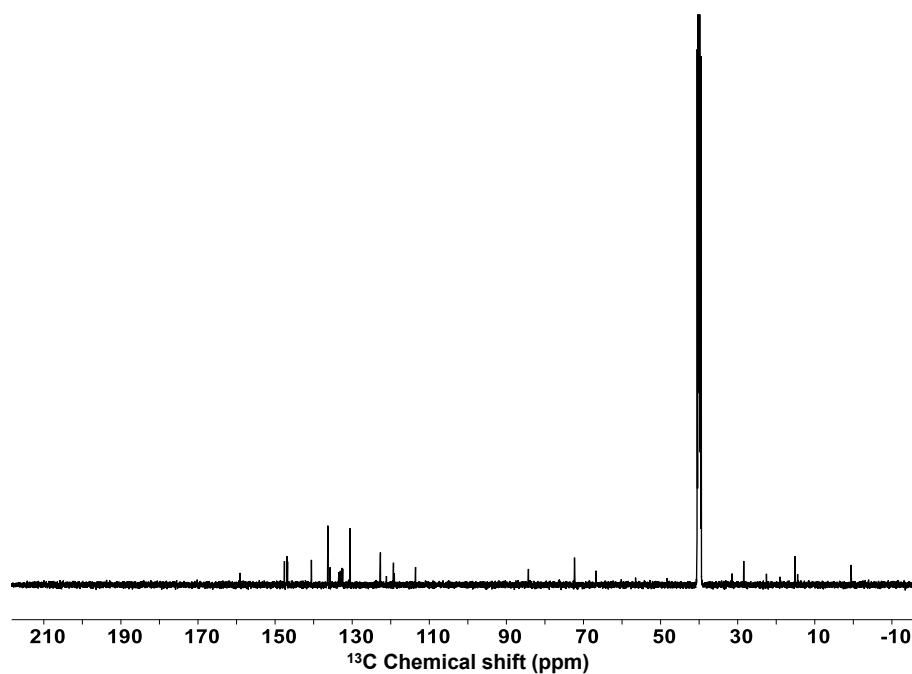**Supplementary Figure 10.** ^{13}C NMR spectrum of **3-TPPAl** in d^6-DMSO at 25 °C.

Supplementary Figure 11. ^{1}H NMR spectrum of **1-TPP** in CDCl$_3$ at 25 °C.

Theoretical mass: 906.0

Supplementary Figure 12. MALDI-TOF-MS spectrum of **1-TPP**.

Supplementary Figure 13. ^{1}H NMR spectrum of **1-TPPAl** in d^6-DMSO at 25 °C. The ring hydrogen peak (-2.8 ppm) disappeared after metallization.

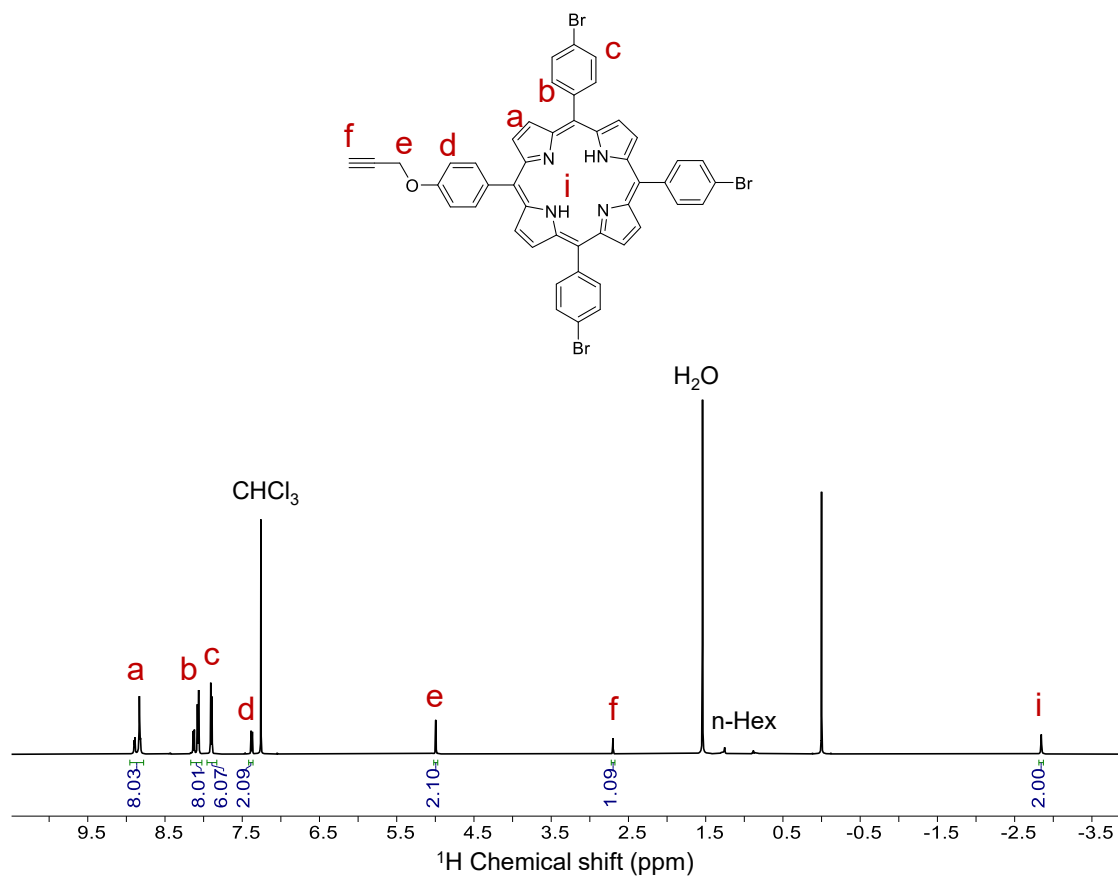**Supplementary Figure 14.** ^{1}H NMR spectrum of **6-TPP** in CDCl$_3$ at 25 °C.

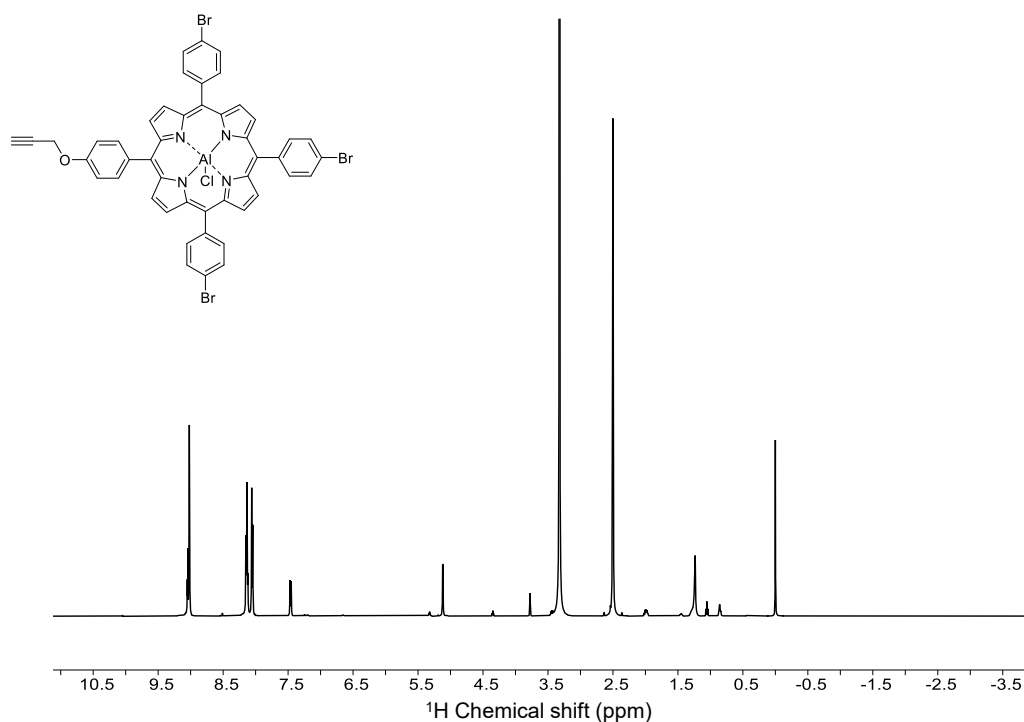**Supplementary Figure 15.** MALDI-TOF-MS spectrum of **6-TPP**.

Supplementary Figure 16. ^{1}H NMR spectrum of **6-TPPAl** in d^6-DMSO at 25 °C. The ring hydrogen peak (-2.8 ppm) disappeared after metallization.

Supplementary Figure 17. ^{1}H NMR spectrum of **10-TPP** in CDCl$_3$ at 25 °C.
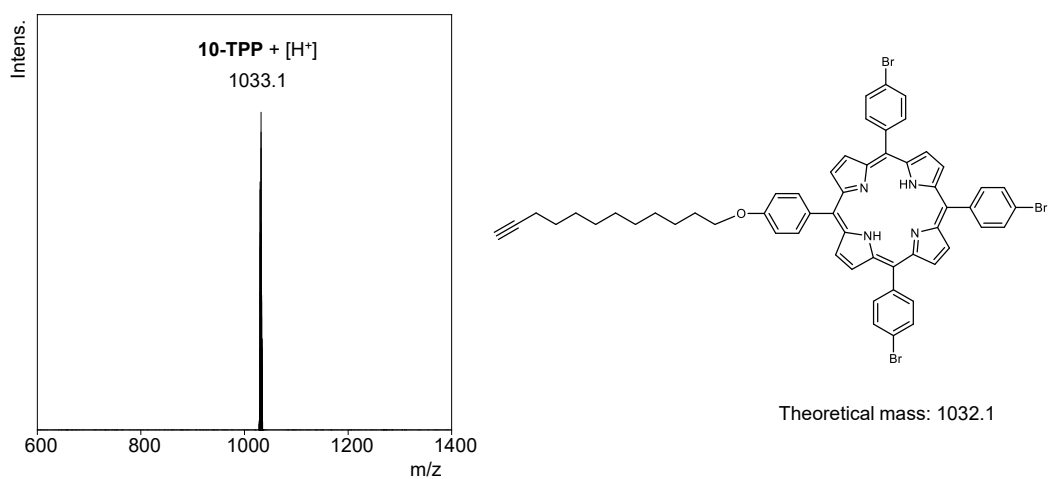
Supplementary Figure 18. MALDI-TOF-MS spectrum of **10-TPP**.

Supplementary Figure 19. ^{1}H NMR spectrum of **10-TPPAl** in d^6-DMSO at 25 °C. The ring hydrogen peak (-2.8 ppm) disappeared after metallization.
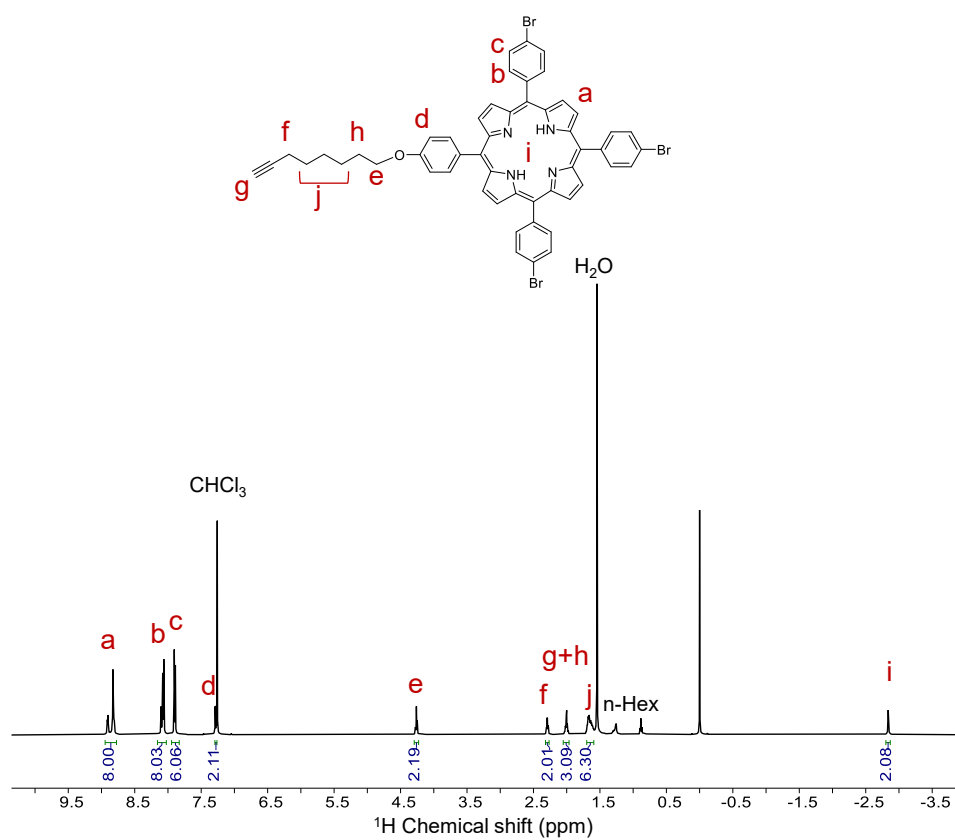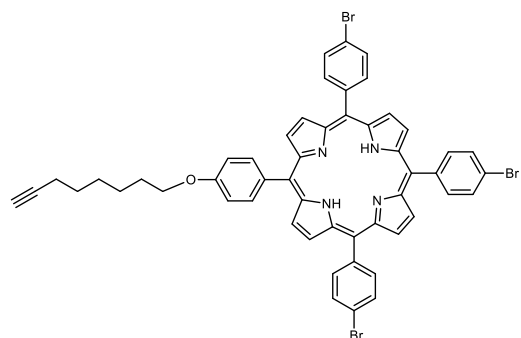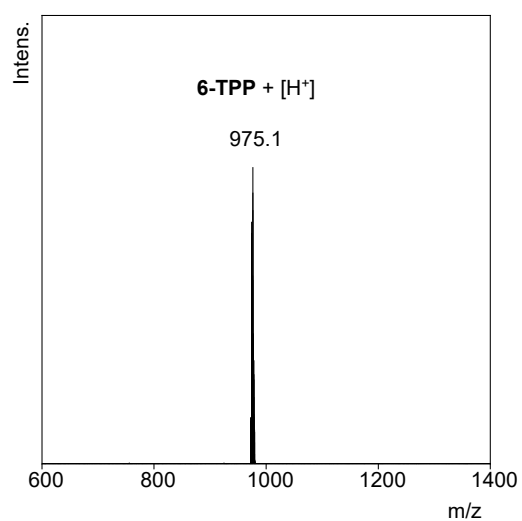

Supplementary Figure 20. ^{1}H NMR spectrum of **1** in CDCl$_3$ at 25 °C.

Supplementary Figure 21. ^{1}H NMR spectrum of DDMAT in CDCl$_3$ at 25 °C.

Supplementary Figure 22. ^{1}H NMR spectrum of RAFT agent (**4**) in CDCl$_3$ at 25 °C.

Supplementary Figure 23. ^{13}C NMR spectrum of RAFT agent (**4**) in CDCl$_3$ at 25 °C.

Supplementary Figure 24. ATR-FT-IR spectrum of RAFT agent (**4**).
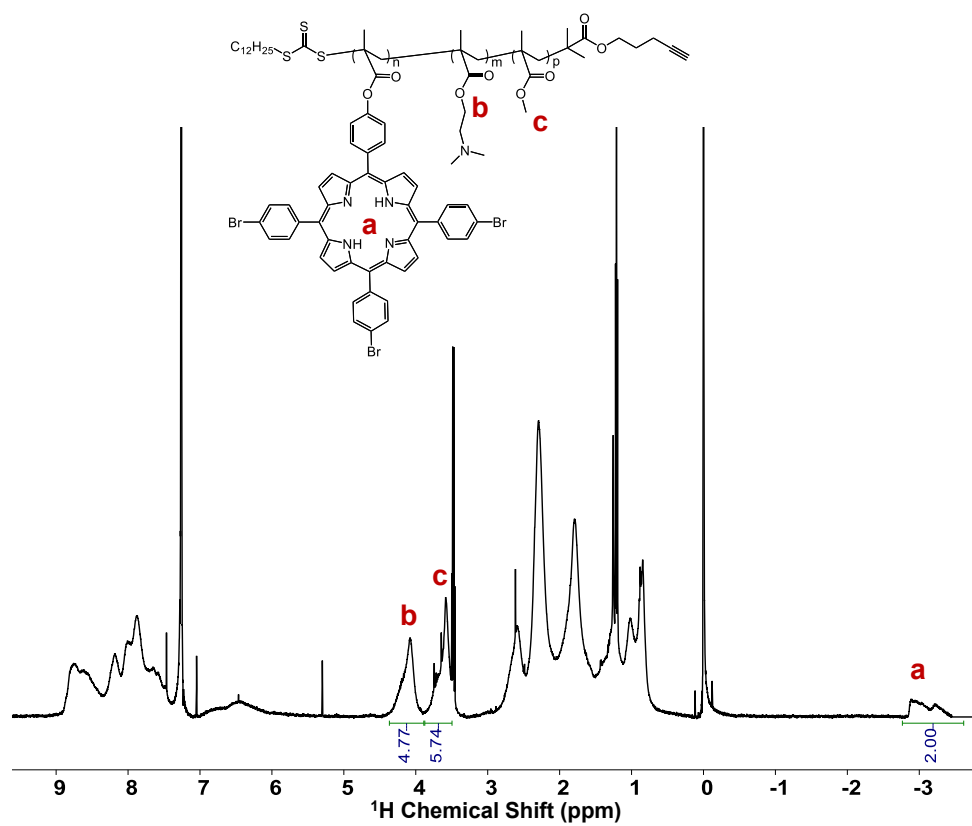
Supplementary Figure 25. ^{1}H NMR spectrum of **BFPL** in CDCl$_3$ at 25 °C.
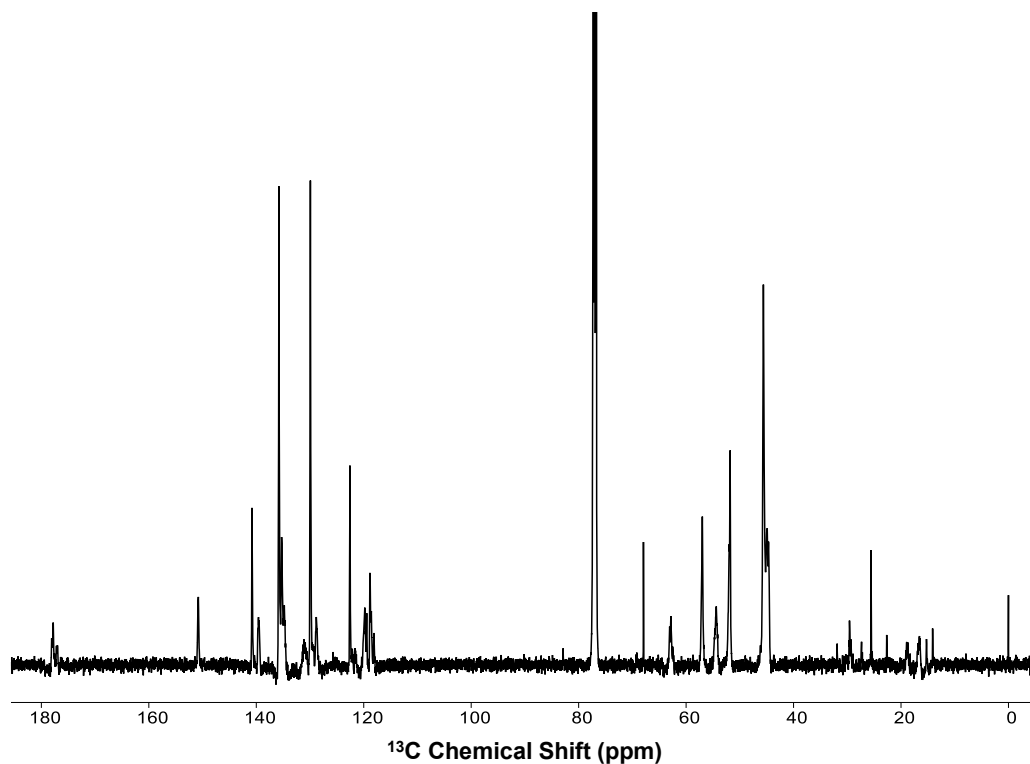
Supplementary Figure 26. ^{13}C NMR spectrum of **BFPL** in CDCl$_3$ at 25 °C.

$M_n = 9.2 \text{ kg·mol}^{-1}$
$Đ = 1.11$
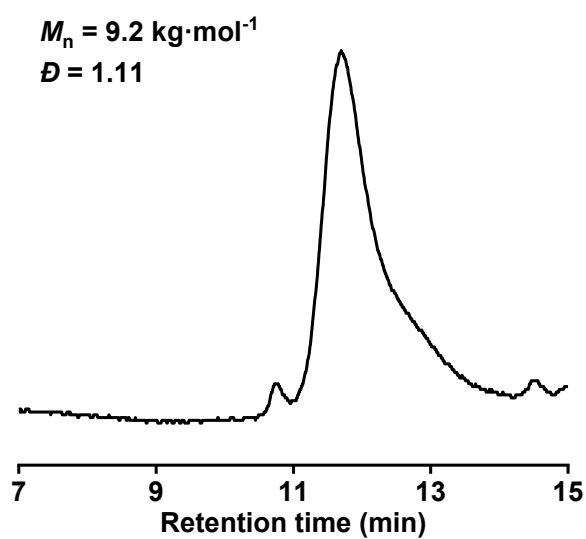
Supplementary Figure 27. GPC curve spectrum of **BFPL** in THF.
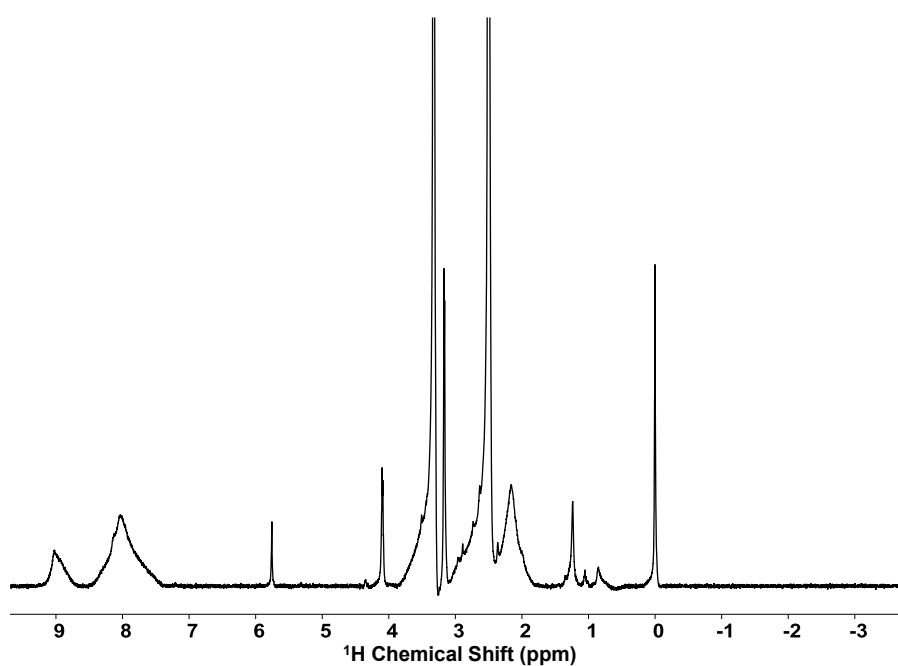
Supplementary Figure 28. ^{1}H NMR spectrum of **BFPC** in d^6-DMSO at 25 °C. The ring hydrogen peak (-2.8 - -3.3 ppm) disappeared after metallization.
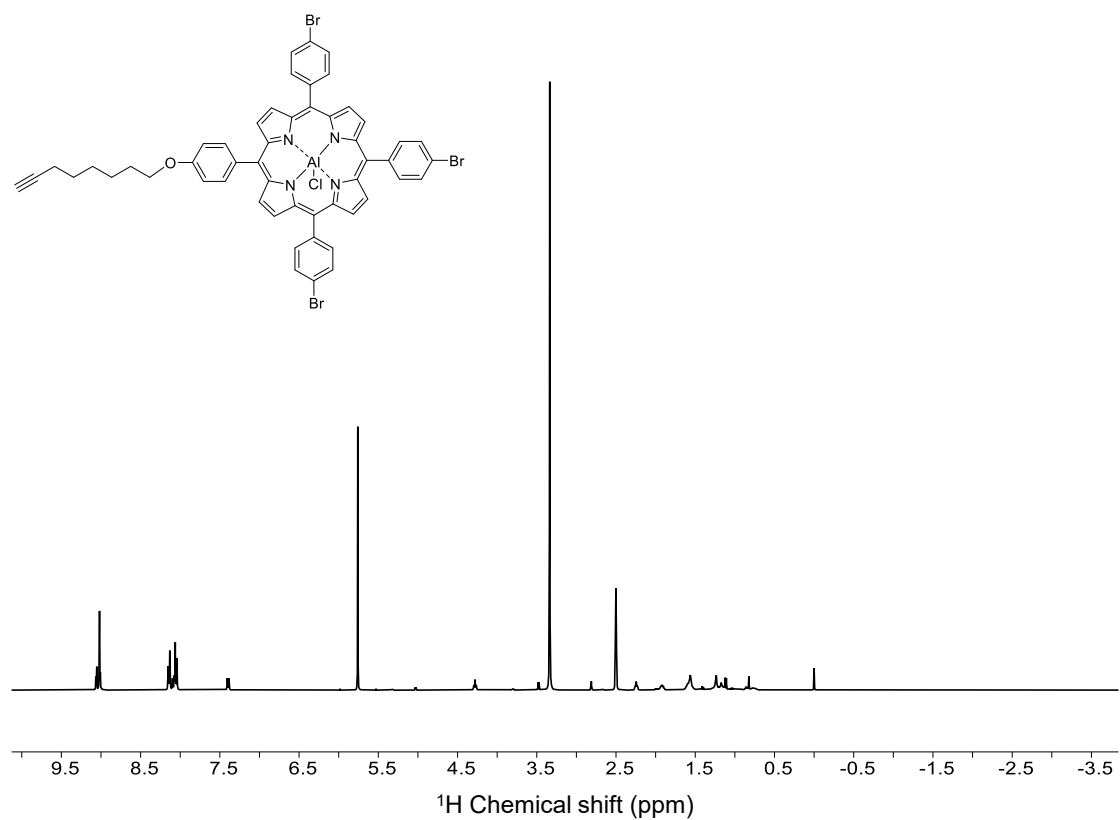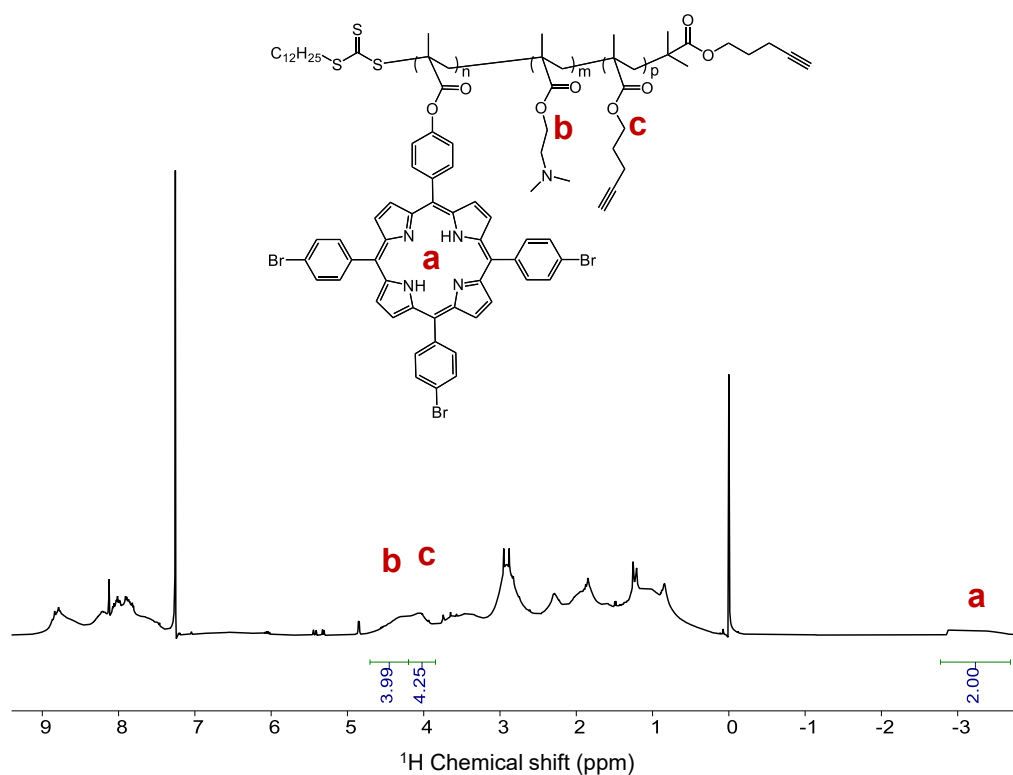
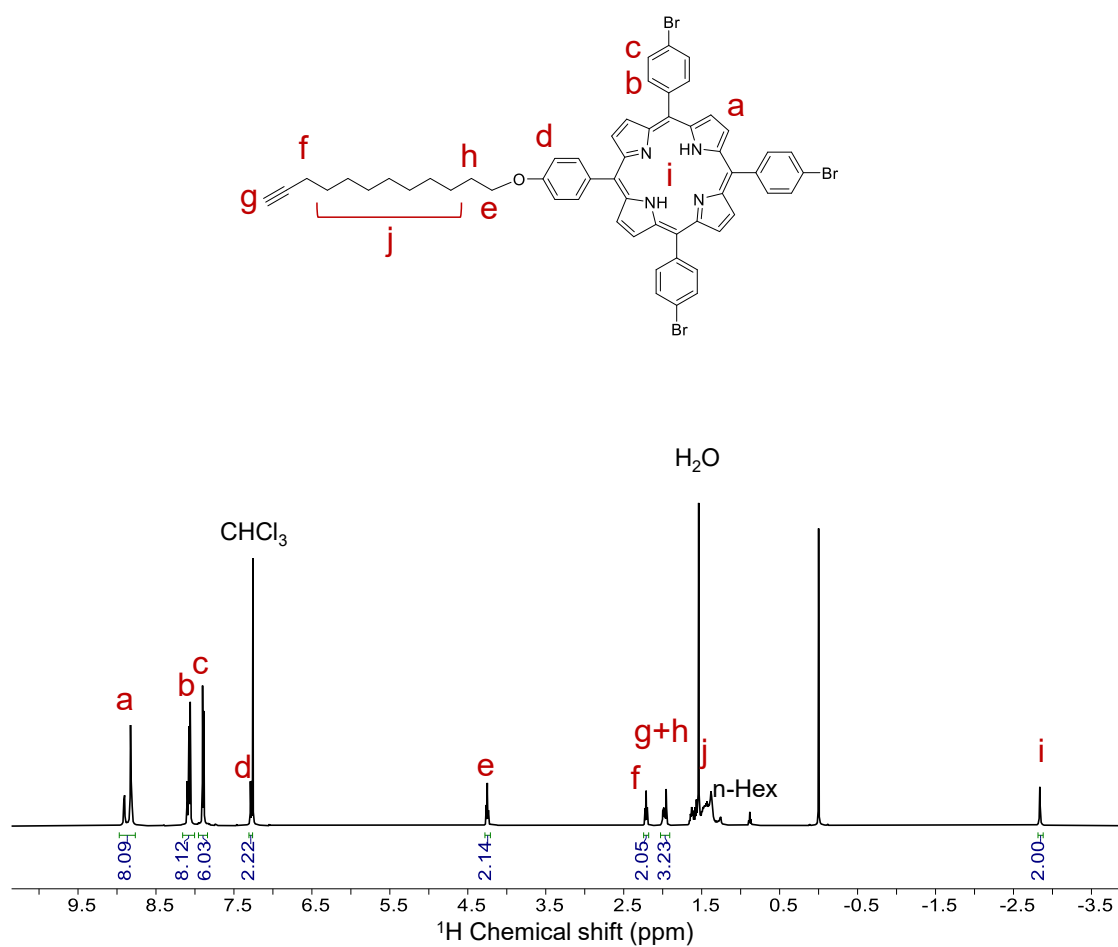**Supplementary Figure 29.** ^1H NMR spectrum of **BFPL'** in CDCl$_3$ at 25 °C.
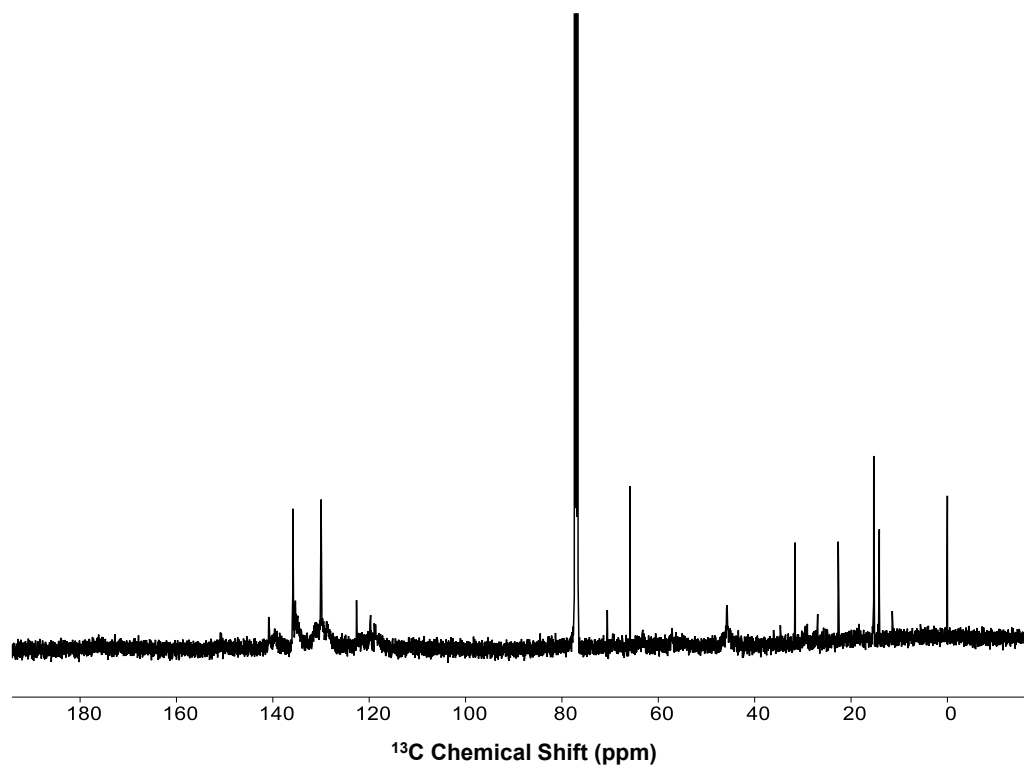
Supplementary Figure 30. ^{13}C NMR spectrum of **BFPL'** in CDCl$_3$ at 25 °C.

M_n = 9.2 kg·mol^{-1}

Đ = 1.13
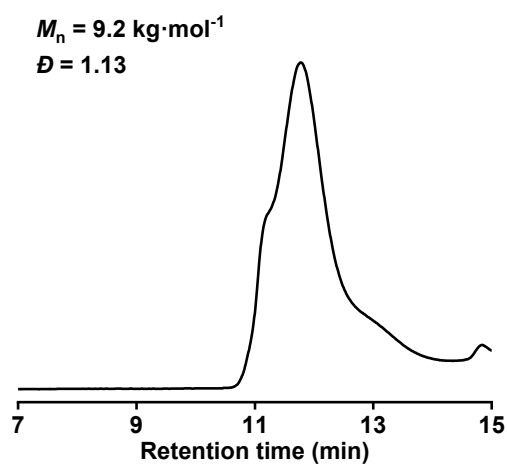
Supplementary Figure 31. GPC curve spectrum of **BFPL'** in THF.
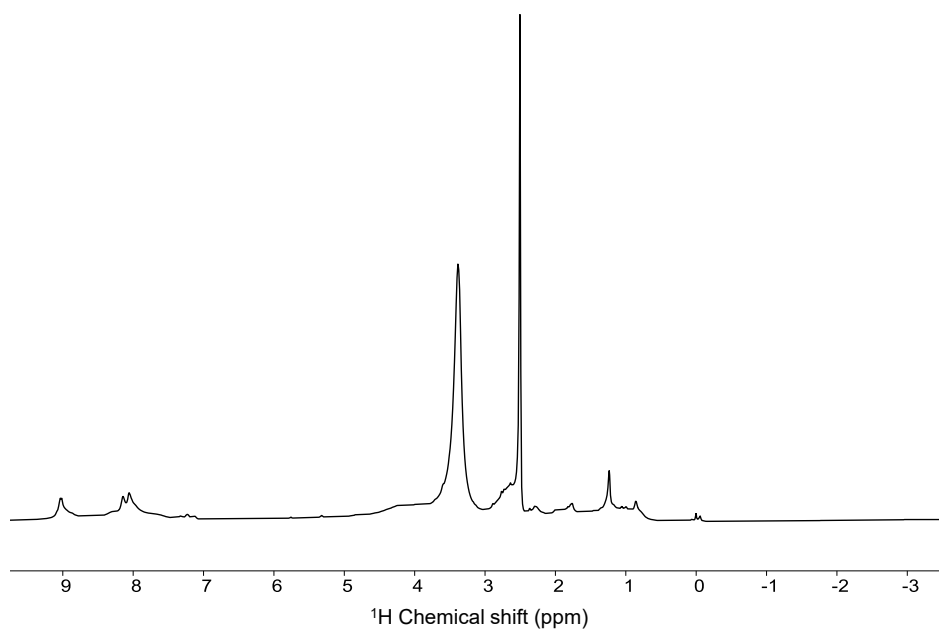
Supplementary Figure 32. ^{1}H NMR spectrum of **BFPC'** in d^6-DMSO at 25 °C. The ring hydrogen peak (-2.8 - -3.3 ppm) disappeared after metallization.
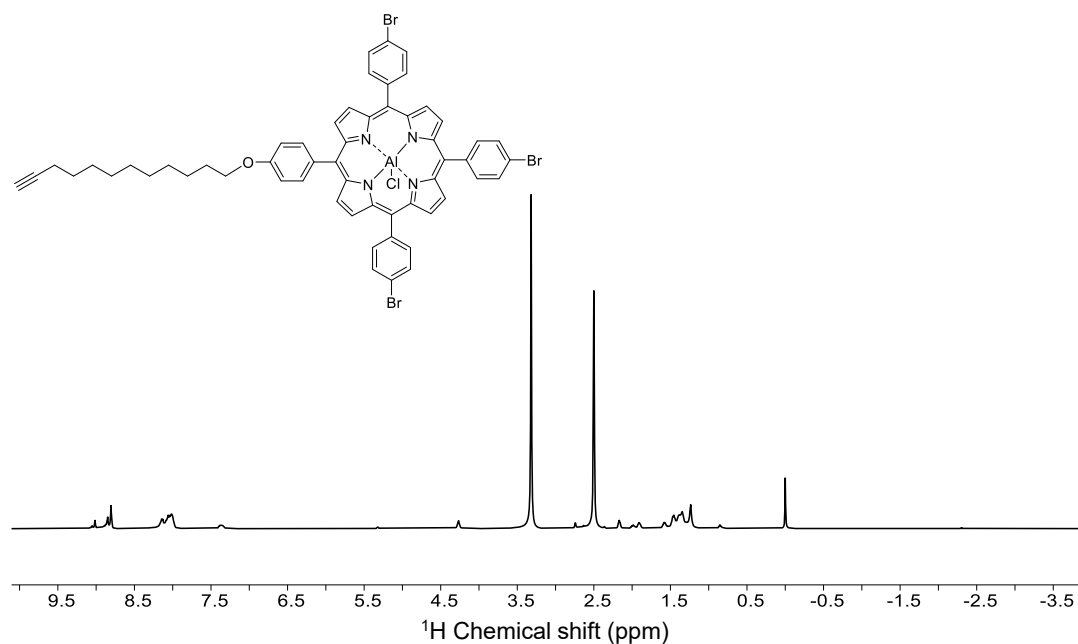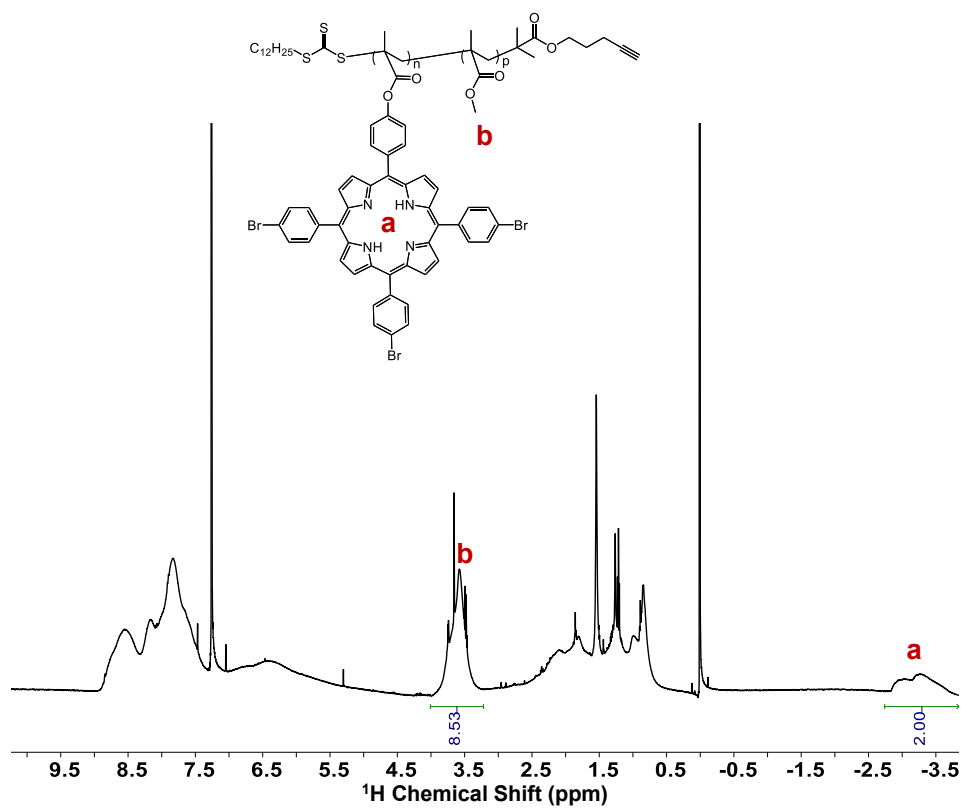
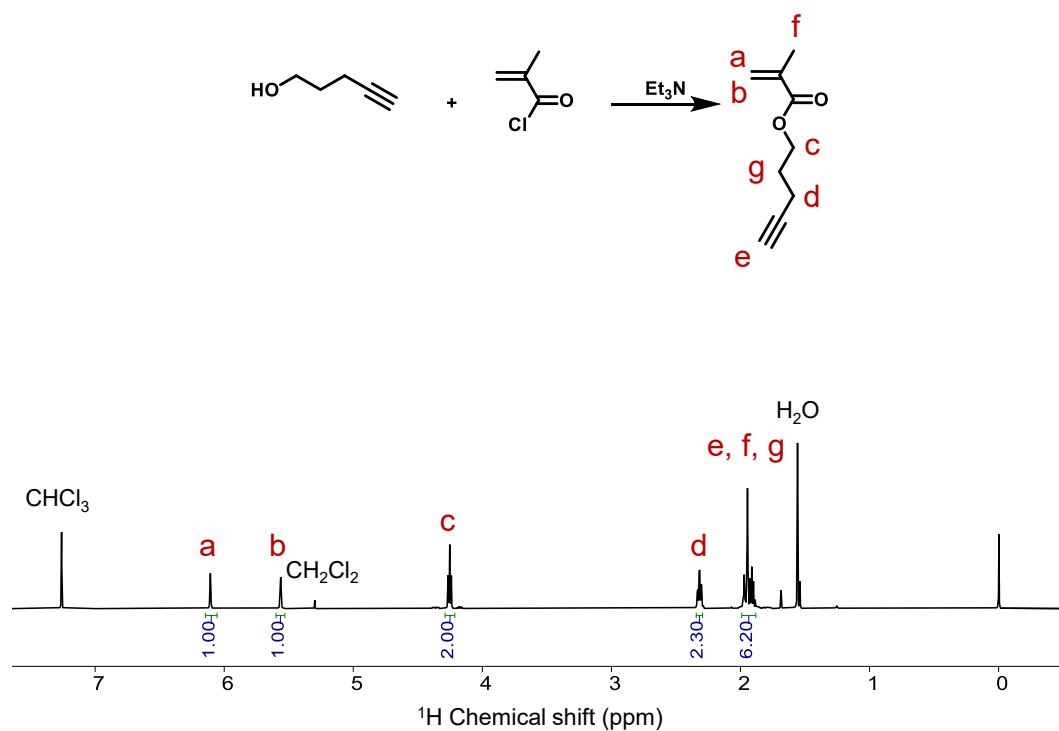**Supplementary Figure 33.** ^{1}H NMR spectrum of **PL** in CDCl$_3$ at 25 °C.
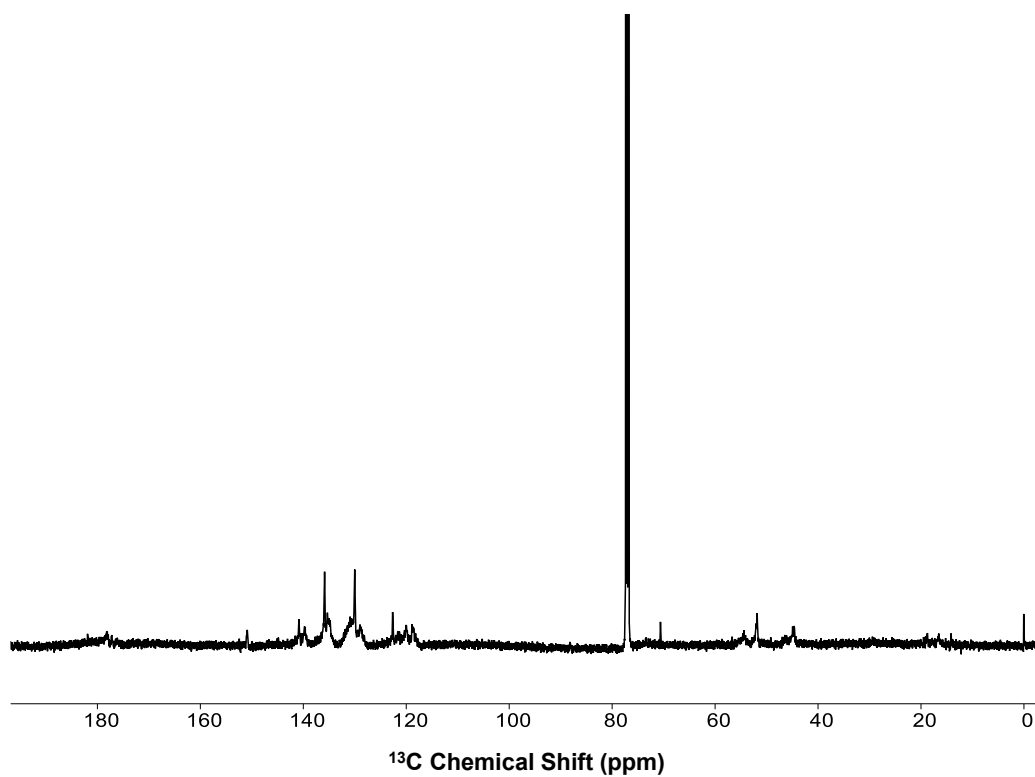
Supplementary Figure 34. ^{13}C NMR spectrum of **PL** in CDCl$_3$ at 25 °C.

M_n = 12.1 kg·mol^{-1}
Đ = 1.05
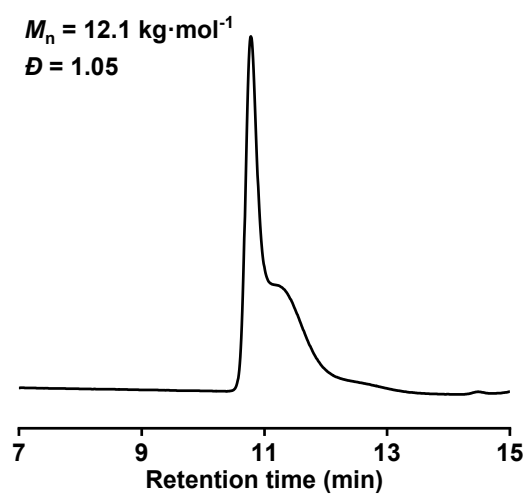
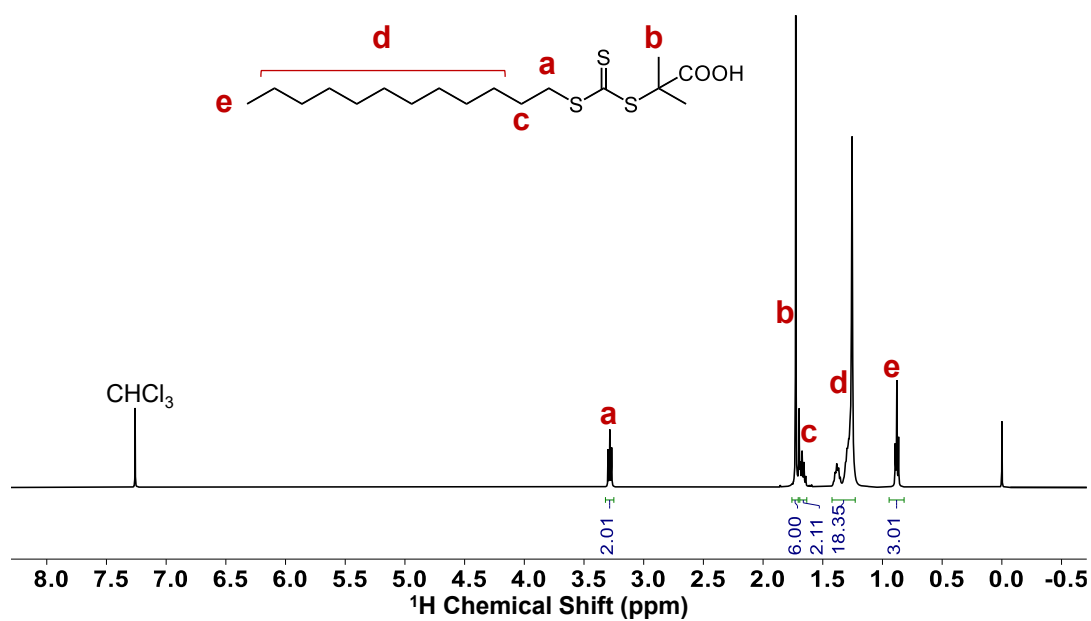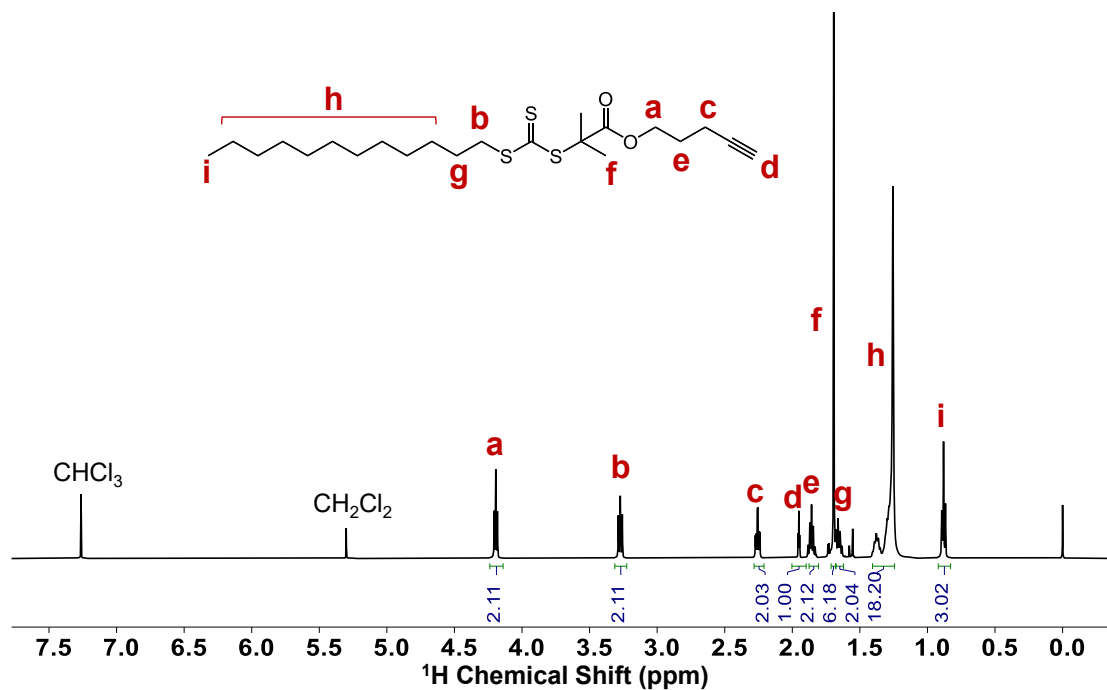**Supplementary Figure 35.** GPC curve spectrum of **PL** in THF.
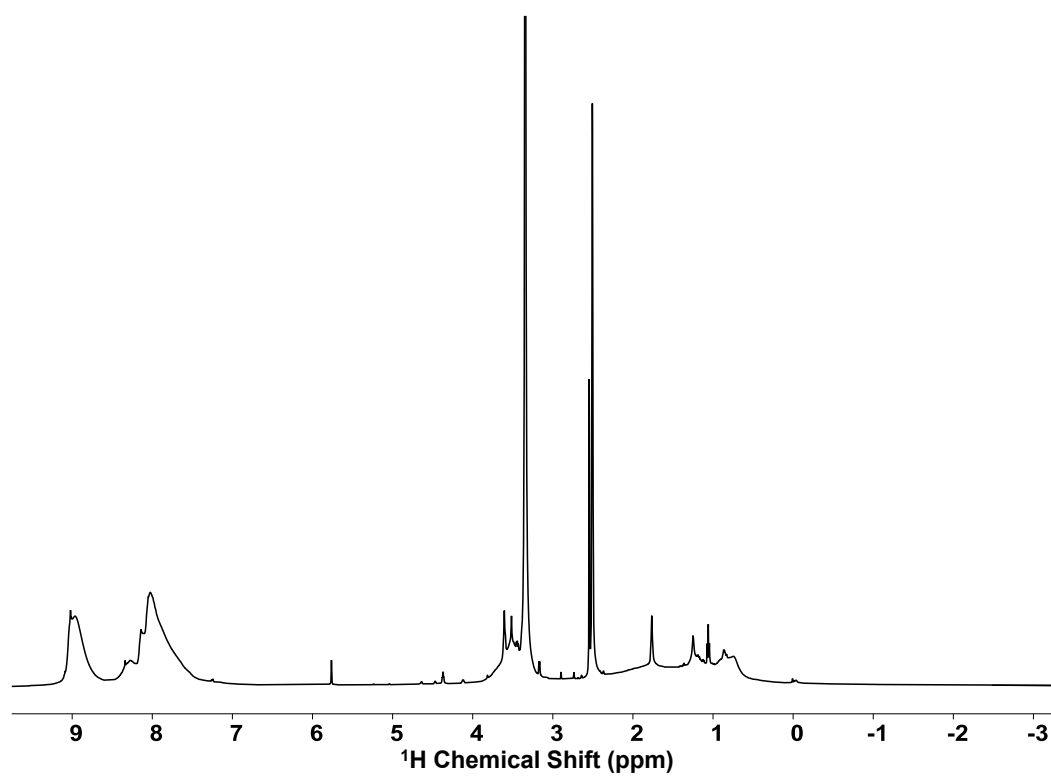
Supplementary Figure 36. ^{1}H NMR spectrum of **PC** in d^6-DMSO at 25 °C. The ring hydrogen peak (-2.8 - -3.3 ppm) disappeared after metallization.
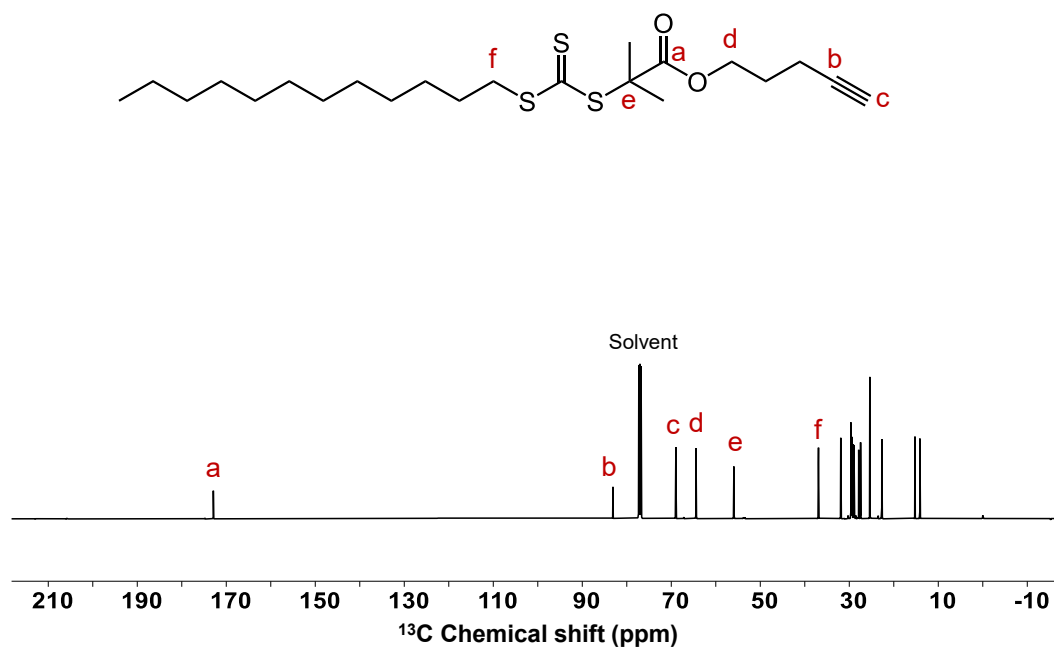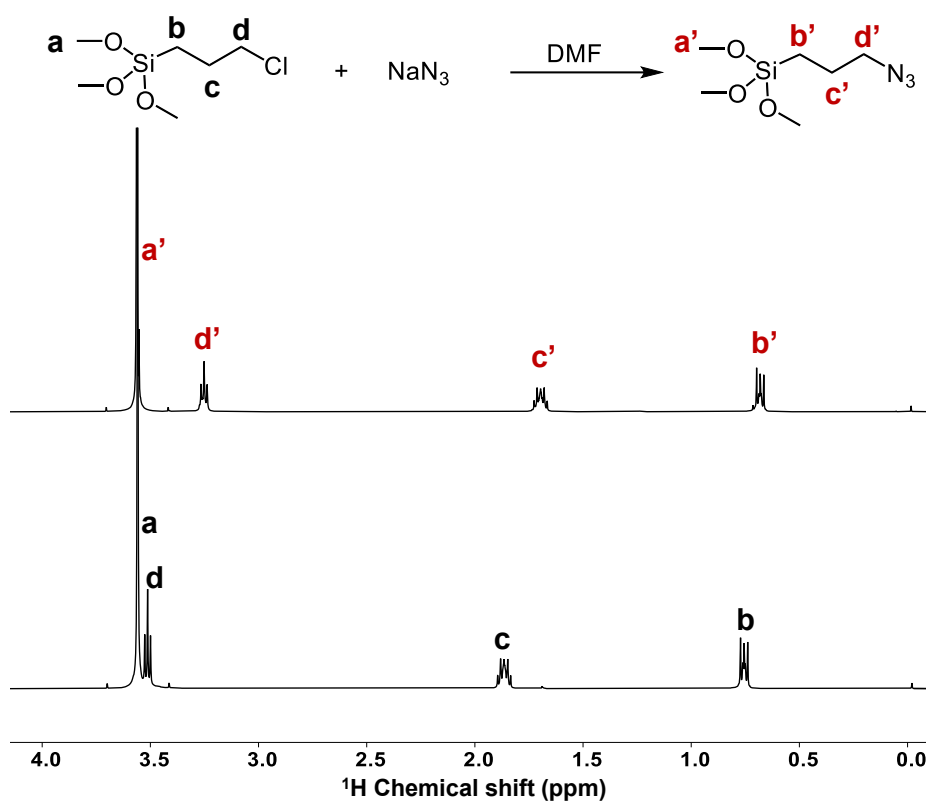
Supplementary Figure 37. ^{1}H NMR spectrum of (3-azidopropyl)trimethoxy silane (**3**) in CDCl$_3$ at 25 °C.
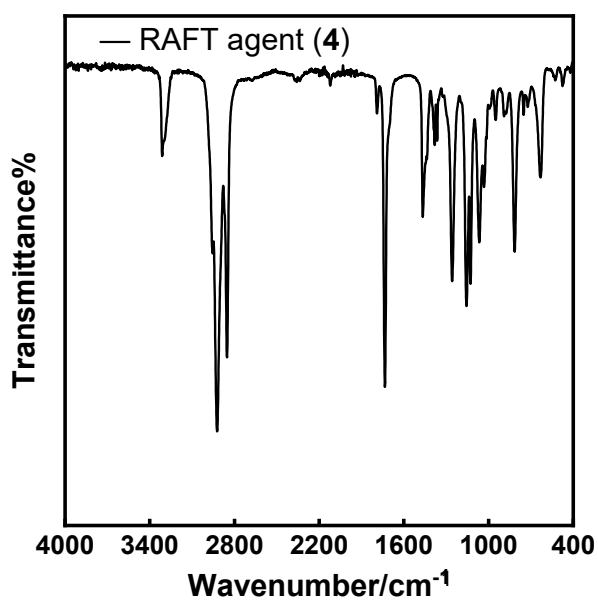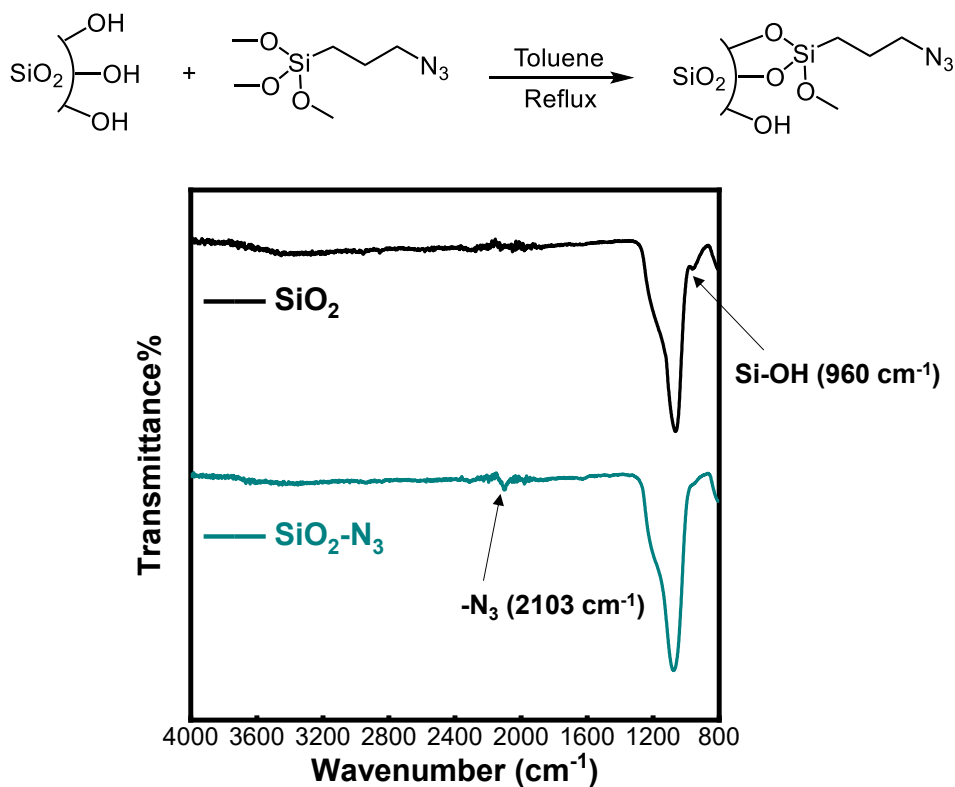

Supplementary Figure 38. ATR-FT-IR spectra of SiO$_2$ and **SiO$_2$-N$_3$**.
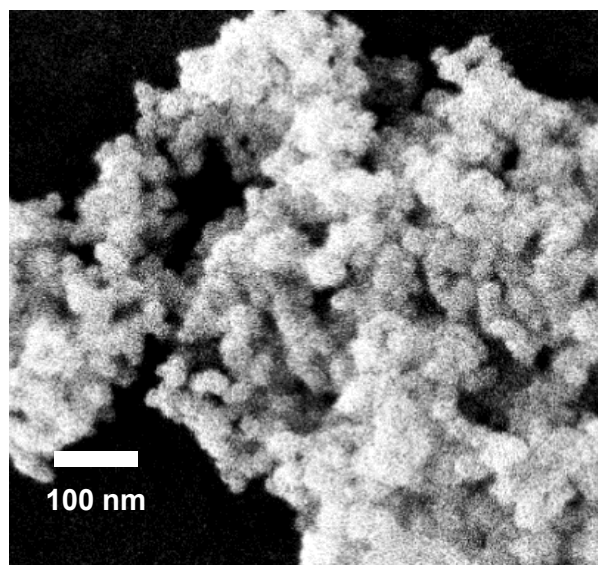
Supplementary Figure 39. SEM image of **SiO$_2$-N$_3$**.

Multi-Point BET Plot

Multi-Point BET

Relative Pressure [P/Po]	Volume @ STP [cc/g]	1 / [W((Po/P) - 1)] [1/g]	Relative Pressure [P/Po]	Volume @ STP [cc/g]	1 / [W((Po/P) - 1)] [1/g]
1.01338e-02	13.3968	6.1143e-01	1.50199e-01	31.5615	4.4807e+00
2.84681e-02	18.9325	1.2384e+00	2.01179e-01	34.7486	5.7989e+00
5.07923e-02	22.6422	1.8909e+00	2.51565e-01	37.5017	7.1713e+00
9.98853e-02	27.6609	3.2099e+00			

MBET summary

Slope =	26.734 1/g
Intercept =	4.603e-01 1/g
Correlation coefficient, r =	0.999609
C constant=	59.084
Surface Area =	128.059 m²/g

Supplementary Figure 40. Multi-point BET plot of **SiO$_2$-N$_3$**. The surface area of **SiO$_2$-N$_3$** is 128 m^2/g.
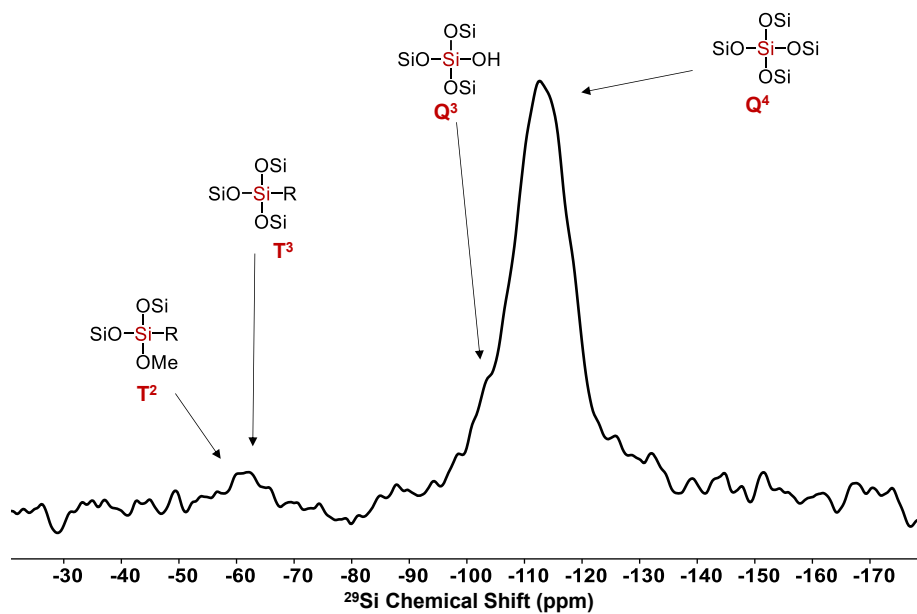
Supplementary Figure 41. Solid-state ^{29}Si NMR spectrum of **SiO₂-N₃**.
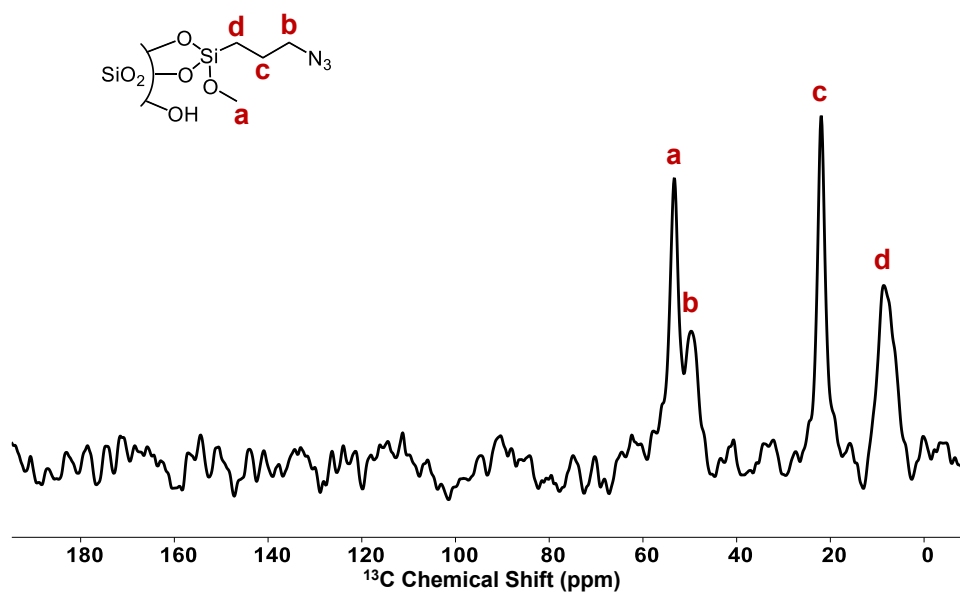
Supplementary Figure 42. Solid-state ^{13}C NMR spectrum of **SiO₂-N₃**.
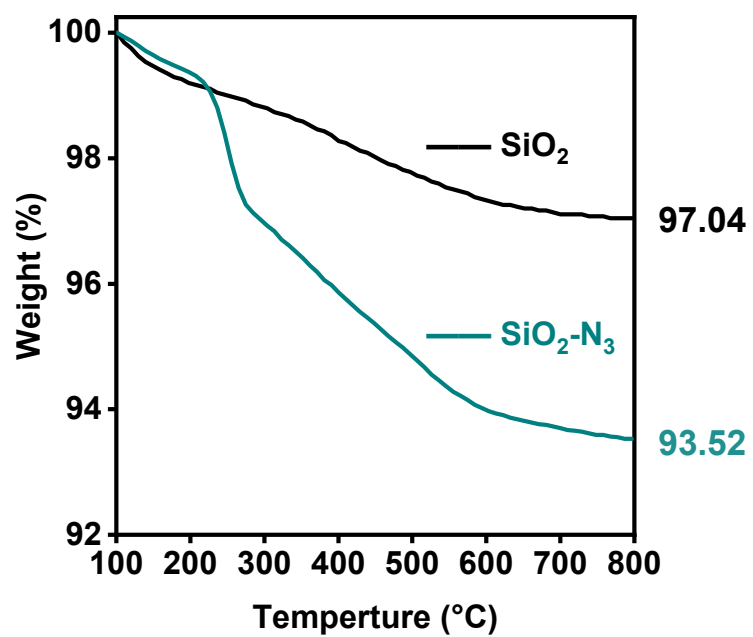
Supplementary Figure 43. TGA curves of SiO_2 and **SiO_2-N_3**. The loading of -N_3 could be calculated as 0.35 mmol/g based on the method of literature[4].
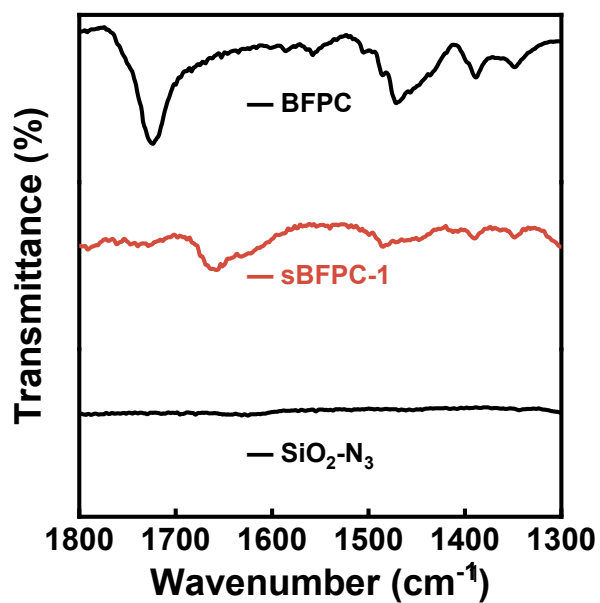
Supplementary Figure 44. ATR-FT-IR spectra of **BFPC**, **sBFPC-1** and **SiO₂-N₃**.
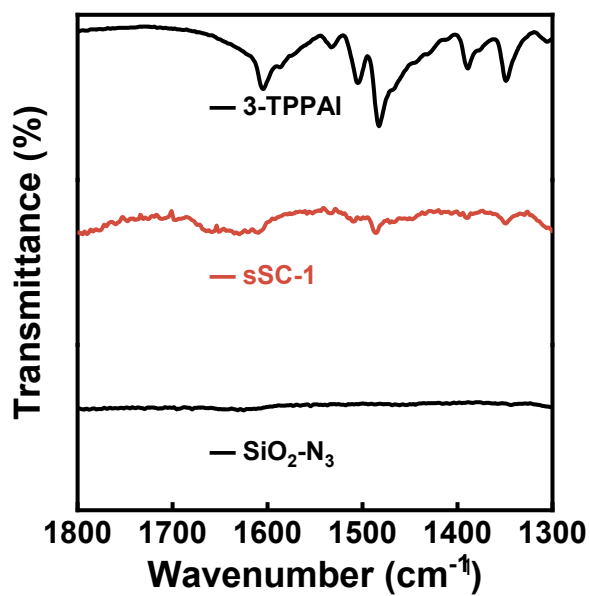
Supplementary Figure 45. ATR-FT-IR spectra of **3-TPPAI**, **sSC-1** and **SiO₂-N₃**.
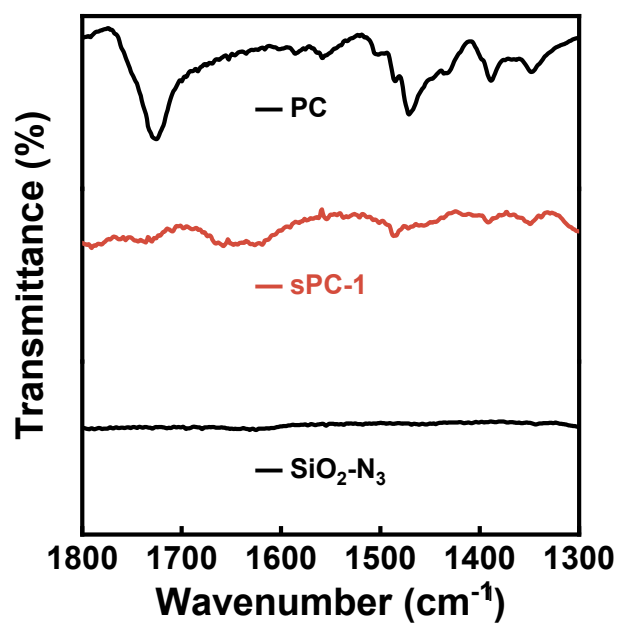
Supplementary Figure 46. ATR-FT-IR spectra of **PC**, **sPC-1** and **SiO$_2$-N$_3$**.
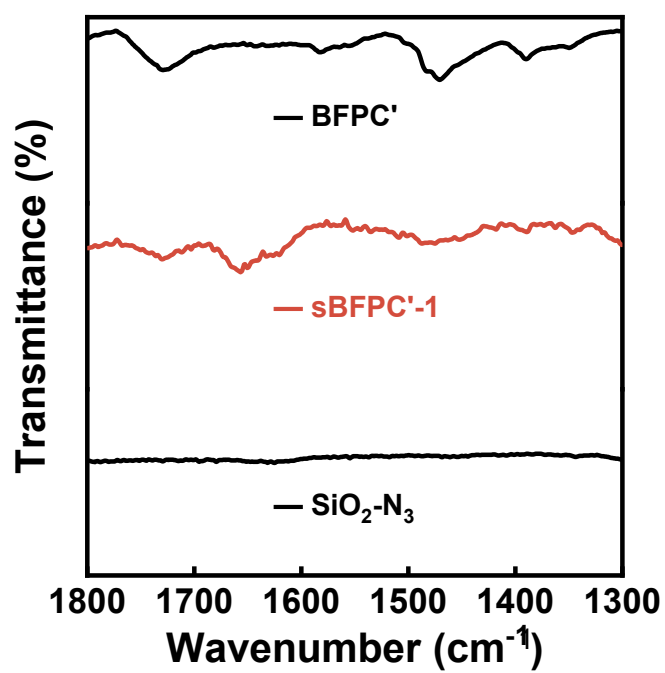
Supplementary Figure 47. ATR-FT-IR spectra of **BFPC'**, **sBFPC'-1** and **SiO$_2$-N$_3$**.
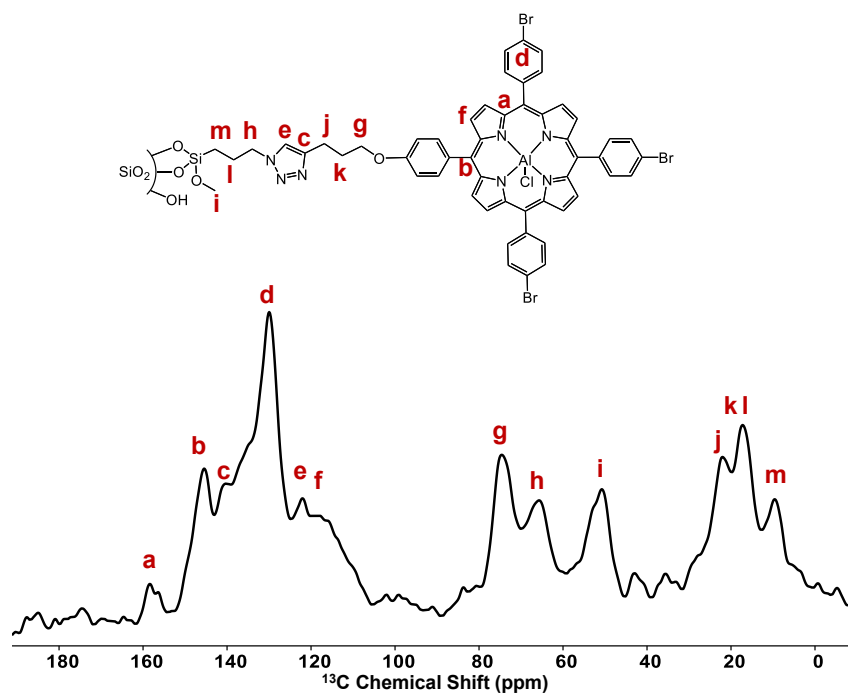
Supplementary Figure 48. Solid-state ^{13}C NMR spectrum of **sSC-1**.
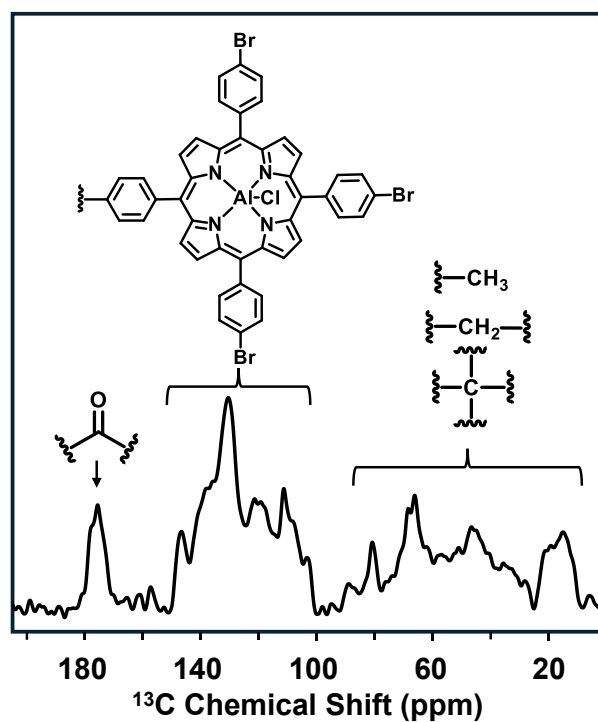
Supplementary Figure 49. Solid-state ^{13}C NMR spectrum of **sBFPC-1**.
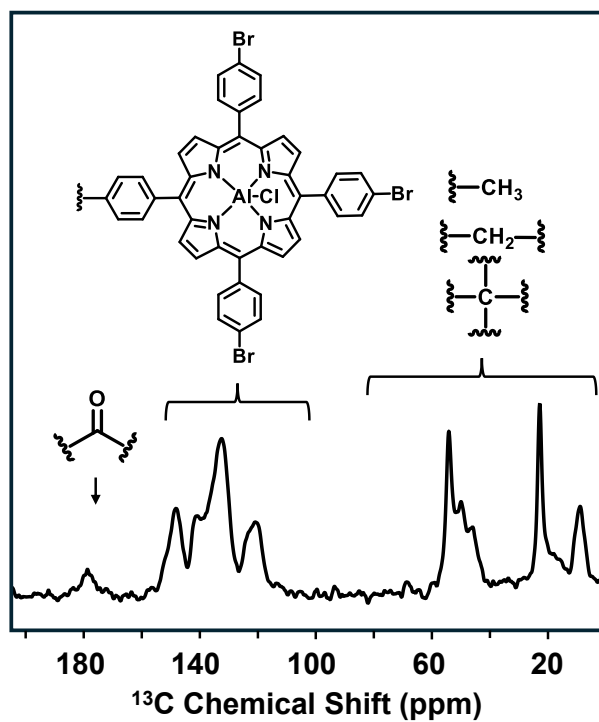
Supplementary Figure 50. Solid-state ^{13}C NMR spectrum of **sPC-1**.
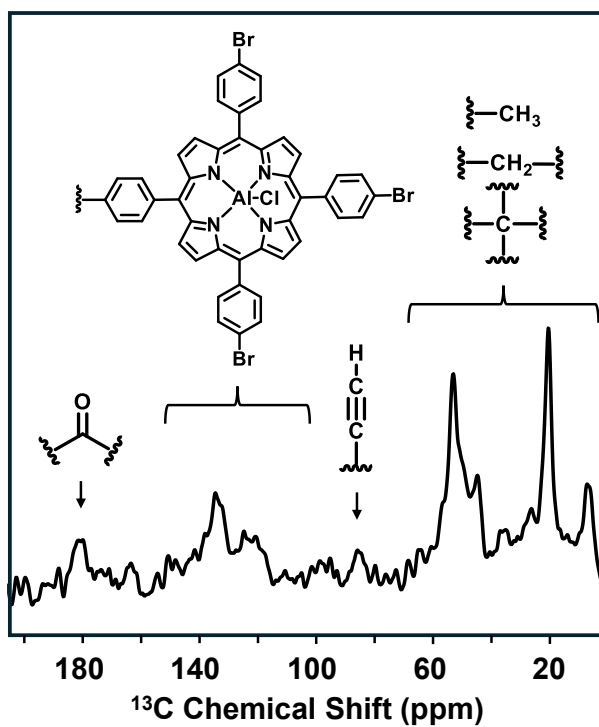
Supplementary Figure 51. Solid-state ^{13}C NMR spectrum of **sBFPC'-1**.
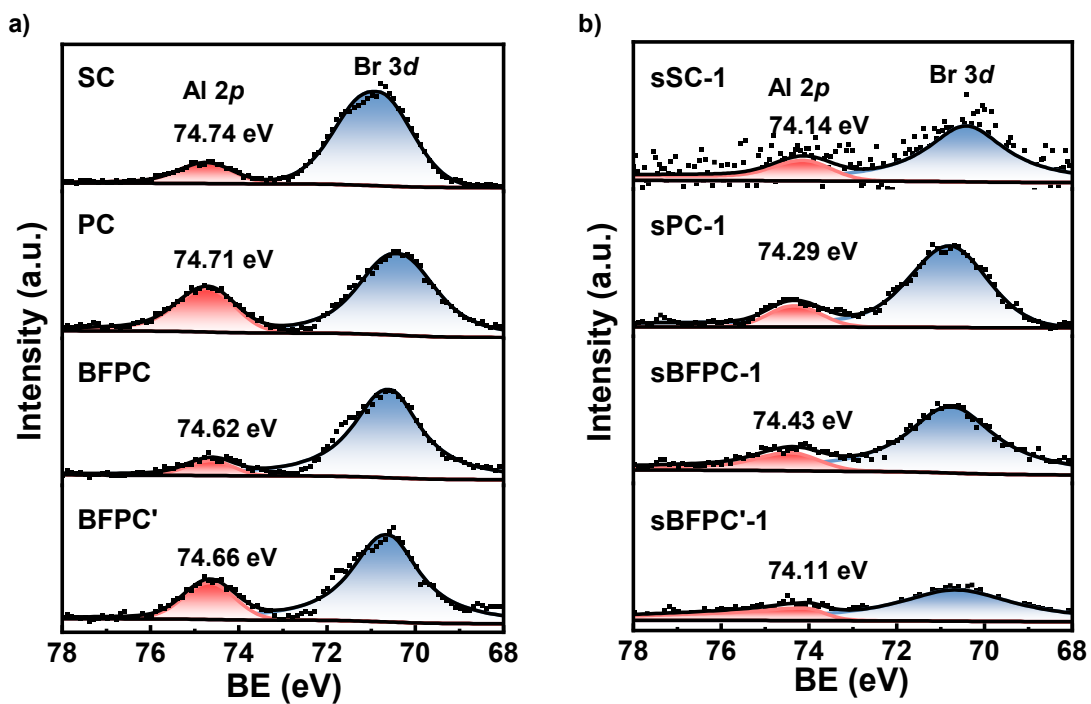
Supplementary Figure 52. a) Comparison of Al 2*p* XPS spectra of **SC** (74.74 eV), **PC** (74.71 eV), **BFPC** (74.62 eV) and **BFPC'** (74.66 eV). b) Comparison of Al 2*p* XPS spectra of **sSC-1** (74.14 eV), **sPC-1** (74.29 eV), **sBFPC-1** (74.43 eV) and **sBFPC'-1** (74.11 eV).
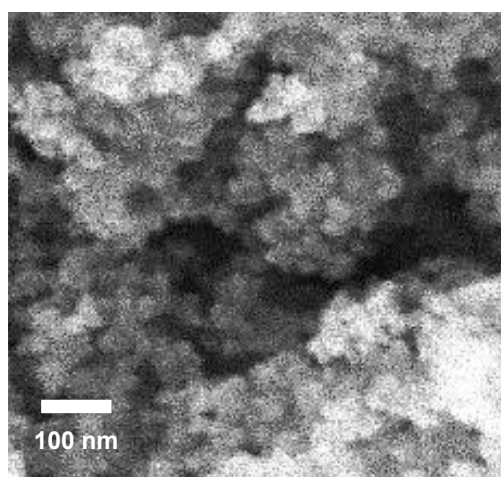
Supplementary Figure 53. SEM image of **sBFPC-1**.

Multi-Point BET Plot

Multi-Point BET

Relative Pressure [P/Po]	Volume @ STP [cc/g]	1 / [W((Po/P) - 1)] [1/g]	Relative Pressure [P/Po]	Volume @ STP [cc/g]	1 / [W((Po/P) - 1)] [1/g]
5.37986e-02	23.6345	1.9248e+00	2.01301e-01	34.4557	5.8526e+00
1.00418e-01	27.9697	3.1932e+00	2.51840e-01	36.9158	7.2957e+00
1.50848e-01	31.5653	4.5029e+00	3.01071e-01	39.6143	8.7003e+00

MBET summary

Slope =	27.303 1/g
Intercept =	4.247e-01 1/g
Correlation coefficient, r =	0.999828
C constant=	65.288
Surface Area =	125.597 m²/g

Supplementary Figure 54. Multi-point BET plot of **sBFPC-1**. The surface area of **sBFPC-1** is 126 m^2/g.
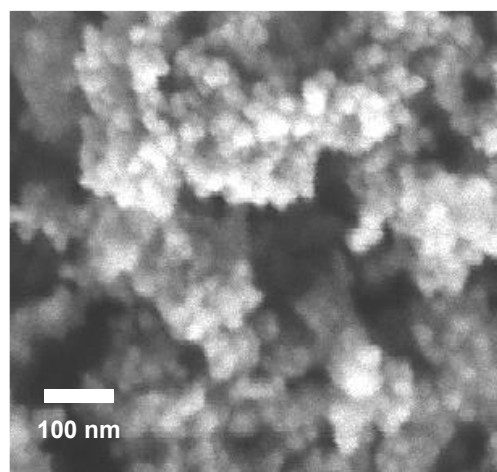
Supplementary Figure 55. SEM image of **sSC-1**.

Multi-Point BET Plot

Multi-Point BET

Relative Pressure [P/Po]	Volume @ STP [cc/g]	1 / [W((Po/P) - 1)] [1/g]	Relative Pressure [P/Po]	Volume @ STP [cc/g]	1 / [W((Po/P) - 1)] [1/g]
5.05179e-02	23.6368	1.8010e+00	2.00053e-01	34.5822	5.7860e+00
1.01717e-01	28.3179	3.1994e+00	2.50234e-01	37.2355	7.1716e+00
1.49768e-01	31.6289	4.4560e+00	3.00281e-01	39.7293	8.6426e+00

MBET summary

Slope =	27.202 1/g
Intercept =	4.042e-01 1/g
Correlation coefficient, r =	0.999815
C constant=	68.300
Surface Area =	126.152 m²/g

Supplementary Figure 56. Multi-point BET plot of **sSC-1**. The surface area of **sSC-1** is 126 m^2/g.
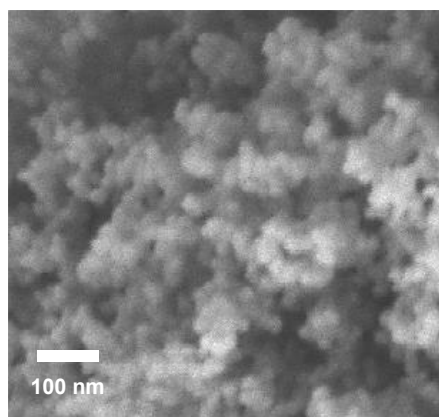
Supplementary Figure 57. SEM image of **sPC-1**.

Multi-Point BET Plot

Multi-Point BET

Relative Pressure [P/Po]	Volume @ STP [cc/g]	1 / [W((Po/P) - 1)] [1/g]	Relative Pressure [P/Po]	Volume @ STP [cc/g]	1 / [W((Po/P) - 1)] [1/g]
5.35145e-02	24.1207	1.8755e+00	2.00305e-01	35.2970	5.6778e+00
1.00313e-01	28.5158	3.1285e+00	2.51248e-01	38.0326	7.0592e+00
1.50941e-01	32.0465	4.4385e+00	3.01828e-01	40.4064	8.5605e+00

MBET summary

Slope =	26.646 1/g
Intercept =	4.242e-01 1/g
Correlation coefficient, r =	0.999659
C constant=	63.821
Surface Area =	128.650 m²/g

Supplementary Figure 58. Multi-point BET plot of **sPC-1**. The surface area of **sPC-1** is 129 m^2/g.
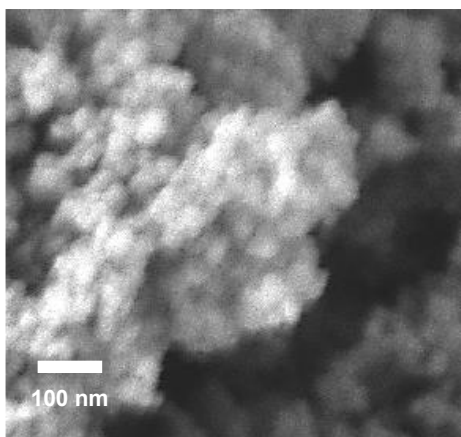
Supplementary Figure 59. SEM image of **sBFPC'-1**.

Multi-Point BET Plot

Multi-Point BET

Relative Pressure [P/Po]	Volume @ STP [cc/g]	1 / [W((Po/P) - 1)] [1/g]	Relative Pressure [P/Po]	Volume @ STP [cc/g]	1 / [W((Po/P) - 1)] [1/g]
2.43947e-02	18.3689	1.0892e+00	1.51933e-01	34.4487	4.1610e+00
5.19933e-02	23.3990	1.8754e+00	2.02059e-01	38.8576	5.2141e+00
7.82764e-02	26.8242	2.5331e+00	2.52219e-01	42.8961	6.2912e+00
1.03692e-01	29.6714	3.1196e+00			

MBET summary

Slope =	22.460 1/g
Intercept =	6.950e-01 1/g
Correlation coefficient, r =	0.998856
C constant=	33.316
Surface Area =	150.398 m²/g

Supplementary Figure 60. Multi-point BET plot of **sBFPC'-1**. The surface area of **sBFPC'-1** is 150 m^2/g.
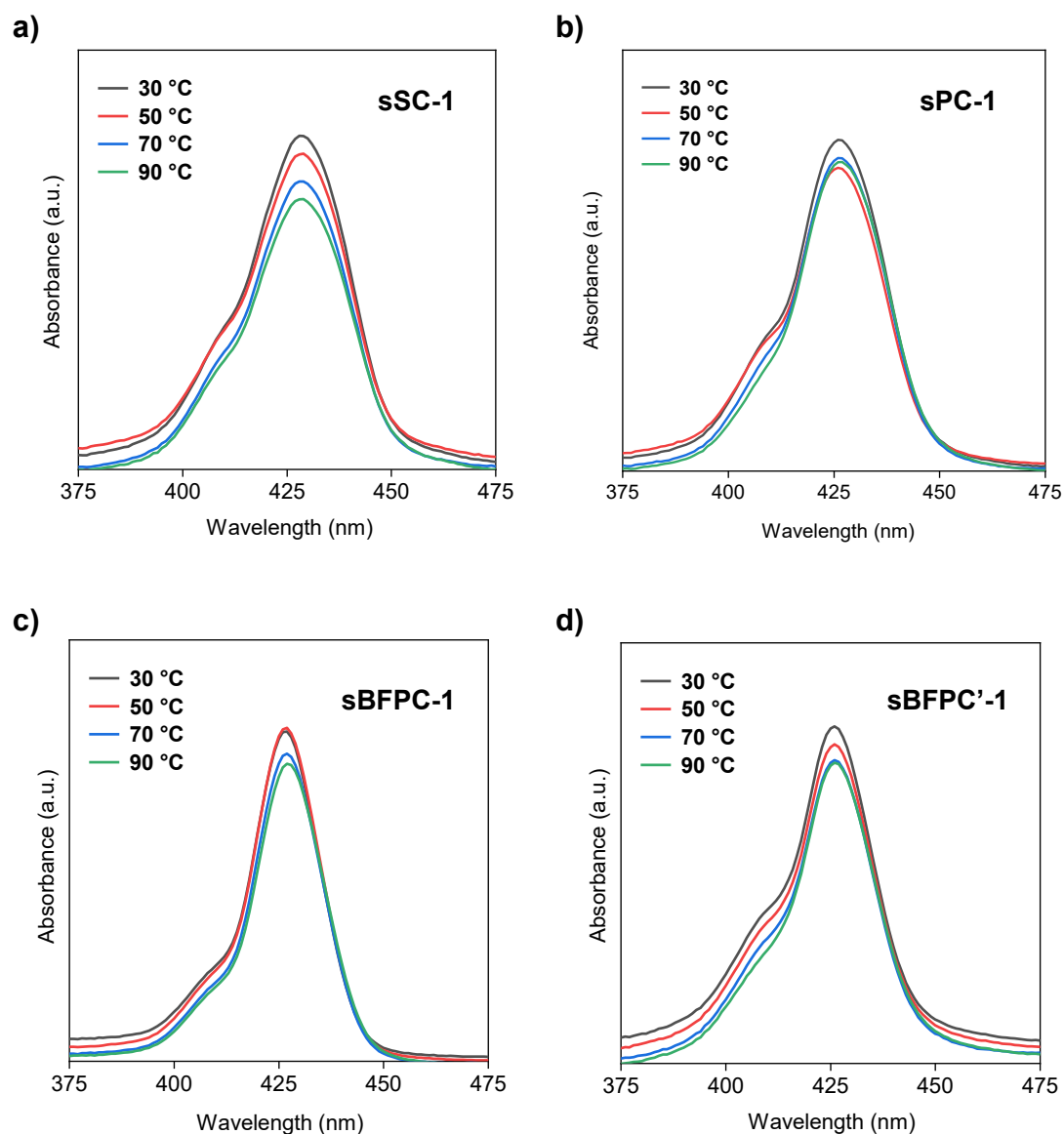
Supplementary Figure 61. The variable-temperature UV-vis absorption spectra of a) **sSC-1**, b) **sPC-1**, c) **sBFPC-1** and d) **sBFPC'-1**. The supported catalysts are dispersed in DMSO (1 mg/mL).
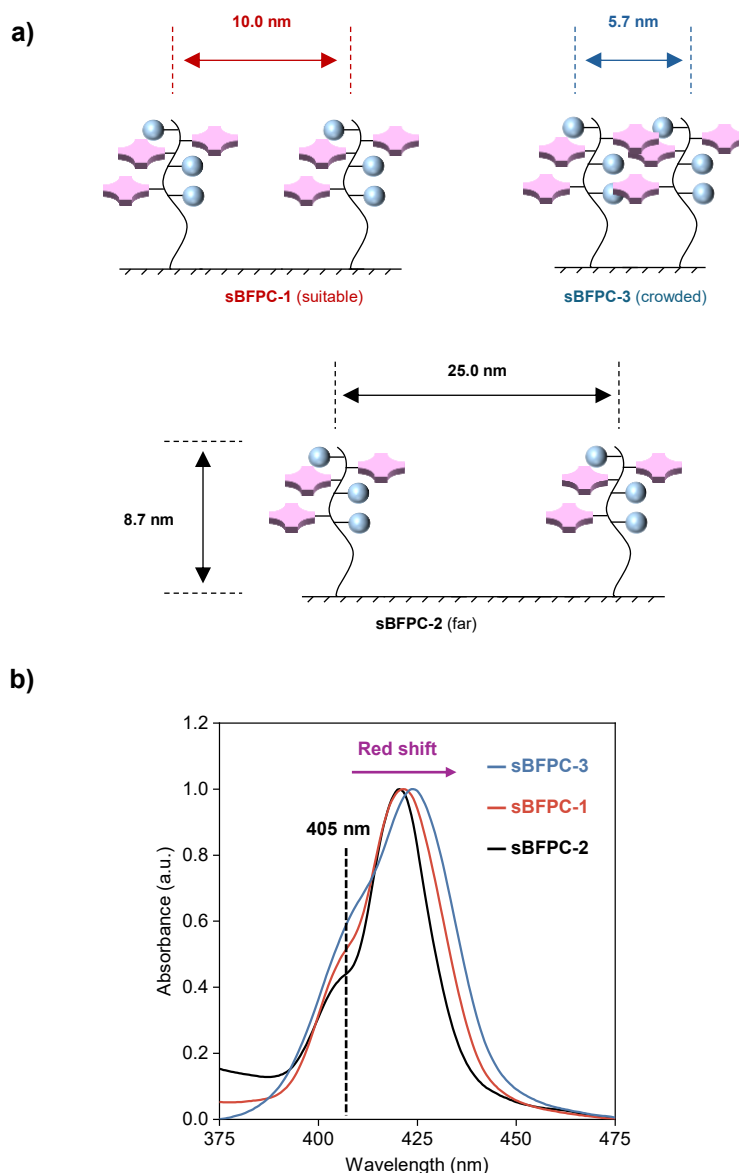
Supplementary Figure 62. a) Schematic illustration of average immobilization site distance of supported polymeric catalysts, which were calculated based on the method of previous literature[5]. b) Comparison of the UV-vis absorption spectra of **sBFPC-1**, **sBFPC-2** and **sBFPC-3**. The supported catalysts are dispersed in the mixture of CH_2Cl_2/CH_3OH (10/1, V/V) at room temperature (1 mg/mL).

General method to analyze the loading of Al-porphyrins

Plot the standard curve

A quantitative amount of freshly prepared homogeneous Al porphyrin (parental catalysts) was dispersed in an aqueous solution of tetrahydrofuran containing sodium hydroxide (0.1 mol/L) and stirred overnight at 40 °C. Subsequently, sodium chloride was added to facilitate the separation of the tetrahydrofuran from the aqueous phase. The tetrahydrofuran solution containing Al porphyrin was partitioned, and the pH of the solution was adjusted to neutral with a small amount of diluted hydrochloric acid. The mixture was transferred to a 25 mL volumetric flask, and the volume was fixed with C_2H_5OH to 25 mL to obtain a standard solution. From this standard solution, aliquots of 0.25, 0.5, 1.0, 2.0, and 3.0 mL were taken and diluted to 100 mL in separate 100 mL volumetric flasks using ethanol. The UV-vis absorption spectra of these dilutions were measured, and a standard curve was plotted

Measure the loading

A quantitative amount of supported catalyst was dispersed in an aqueous solution of tetrahydrofuran containing sodium hydroxide (0.1 mol/L) and stirred overnight at 40 °C. Subsequently, sodium chloride was added to facilitate the separation of the tetrahydrofuran from the aqueous phase. The tetrahydrofuran solution containing Al porphyrin was partitioned, and the pH of the solution was adjusted to neutral with a small amount of diluted hydrochloric acid. The supernatant was transferred to a 100 mL volumetric flask, and the volume was fixed with C_2H_5OH to 100 mL. The UV-vis absorption spectrum of the solution was recorded, and the intensity of the absorption was measured as A. The catalyst loading can be calculated from the standard curve.
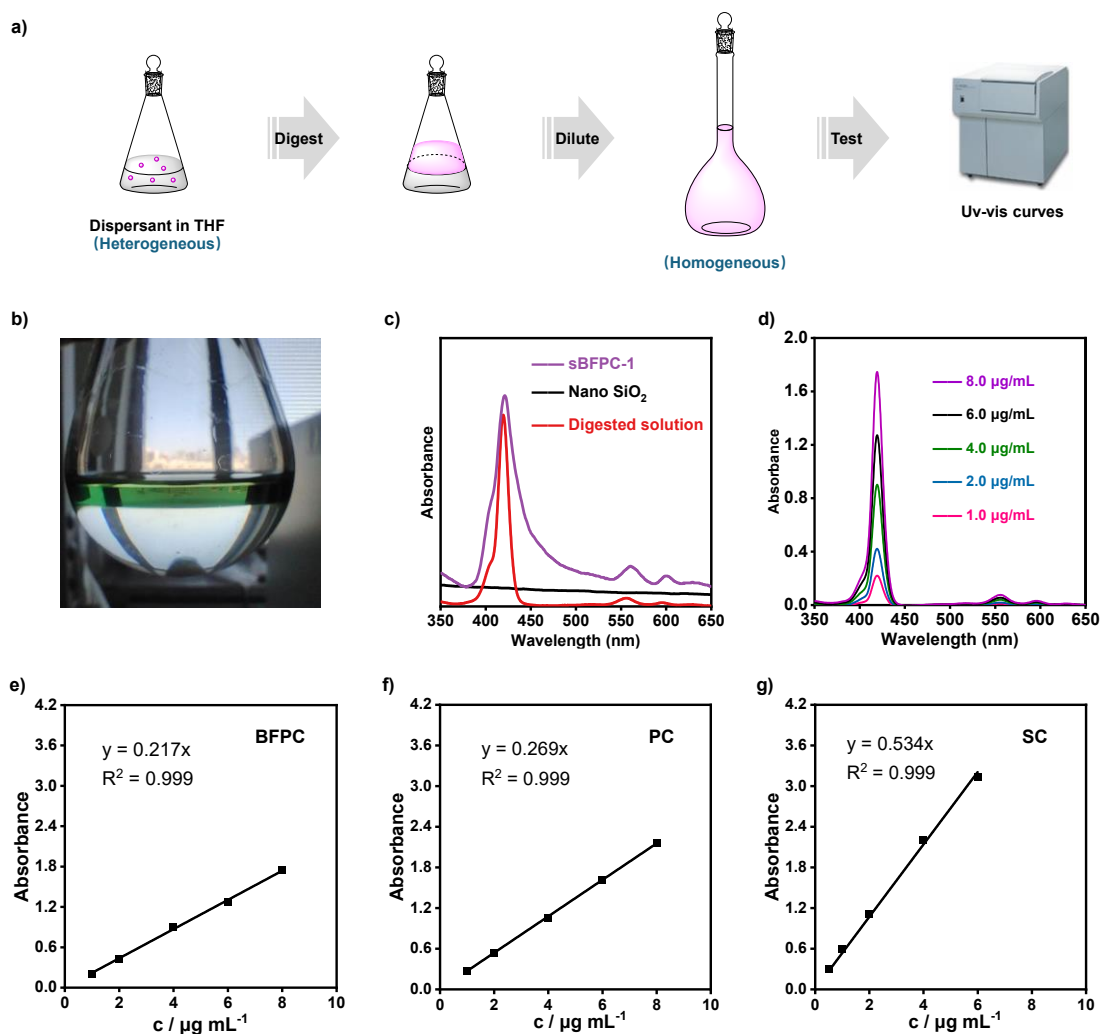
Supplementary Figure 63. a) Cartoon models of the digest operation and UV-vis test of Al porphyrin. b) The picture of digested solution of **sBFPC-1**, where the organic phase is transparent, indicating complete hydrolysis of the nanoparticle. c) UV-vis spectrums of dispersion of **sBFPC-1** (purple curve), nano SiO_2 (black curve) and digested solution (red curve). d) UV-vis spectrums of standard samples (**BFPC**) prepared by digest operation. The calibration curve of e) digested **BFPC**, f) **PC** and g) **SC** plotted by the absorbance at 422 nm.

Supplementary Scheme 7. Calculation method to determinate the loading.

The homogeneous catalyst porphyrin content : $w\% = \dfrac{M * n}{M_2} * 100\%$

The molar absorption coefficient : $\varepsilon = \dfrac{k}{w\%} * M * 1000$

The quantity of active sites: Loading $= \dfrac{A * V}{k * m * M}$

Supplementary Table 1. The unit and meaning of each symbol used to calculate the loading.

Symbol	Unit	Meaning
M	g/mol	The relative molecular mass of aluminum porphyrin
n	/	The number of aluminum porphyrin units per polymeric catalyst chain
M_2	g/mol	The molecular weight of polymeric catalyst obtained by GPC
w%	/	The homogeneous catalyst porphyrin content
k	mL/(µg*cm)	The slope of the standard curve of UV-vis spectrum
ε	L/(mol*cm)	The molar absorption coefficient of digested aluminum porphyrin
m	g	The mass of immobilized catalyst used to digest
V	mL	The volume of the volumetric bottle
A	/cm	The absorbance of diluted digest solution
Loading	µmol/g	The loading of immobilized catalyst

Supplementary Table 2. Information of homogeneous catalysts and immobilized catalysts.

Corresponding homogeneous catalyst	M_n (Đ)	n	ε	Immobilized catalyst	Loading (µmol Al/g)
BFPC	9.2 kg/mol (1.11)	6	3.3 * 10⁵	**sBFPC-2**	2.1
				sBFPC-1	13.0
				sBFPC-3	38.0
BFPC'	9.2 kg/mol (1.13)	6		**sBFPC'-1**	17.2
PC	12.1 kg/mol (1.05)	9.2	3.5 * 10⁵	**sPC-1**	15.1
SC	1.0 kg/mol	1	5.4 * 10⁵	**sSC-1**	12.3
				sSC-2	45.2
				sSC-3	95.5
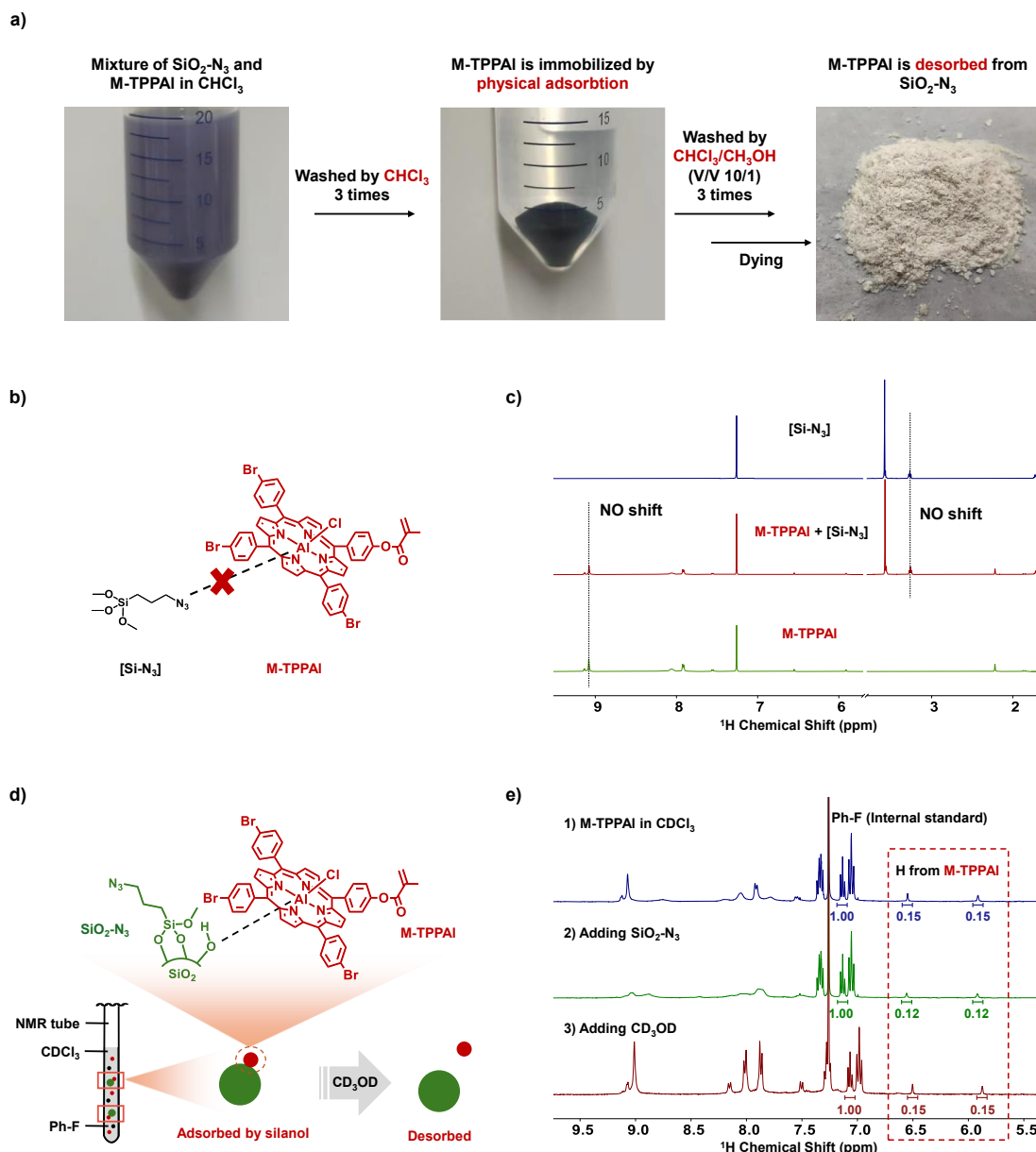
Supplementary Figure 64. a) Comparison of results for non-polar versus polar condition treatments. b) The schematic of no interaction between (3-azidopropyl)trimethoxy silane (**Si-N₃**) and **M-TPPAl**. c) ^1H NMR spectrums of **Si-N₃**, **M-TPPAl** and their mixture in CDCl₃ at 25 °C. d) Schematic of the interaction between Al porphyrin and SiO₂-N₃ regulated by solvent. e) Investigation of the state of Al porphyrin in the suspension of **SiO₂-N₃** monitored by NMR spectroscopy.

The physically adsorbed **M-TPPAl** cannot be washed out by non-polar solvents such as CHCl₃, indicating an interaction between **SiO₂-N₃** and **M-TPPAl**. Desorption of **M-TPPAl** is easily achieved when a polar organic solvent, such as CH₃OH, is used, suggesting that the interaction is unstable under polar conditions. The ^1H NMR spectrum of mixture of **Si-N₃** and **M-TPPAl** (Supplementary Fig. 64c) shows no interaction between

Si-N$_3$ and **M-TPPAl**. The result suggests that residual surface silanol is responsible for the adsorption of Al porphyrin (Supplementary Fig. 64d). In ^{1}H NMR monitoring experiments, **M-TPPAl** and fluorobenzene (Ph-F, internal standard) were dissolved in a 0.15:1 molar ratio in CDCl$_3$. After adding **SiO$_2$-N$_3$** and dispersing it by sonication, ^{1}H NMR revealed a reduction in the signal of **M-TPPAl** from 15% to 12% of the internal standard, accompanied by a blurring of the peak split (9.5-7.5 ppm). This observation indicates partial adsorption of Al porphyrin onto silica in non-polar solvents, which restricts the mobility of molecular catalyst. Upon adding a drop of CD$_3$OD (a polar solvent) to the dispersion, the peak of **M-TPPAl** reverted to 15%, with sharpened peak splitting, indicating desorption due to the solvent's polarity. Therefore, polar conditions are favorable for the conformational stretching of supported catalyst chain.

Basic principles of solvent relaxation nuclear magnetic resonance

Supplementary Scheme 8. The basic principles of solvent relaxation NMR

Substrate
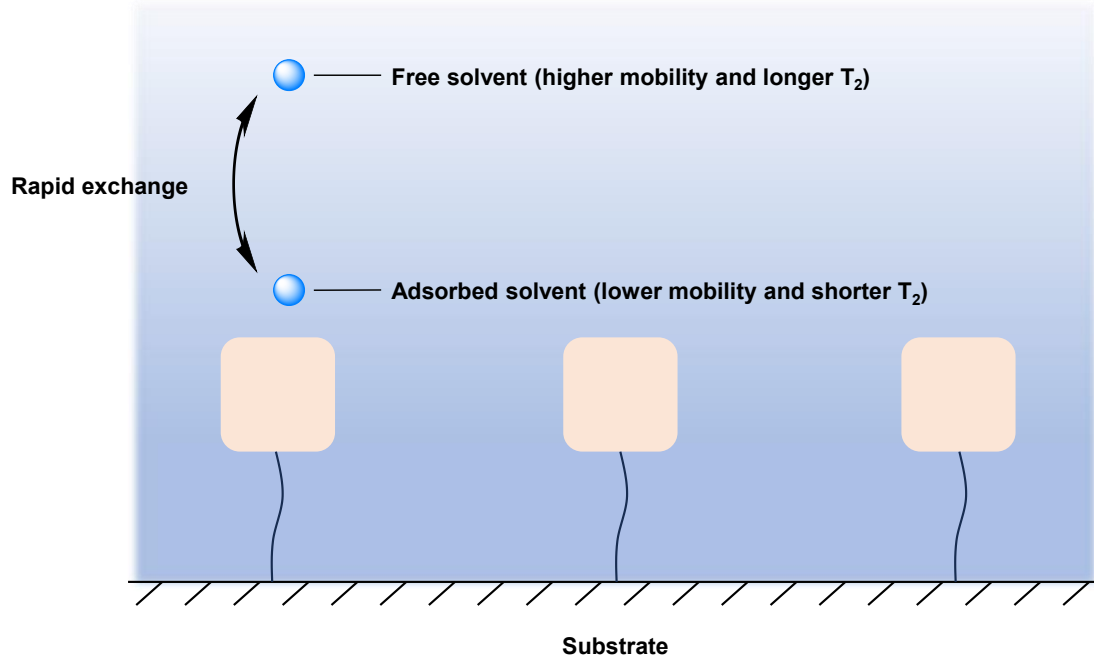
In a simple suspension system, solvent molecules exist in two environments: in the bulk solution (free) and at the particle surface (absorbed) [6]. Protons within solvent molecules in bulk solution have a longer relaxation time (T_{2f}) than those at the surface (T_{2b}), due to their faster mobility and differing magnetic interactions[7]. Although the solvent molecules display distinct relaxation behaviors within the suspension system, a single-exponential magnetization can be obtained because of a rapid exchange between these molecules. The T_2 relaxation NMR test provides the echo height $M(t)$ as a function of time t, which can be expressed as eq (1). The dynamically averaged relaxation rate of the system is related to the fraction of solvent molecules in each state, as described by eq (2).

$$M(t) = M(0)e^{(-t/T_2)} \quad (1)$$

$$\frac{1}{T_2} = \frac{1-p_b}{T_{2f}} + \frac{p_b}{T_{2b}} \quad (2)$$

where T_2 is the observed relaxation time and p_b is the fraction of protons in the bound environment. It is convenient to define relaxation rate R_2, R_{2f}, R_{2b} as $1/T_2$, $1/T_{2f}$, $1/T_{2b}$, respectively. Thus, the average relaxation rate can be described by eq (3).

$$R_2 = (1 - p_b)R_{2f} + p_b R_{2b} \quad (3)$$

For the specific suspension, the specific relaxation rate constant, R_{sp}, describes the relaxation rate with respect to the pure solvent (R_{2f}) and can be calculated using eq (4).

$$R_{sp} = \frac{R_2}{R_{2f}} - 1 \qquad (4)$$

R_{sp} can also be given as eq (5) from eq (3) and eq (4):

$$R_{sp} = (\frac{R_b}{R_{2f}} - 1)p_b \qquad (5)$$

For the supported catalysts tested in this work, the volume fraction times the specific surface area ($V_{solid} \cdot V_{liquid}^{-1} \cdot S_{BET}$) is similar across the sample, which can be considered the same p_b[8]. Consequently, an increase in R_{sp} implies that the system is relaxing more efficiently, indicating lower solvent mobility at the surface.

Previous work of preparation of CO$_2$-polyols synthesized by PO and CO$_2$.

Utilizing carbon dioxide (CO$_2$) to prepare high-value products is advantageous for both academic and industrial communities[9-11]. One effective route is the ring-opening copolymerization (ROCOP) of CO$_2$ and epoxides to yield polycarbonates[12-14], a process first reported by Inoue and co-workers[15]. Propylene oxide (PO), an inexpensive commodity epoxide, is particularly attractive epoxide for producing high-molar-mass polymers and low-molar-mass CO$_2$-derived polyols. While outstanding progress has been achieved in synthesizing high-molar-mass polymers[16-20], research on the preparation of low-molar-mass CO$_2$-polyols has advanced more slowly. These polyols typically consist of two or more hydroxyl end-capped polypropylene carbonate (PPC) or polyether carbonate (PEC) (Supplementary Scheme 9). Compared to the high carbonate unit content of PPC polyols (CU% ≥ 99%), the coexisting carbonate/ether structure in PEC polyols provides the advantages of both polyester and polyether polyols, including lower glass transition temperatures and viscosities, making them suitable for use in polyurethane applications[21].

Supplementary Scheme 9. Synthesis of CO$_2$-polyols prepared by RD-ROCOP of PO/CO$_2$.
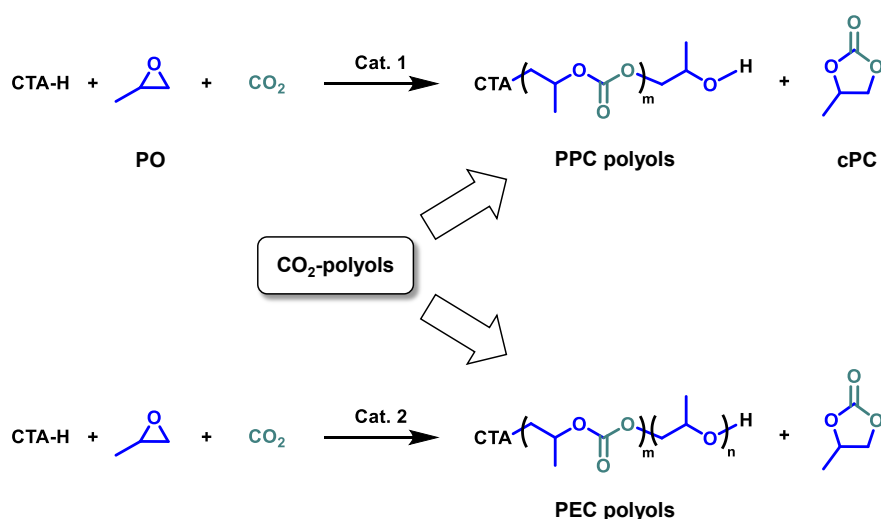
The most effective method for preparing CO$_2$-polyols is telomerization of PO and CO$_2$ through the addition of protic chain transfer agent (CTA), such as carboxylic acids, alcohols, or phenols[22-24]. In reversible-deactivation ring-opening copolymerization (RD-ROCOP), rapid and reversible proton transfer occurs between dormant and active chains,

allowing for the tailoring of polymer molar mass by varying CTA loadings[23]. However, the catalytic performance generally declines significantly at high CTA loadings due to two main factors: 1) reduced activation of the monomer 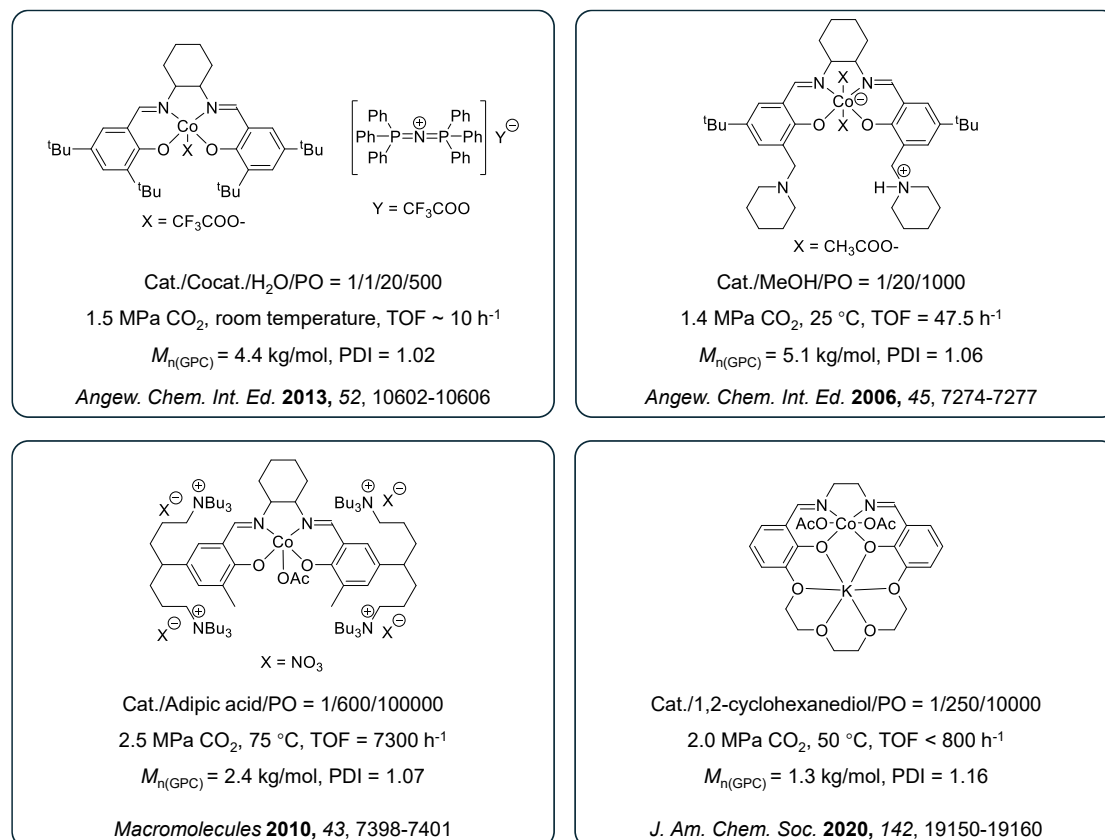resulting from the competitive coordination of CTA to the Lewis acid, and 2) decreased nucleophilicity of the anionic chain ends due to hydrogen bonding with the CTA[25]. Specifically, it is challenging to produce ultra-low molecular weight (ULMW, < 1000 g/mol) CO_2-polyols under high CTA loadings, which are essential soft segments for the production of polyurethane foams[26]. In other words, proton tolerance is a critical factor to consider in RD-ROCOP. To compare the proton tolerance of different catalytic systems, a parameter 'p' was defined as the maximum molar ratio of active protons to catalyst at which the catalyst remains effective. Numerous studies have demonstrated that the synergistic effect is significant in enhancing proton tolerance (Supplementary Schemes 10-11), where active sites collaborate to catalyze various reaction steps[27, 28]. The binary catalytic system, characterized by synergy between two molecules, suffers from low activity and requires high catalyst loading to prepare polyols, usually used with low CTA loading ($p < 40$) [29, 30]. To overcome the limitations, Nozaki and co-workers, along with many others, developed a strategy for constructing bifunctional catalysts, in which the catalyst and cocatalyst are covalently bonded[17, 31-33]. This innovation, benefiting from intramolecular synergy, has led to a remarkable improvement in catalytic performance in terms of activity, selectivity, and proton tolerance (p: 100~1200)[34-36]. The intramolecular synergy endows bifunctional catalysts with resilience against inhibition pathways caused by alcohol chains[25]. Simultaneously, a series of dinuclear complexes exhibiting intermetallic synergy have been developed and can function without any cocatalyst[37-39]. Recently, our group introduced multisite intramolecular synergy into catalytic design, achieving p of 16666[40, 41]. However, the aforementioned catalysts displayed decreasing activity with increasing CTA equivalents at very dilute concentrations. Additionally, the difficulty in separating catalysts from products results in high costs, toxic residues, color issues, and premature polymer degradation. Although evidence suggests that synergistic effects exist on the surfaces of heterogeneous catalysts, such as double metal cyanide complexes (DMCC) and zinc glutarate catalysts[42-44], they are less controllable in terms of selectivity and

molecular weight distribution. Merrifield resin has also been reported to load catalysts for better control over molecular weight[45]; however, the activity remains low (TOF ~ 500 h^{-1} at 70 °C). It continues to be a challenge to construct a separable catalytic system that exhibits high activity, controllability, and proton tolerance for the synthesis of CO_2-polyols

Supplementary Scheme 10. Previous work of preparation of polypropylene carbonate (PPC) polyols.

$X = CF_3COO-$

$Y = CF_3COO$

Cat./Cocat./H$_2$O/PO = 1/1/20/500

1.5 MPa CO_2, room temperature, TOF ~ 10 h^{-1}

$M_{n(GPC)}$ = 4.4 kg/mol, PDI = 1.02

Angew. Chem. Int. Ed. **2013**, *52*, 10602-10606

$X = CH_3COO-$

Cat./MeOH/PO = 1/20/1000

1.4 MPa CO_2, 25 °C, TOF = 47.5 h^{-1}

$M_{n(GPC)}$ = 5.1 kg/mol, PDI = 1.06

Angew. Chem. Int. Ed. **2006**, *45*, 7274-7277

$X = NO_3$

Cat./Adipic acid/PO = 1/600/100000

2.5 MPa CO_2, 75 °C, TOF = 7300 h^{-1}

$M_{n(GPC)}$ = 2.4 kg/mol, PDI = 1.07

Macromolecules **2010**, *43*, 7398-7401

Cat./1,2-cyclohexanediol/PO = 1/250/10000

2.0 MPa CO_2, 50 °C, TOF < 800 h^{-1}

$M_{n(GPC)}$ = 1.3 kg/mol, PDI = 1.16

J. Am. Chem. Soc. **2020**, *142*, 19150-19160

Supplementary Scheme 11. Previous work of preparation of polyether carbonate (PEC) polyols.
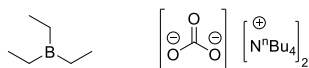
Et$_3$B/*Tertra*-butylammonium carbonate/PO = 2.8/1/10

1.0 MPa CO$_2$, 40 °C, TOF ~ 3 h^{-1}

CU% = 90%, $M_{n(GPC)}$ = 1.1 kg/mol, PDI = 1.4

Macromolecules **2019**, *52*, 2431-2438
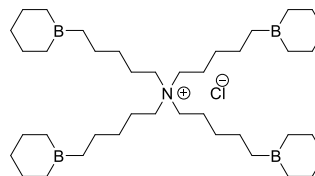
Cat./1,4-benzenedimethanol/PO = 1/100/20000

1.0 MPa CO$_2$, 70 °C, TOF = 870 h^{-1}

CU% = 45%, $M_{n(GPC)}$ = 6.9 kg/mol, PDI = 1.09

Macromolecules **2023**, *56*, 892-898
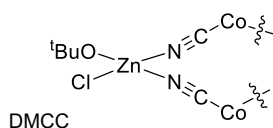
DMCC

Sebacic acid/PO = 1/15.1

4.0 MPa CO$_2$, 80 °C, 5 h

Productivity = 2.4 kg/g catalyst

CU% = 42%, $M_{n(GPC)}$ = 1.2 kg/mol, PDI = 1.21

J. Polym. Sci., Part A: Polym. Chem. **2012**, *50*, 5177-5184
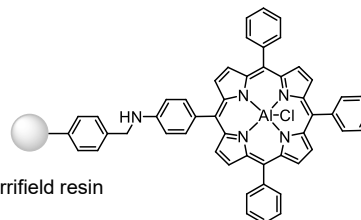
Merrifield resin

Cat./Sebacic acid/PO = 1/8000/40000

3.0 MPa CO$_2$, 70 °C, TOF ~ 500 h^{-1}

CU% = 31%, $M_{n(GPC)}$ = 0.6 kg/mol, PDI = 1.00

Angew. Chem. Int. Ed. **2023**, *62*, e202305186
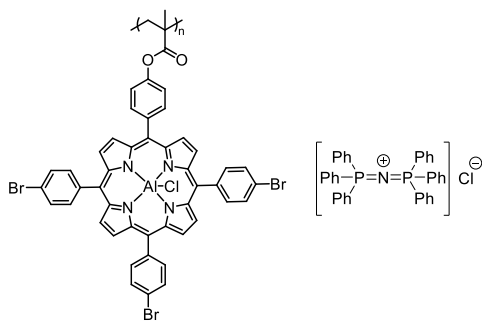
Cat./Cocat./Sebacic acid/PO = 1/1/8333/50000

6.0 MPa CO$_2$, 60 °C, TOF = 1580 h^{-1}

CU% = 37%, $M_{n(GPC)}$ = 0.5 kg/mol, PDI = 1.06

Chin. Chem. Lett. **2023**, *34*, 108011

Calculation method of polymerization results
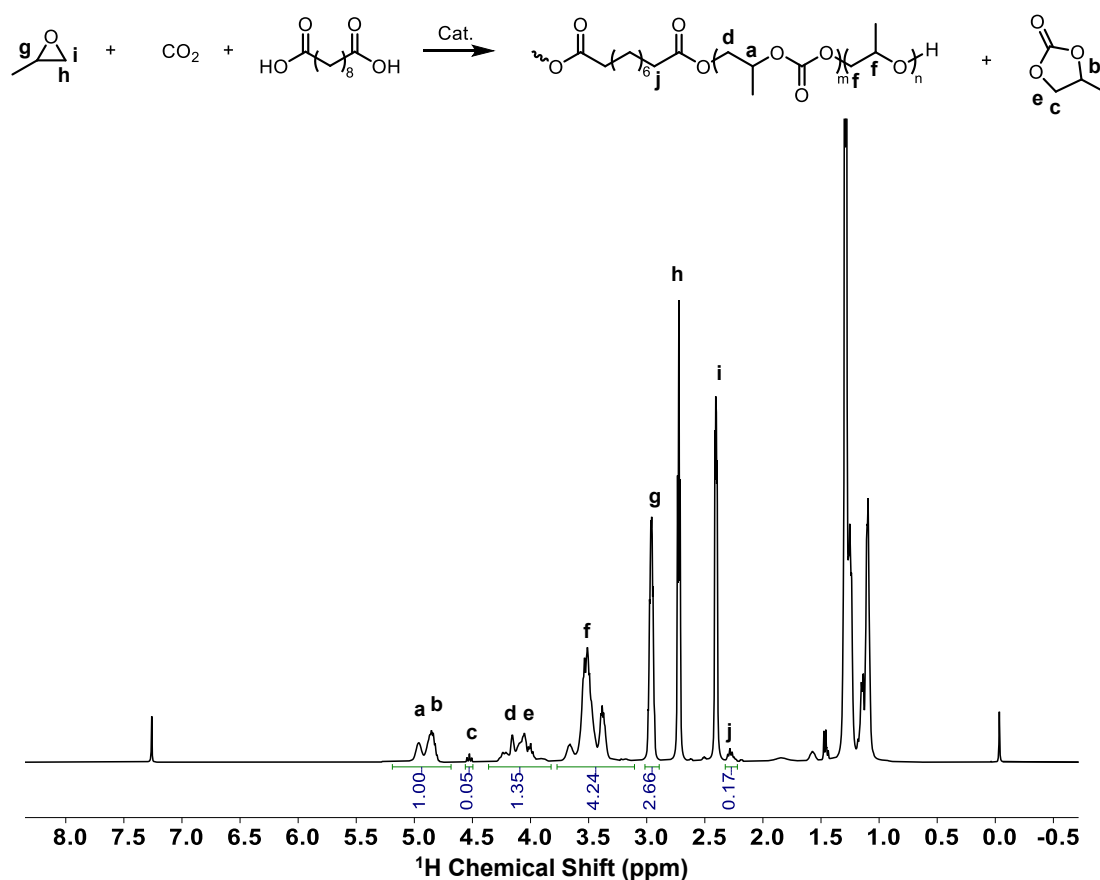
Supplementary Figure 65. Crude ^1H NMR spectrum of CO_2-polyol using sebacic acid as chain transfer agent (entry 2, Supplementary Table 3).

Calculation methods for determination of PO conversion, polymer selectivity, carbonate unit and the theoretical molecular weight of obtained polymers:

$$Conversion = \frac{A_{5.1-4.7}+A_{4.5}+A_{4.3-3.9}+A_{3.7-3.3}}{A_{5.1-4.7}+A_{4.5}+A_{4.3-3.9}+A_{3.7-3.3}+3\times A_{2.9}}\times 100\%$$

$$Polymer\ selectivity = \frac{102\times(A_{5.1-4.7}-2\times A_{4.5}+A_{4.3-3.9})+58\times A_{3.7-3.3}}{102\times(A_{5.1-4.7}+A_{4.5}+A_{4.3-3.9})+58\times A_{3.7-3.3}}\times 100\%$$

$$Carbonate\ unit = \frac{A_{5.1-4.7}-2\times A_{4.5}+A_{4.3-3.9}}{A_{5.1-4.7}-2\times A_{4.5}+A_{4.3-3.9}+A_{3.7-3.3}}\times 100\%$$

$$M_n^{theo.} = M_{CTA} + \frac{[PO]\times Conversion\times Polymer\ selectivity\times[102\times CU+58\times(1-CU)]}{[CTA]}$$

Calculation methods for determination of TOF and productivity of catalysts:

$$TOF = \frac{[PO] \times Conversion}{[Al] \times Time}$$

$$Productivity = \frac{m_{polyol}}{m_{TPPAl}}$$

$$= \frac{[CTA] \times M_{CTA} + [PO] \times Conversion \times Polymer\ selectivity \times [102 \times CU + 58 \times (1 - CU)]}{[Al] \times M_{TPPAl}}$$

Results of Telomerization of PO/CO$_2$

Supplementary Table 3. Optimization of conditions for telomerization of PO/CO$_2$ in the presence of SA. [a]

Entry	Cat.	[Al]/SA/M$_0$[b]	p[c]	T (°C)	P (MPa)	Conv. (%)[d]	TOF (h^{-1})[e]	Polymer (%)[f]	CU (%)[g]	$M_n^{theo.}$ (kg/mol)[h]	M_n^{GPC} (kg/mol)[i]	$Đ$[i]	Productivity (kg/g)[j]
1	**sBFPC-1**	1/2000/200000	4*10^3	50	3	13	722	>99	38	1.1	1.2	1.07	2.5
2	**sBFPC-1**	1/2000/200000	4*10^3	70	3	45	2500	97	35	3.4	2.7	1.06	7.2
3	**sBFPC-1**	1/2000/200000	4*10^3	90	3	56	3111	88	35	3.8	2.8	1.06	8.1
4	**sBFPC-1**	1/2000/200000	4*10^3	70	1	34	1880	85	27	2.2	1.8	1.38	4.7
5	**sBFPC-1**	1/2000/200000	4*10^3	70	5	40	2236	95	42	3.1	3.0	1.18	6.6
6	**sBFPC-1**	1/0/200000	0	70	3	37	2070	91	34	5400.0	66.5	1.52	5.4

[a] The polymerization reactions were carried out in neat 4 mL PO in the presence of SA for 36 h. [b] The feed molar ratio. [c] p was the molar ratio of active proton to catalyst (p = [H]/[Al]). [d] Conversion of PO, determined by ^{1}H NMR analysis of crude reaction mixture. [e] Turnover frequency (TOF) = number of moles of PO consumed/(number of moles [Al]*time). [f] Weight percentage of polyols over cPC. [g] The content of carbonate units in polyols determined by ^{1}H NMR. [h] Theoretical molecular weight of the polyols calculated according to the conversion of PO, selectivity and CU content. [i] The molecular weight and polymer dispersity index determined by gel permeation chromatography (GPC) in THF at 25 °C, calibrated with polystyrene standards. [j] Kilogram polyol per gram Al porphyrin, calculated by $m_{polyol}/m_{Al\ porphyrin}$.

Supplementary Table 4. Telomerization of PO/CO_2 in the presence of SA catalyzed by different supported catalysts. [a]

Entry	Cat.	[Al]/PPNCl/SA/M_0[b]	p[c]	Conv. (%)[d]	TOF (h^{-1})[e]	Polymer (%)[f]	CU (%)[g]	$M_n^{theo.}$ (kg/mol)[h]	M_n^{GPC} (kg/mol)[i]	Đ[i]	Productivity (kg/g)[j]
1	**sBFPC-1**	1/0/2000/200000	$4*10^3$	45	2500	97	35	3.4	2.7	1.06	7.2
2	**sSC-1**	1/0/2000/200000	$4*10^3$	2	111	94	26	0.3	-	-	0.3
3	**sPC-1**	1/0/2000/200000	$4*10^3$	18	1000	98	24	1.4	1.0	1.62	3.0
4	**sBFPC'-1**	1/0/2000/200000	$4*10^3$	21	1160	95	36	1.7	0.9	1.23	3.5
5	**sSC-1**	1/1/2000/200000	$4*10^3$	5	256	96	67	0.6	-	-	1.3
6	**sPC-1**	1/1/2000/200000	$4*10^3$	39	2141	88	36	2.7	2.0	1.05	5.8
7	**sBFPC-2**	1/0/2000/200000	$4*10^3$	17	944	87	33	1.3	1.5	1.31	2.7
8	**sBFPC-3**	1/0/2000/200000	$4*10^3$	34	1889	92	38	2.7	2.4	1.05	5.4
9	**SiO_2-N_3**	0/0/2000/200000	-	<1	-	-	-	-	-	-	-

[a] The polymerization reactions were carried out in neat 4 mL PO under CO_2 pressure of 3 MPa at 70 °C in the presence of SA for 36 h. [b] The feed molar ratio. [c] p was the molar ratio of active proton to catalyst (p = [H]/[Al]). [d] Conversion of PO, determined by ^{1}H NMR analysis of crude reaction mixture. [e] Turnover frequency (TOF) = number of moles of PO consumed/(number of moles [Al]*time). [f] Weight percentage of polyols over cPC. [g] The content of carbonate units in polyols determined by ^{1}H NMR. [h] Theoretical molecular weight of the polyols calculated according to the conversion of PO, selectivity and CU content. [i] The molecular weight and polymer dispersity index determined by gel permeation chromatography (GPC) in THF at 25 °C, calibrated with polystyrene standards. [j] Kilogram polyol per gram Al porphyrin, calculated by $m_{polyol}/m_{Al\ porphyrin}$.

Supplementary Figure 66. GPC curves of CO_2-polyols made by different supported catalysts (entries 1, 3, 4 Supplementary Table 4; entry 1, Supplementary Table 5).

Supplementary Table 5. Performance comparison of different supported single-site Al porphyrin catalysts with different loadings and linker lengths. [a]

sSC-1 (12.3 µmol Al/g)

sSC-2 (45.2 µmol Al/g)

sSC-3 (95.5 µmol Al/g)

sSC-4 (48.4 µmol Al/g)

sSC-5 (45.1 µmol Al/g)

sSC-6 (45.6 µmol Al/g)

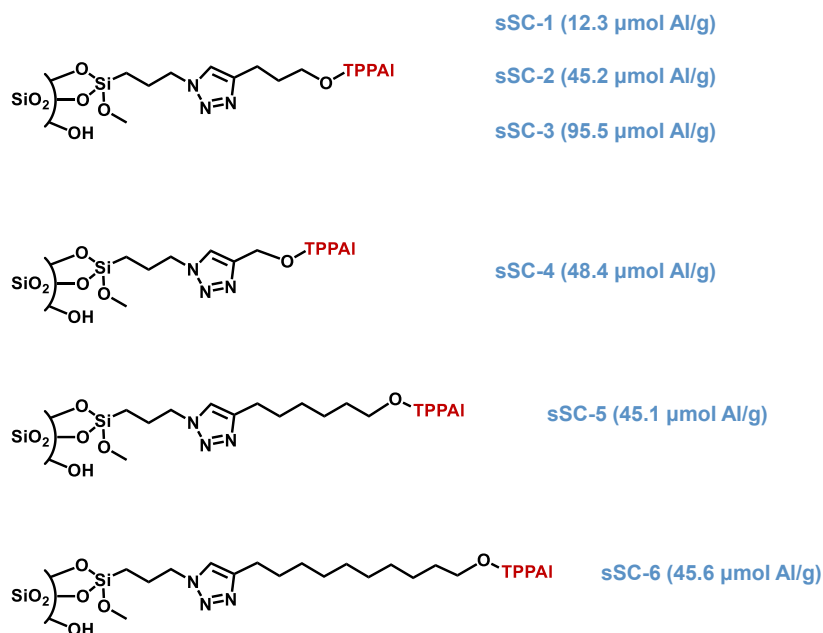| Entry	Cat.	[Al]/PPNCl/SA/M_0[b]	p[c]	t (h)	Conv. (%)[d]	TOF (h^{-1})[e]	Polymer (%)[f]	CU (%)[g]	$M_n^{theo.}$ (kg/mol)[h]	M_n^{GPC} (kg/mol)[i]	$Ð$[i]	Productivity (kg/g)[j]
1	sSC-1	1/0/100/10000	200	24	34	140	96	26	2.5	1.8	2.22	0.26
2	sSC-1	1/1/100/10000	200	24	59	246	84	30	4.4	2.8	1.74	0.39
3	sSC-2	1/0/100/10000	200	24	51	211	95	28	3.6	1.9	1.71	0.38
4	sSC-3	1/0/100/10000	200	24	46	191	97	29	3.4	1.6	2.54	0.36
5	sSC-4	1/0/100/10000	200	24	46	193	93	22	3.3	2.0	2.00	0.33
6	sSC-5	1/0/100/10000	200	24	42	173	94	25	3.1	2.0	1.82	0.31
7	sSC-6	1/0/100/10000	200	24	55	230	91	32	2.6	1.6	1.46	0.40

[a] The polymerization reactions were carried out in neat 4 mL PO under CO_2 pressure of 3 MPa at 70 °C in the presence of CTA. [b] The feed molar ratio. [c] p was the molar ratio of active proton to catalyst (p = [H]/[Al]). [d] Conversion of PO, determined by ^{1}H NMR analysis of crude reaction mixture. [e] Turnover frequency (TOF) = number of moles of PO consumed/(number of moles [Al]*time). [f] Weight percentage of polyols over cPC. [g] The content of carbonate units in polyols determined by ^{1}H NMR. [h] Theoretical molecular weight of the polyols calculated according to the conversion of PO, selectivity and CU content. [i] The molecular weight and polymer dispersity index determined by gel permeation chromatography (GPC) in THF at 25 °C, calibrated with polystyrene standards. [j] Kilogram polyol per gram Al porphyrin, calculated by $m_{polyol}/m_{Al\ porphyrin}$.

Supplementary Table 6. Comparison of performance of **BFPC** and **sBFPC-1** at different ratio of SA. [a]

Entry	Cat.	[Al]/SA/M_0[b]	p[c]	t (h)	Conv. (%)[d]	TOF (h^{-1})[e]	Polymer (%)[f]	CU (%)[g]	$M_n^{theo.}$ (kg/mol)[h]	M_n^{GPC} (kg/mol)[i]	Đ[i]	Productivity (kg/g)[j]
1[L]	BFPC	1/2000/200000	$4*10^3$	36	50	2789	94	41	3.8	4.5	1.04	8.0
2	sBFPC-1	1/2000/200000	$4*10^3$	36	45	2500	97	35	3.4	2.7	1.06	7.2
3[L]	BFPC	1/4000/200000	$8*10^3$	36	55	3055	94	43	2.1	2.3	1.05	9.3
4	sBFPC-1	1/4000/200000	$8*10^3$	36	54	3000	92	39	2.1	1.8	1.04	8.8
5[L]	BFPC	1/20000/200000	$4*10^4$	36	55	3055	93	44	0.6	0.7	1.04	12.7
6	sBFPC-1	1/20000/200000	$4*10^4$	36	58	3222	90	44	0.7	0.8	1.04	12.9
7[L]	BFPC	1/40000/200000	$8*10^4$	36	56	3128	99	57	0.5	0.6	1.01	18.4
8	sBFPC-1	1/40000/200000	$8*10^4$	36	62	3240	99	59	0.5	0.6	1.01	19.4
9[M]	BFPC	1/160000/8000000	$3.2*10^5$	144	66	2777[k]	98	47	0.6	0.6	1.01	58.7[k]
10[L]	sBFPC-1	1/160000/8000000	$3.2*10^5$	144	73	3167[k]	95	44	0.5	0.6	1.01	62.4[k]
11	-	0/40000/200000	-	144	16	-	100	47	0.3	0.5	1.00	-
12[N]	sBFPC-1	1/40000/200000	$8*10^4$	36	67	3722	99	45	0.5	0.6	1.03	19.5

[a] The polymerization reactions were carried out in neat 4 mL PO under CO_2 pressure of 3 MPa at 70 °C in the presence of SA. [b] The feed molar ratio. [c] p was the molar ratio of active proton to catalyst (p = [H]/[Al]). [d] Conversion of PO, determined by ^{1}H NMR analysis of crude reaction mixture. [e] Turnover frequency (TOF) = number of moles of PO consumed/(number of moles [Al]*time). [f] Weight percentage of polyols over cPC. [g] The content of carbonate units in polyols determined by ^{1}H NMR. [h] Theoretical molecular weight of the polyols calculated according to the conversion of PO, selectivity and CU content. [i] The molecular weight and polymer dispersity index determined by gel permeation chromatography (GPC) in THF at 25 °C, calibrated with polystyrene standards. [j] Kilogram polyol per gram Al porphyrin, calculated by $m_{polyol}/m_{Al\ porphyrin}$. [k] Blank experimental result was subtracted based on the results of entry 11. [L] 20 mL PO was used. [M] 40 mL PO was used. [N] 2 L PO was used.

M_n kg/mol ($Đ$)	M_0/CTA
— 2.7 (1.06)	100
— 1.8 (1.04)	50
— 0.8 (1.04)	10
— 0.6 (1.01)	5
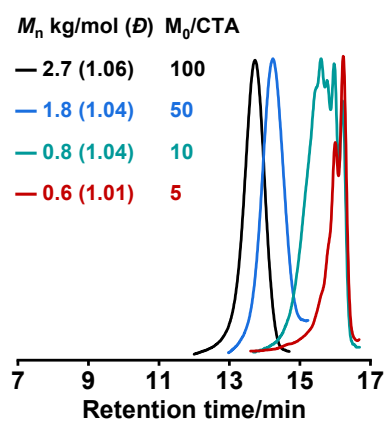
Supplementary Figure 67. GPC curves of CO_2-polyols made by **sBFPC-1** (entries 2, 4, 6, 8, Supplementary Table 6).

It is notable that GPC can distinguish chain lengths in the very low molar mass regime, so the curves exhibited several sharp peaks for the ULMW CO_2-polyols[46].

Supplementary Table 7. Comparison of reaction processes catalyzed by **BFPC** and **sBFPC-1**. [a]

| Entry	Cat.	[Al]/SA/M$_0$[b]	p[c]	t (h)	Conv. (%)[d]	TOF (h^{-1})[e]	Polymer (%)[f]	CU (%)[g]	$M_n^{theo.}$ (kg/mol)[h]	M_n^{GPC} (kg/mol)[i]	Đ[i]	Productivity (kg/g)[j]
1	**BFPC**	1/2000/200000	4*10^3	9	11	2449	99	59	1.1	0.6	1.05	2.4
2	**sBFPC-1**	1/2000/200000	4*10^3	9	12	2725	99	53	1.2	0.8	1.05	2.5
3	**BFPC**	1/2000/200000	4*10^3	18	24	2670	97	47	2.0	1.3	1.05	4.3
4	**sBFPC-1**	1/2000/200000	4*10^3	18	22	2411	97	41	1.8	1.1	1.06	3.9
5	**BFPC**	1/2000/200000	4*10^3	27	39	2877	98	44	3.1	2.1	1.06	6.7
6	**sBFPC-1**	1/2000/200000	4*10^3	27	36	2673	97	42	2.9	1.8	1.05	6.1
7	**BFPC**	1/2000/200000	4*10^3	36	50	2789	94	41	3.8	4.5	1.04	8.0
8	**sBFPC-1**	1/2000/200000	4*10^3	36	45	2500	97	35	3.4	2.7	1.06	7.2

[a] The polymerization reactions were carried out in neat PO (4 mL for **sBFPC-1**, 20 mL for **BFPC**) under CO$_2$ pressure of 3 MPa at 70 °C in the presence of SA. [b] The feed molar ratio. [c] p was the molar ratio of active proton to catalyst (p = [H]/[Al]). [d] Conversion of PO, determined by ^{1}H NMR analysis of crude reaction mixture. [e] Turnover frequency (TOF) = number of moles of PO consumed/(number of moles [Al]*time). [f] Weight percentage of polyols over cPC. [g] The content of carbonate units in polyols determined by ^{1}H NMR. [h] Theoretical molecular weight of the polyols calculated according to the conversion of PO, selectivity and CU content. [i] The molecular weight and polymer dispersity index determined by gel permeation chromatography (GPC) in THF at 25 °C, calibrated with polystyrene standards. [j] Kilogram polyol per gram Al porphyrin, calculated by m$_{polyol}$/m$_{Al\ porphyrin}$.

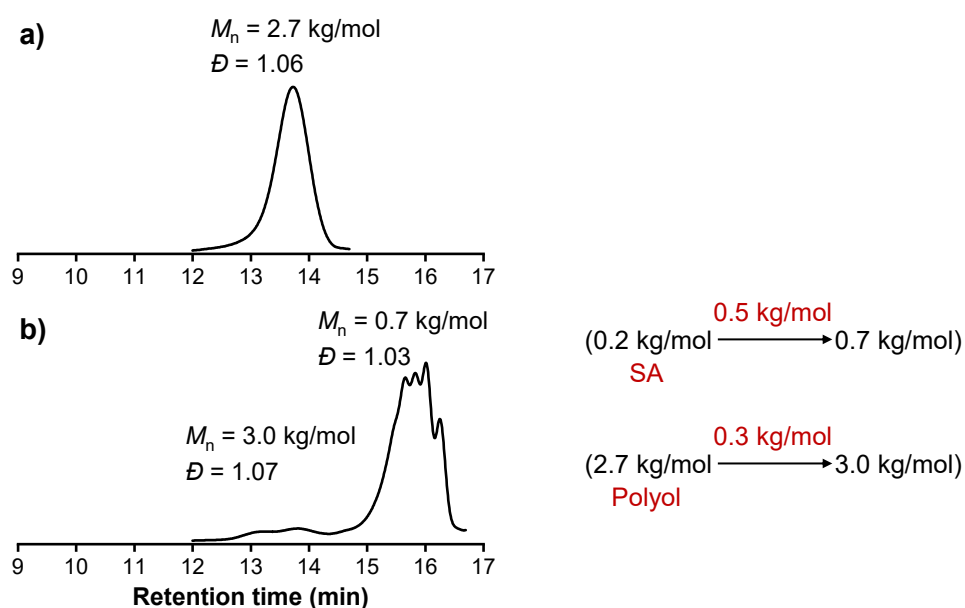**Supplementary Table 8.** Telomerization of PO/CO_2 in the presence of different CTA catalyzed by **sBFPC-1**. [a]

sBFPC-1

PEC polyols

cPC (byproduct)

CTA:

SA   AA   SuA   OA

BPA   PEG$_{300}$ TMA   BTC
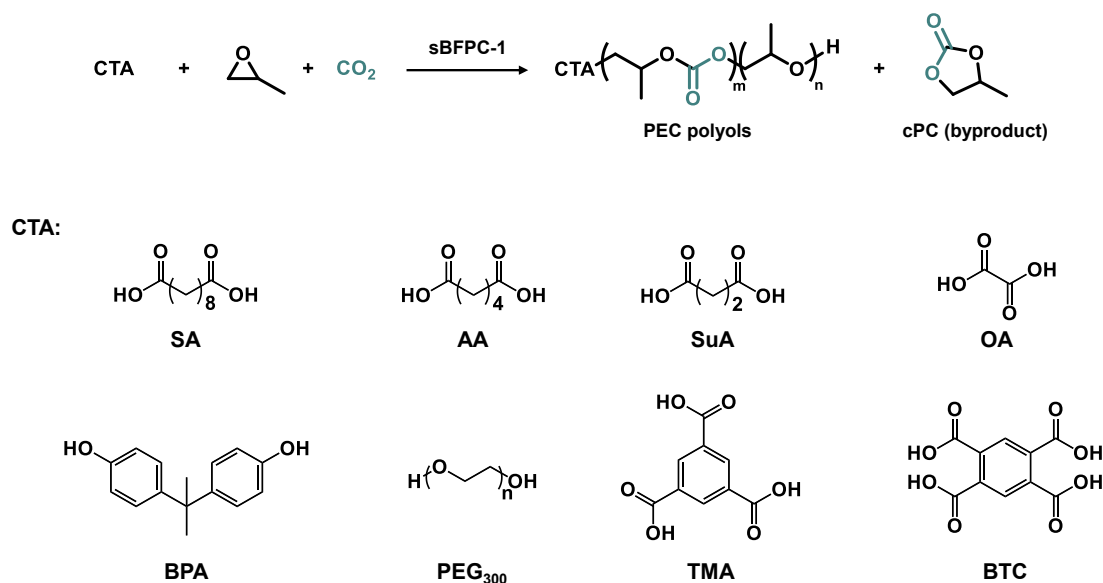
Entry	CTA	[Al]/CTA/M$_0$[b]	p[c]	Conv. (%)[d]	TOF (h^{-1})[e]	Polymer (%)[f]	CU (%)[g]	(Poylyester + polycarbonate)[g]	$M_n^{theo.}$ (kg/mol)[h]	M_n^{GPC} (kg/mol)[i]	Đ[i]	Productivity (kg/g)[j]
1	SA	1/40000/200000	8*10^4	62	3240	99	59	74	0.5	0.6	1.01	19.4
2	AA	1/40000/200000	8*10^4	77	4278	95	24	58	0.4	0.5	1.01	16.9
3	SuA	1/40000/200000	8*10^4	78	4333	97	38	55	0.4	0.5	1.01	17.0
4	OA	1/40000/200000	8*10^4	97	5389	99	33	53	0.4	1.5	1.16	18.6
5	PEG$_{300}$	1/40000/200000	8*10^4	62	3463	89	38	38	0.5	0.6	1.03	21.0
6	BPA	1/40000/200000	8*10^4	60	3354	97	5	5	0.4	0.6	1.01	17.1
7	TMA	1/40000/200000	1.2*10^5	90	4995	95	20	47	0.6	0.7	1.03	23.2
8	BTC	1/40000/200000	1.6*10^5	99	5319	99	22	49	0.6	0.9	1.07	25.3

[a] The polymerization reactions were carried out in neat 4 mL PO under CO_2 pressure of 3 MPa at 70 °C in the presence of CTA for 36 h catalyzed by **sBFPC-1**. [b] The feed molar ratio. [c] p was the molar ratio of active proton to catalyst (p = [H]/[Al]). [d] Conversion of PO, determined by ^{1}H NMR analysis of crude reaction mixture. [e] Turnover frequency (TOF) = number of moles of PO consumed/(number of moles [Al]*time). [f] Weight percentage of polyols over cPC. [g] The content of carbonate units and ester + carbonate units in polyols determined by ^{1}H NMR. The ester unit is high in the ultra-low molecular weight (< 1000 g/mol) CO_2-polyols when using acid as CTA so it cannot be ignored. [h] Theoretical molecular weight of the polyols calculated according to the conversion of PO, selectivity and CU content. [i] The molecular weight and polymer dispersity index determined by gel permeation chromatography (GPC) in THF at 25 °C, calibrated with polystyrene standards. [j] Kilogram polyol per gram Al porphyrin, calculated by $m_{polyol}/m_{Al porphyrin}$.
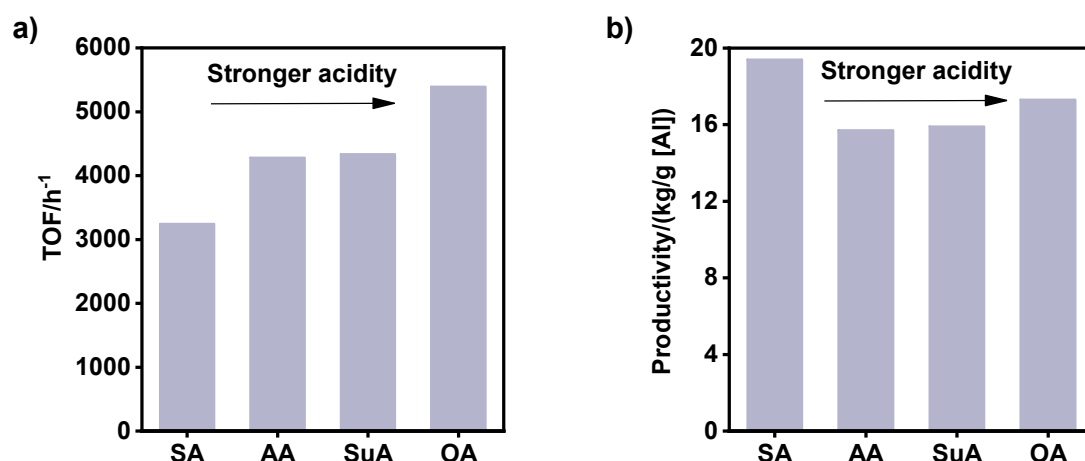
Supplementary Figure 68. a) Comparison of TOF of **sBFPC-1** using different acidic CTA (entries 1-4, Supplementary Table 8). b) Comparison of productivity of **sBFPC-1** using different acidic CTA. TOF and productivity have different trends due to different calculation methods (Supplementary Figure 65).

Supplementary Figure 69. GPC curves of polyols. a) Polyol **a** prepared using SA as CTA (entry 1, Supplementary Table S4). b) Polyol **b** prepared using mixture of polyol **a** and SA (1/1, m/m) as CAT. Conditions: The polymerization reactions were carried out in neat 4 mL PO under CO_2 pressure of 3 MPa at 70 °C in the presence of CTA for 24 h. The results showed polymer grows faster on SA than on polyol **a**.

Supplementary Table 9. Telomerization of other substituted epoxide and CO_2 in the presence of SA catalyzed by **sBFPC-1**. [a]
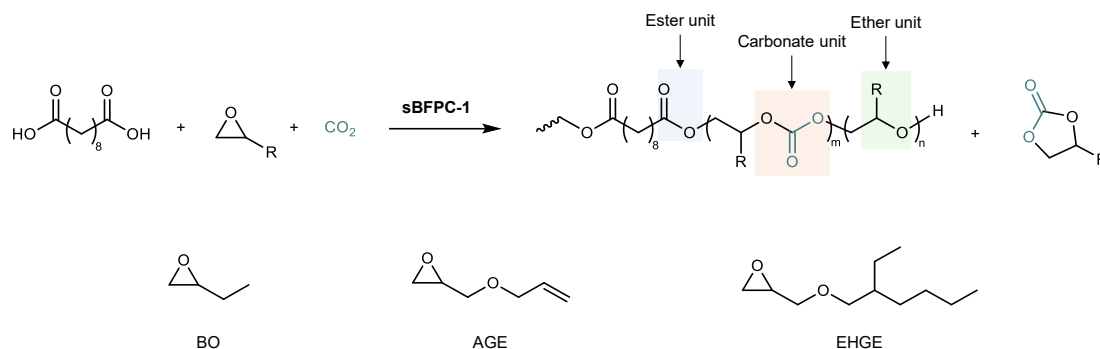

Entry	Mon.	[Al]/SA/M_0[b]	p[c]	Conv. (%)[d]	TOF (h^{-1})[e]	Polymer (%)[f]	CU (%)[g]	(Polyester + polycarbonate)[h]	M_n^{GPC} (kg/mol)[i]	$Đ$[i]	Productivity (kg/g)[j]
1	BO	1/40000/200000	$8*10^4$	55	3056	99	20	58	0.6	1.01	18.0
2	AGE	1/40000/200000	$8*10^4$	39	2167	99	30	65	0.5	1.01	16.9
3	EHGE	1/40000/200000	$8*10^4$	22	1222	99	31	74	0.5	1.03	8.4

[a] The polymerization reactions were carried out in neat 4 mL monomers under CO_2 pressure of 3 MPa at 70 °C in the presence of SA for 36 h catalyzed by **sBFPC-1**. [b] The feed molar ratio. [c] p was the molar ratio of active proton to catalyst (p = [H]/[Al]). [d] Conversion of monomer, determined by ^1H NMR analysis of crude reaction mixture. [e] Turnover frequency (TOF) = number of moles of monomer consumed/(number of moles [Al]*time). [f] Weight percentage of polyols over cPC. [g] The content of carbonate units in polyols determined by ^1H NMR. [h] The content of ester and carbonate units in polyols determined by ^1H NMR. The ester unit is high in the ultra-low molecular weight (< 1000 g/mol) CO_2-polyols so it cannot be ignored. [i] The molecular weight and polymer dispersity index determined by gel permeation chromatography (GPC) in THF at 25 °C, calibrated with polystyrene standards. [j] Kilogram polyol per gram Al porphyrin, calculated by $m_{polyol}/m_{Al\ porphyrin}$.
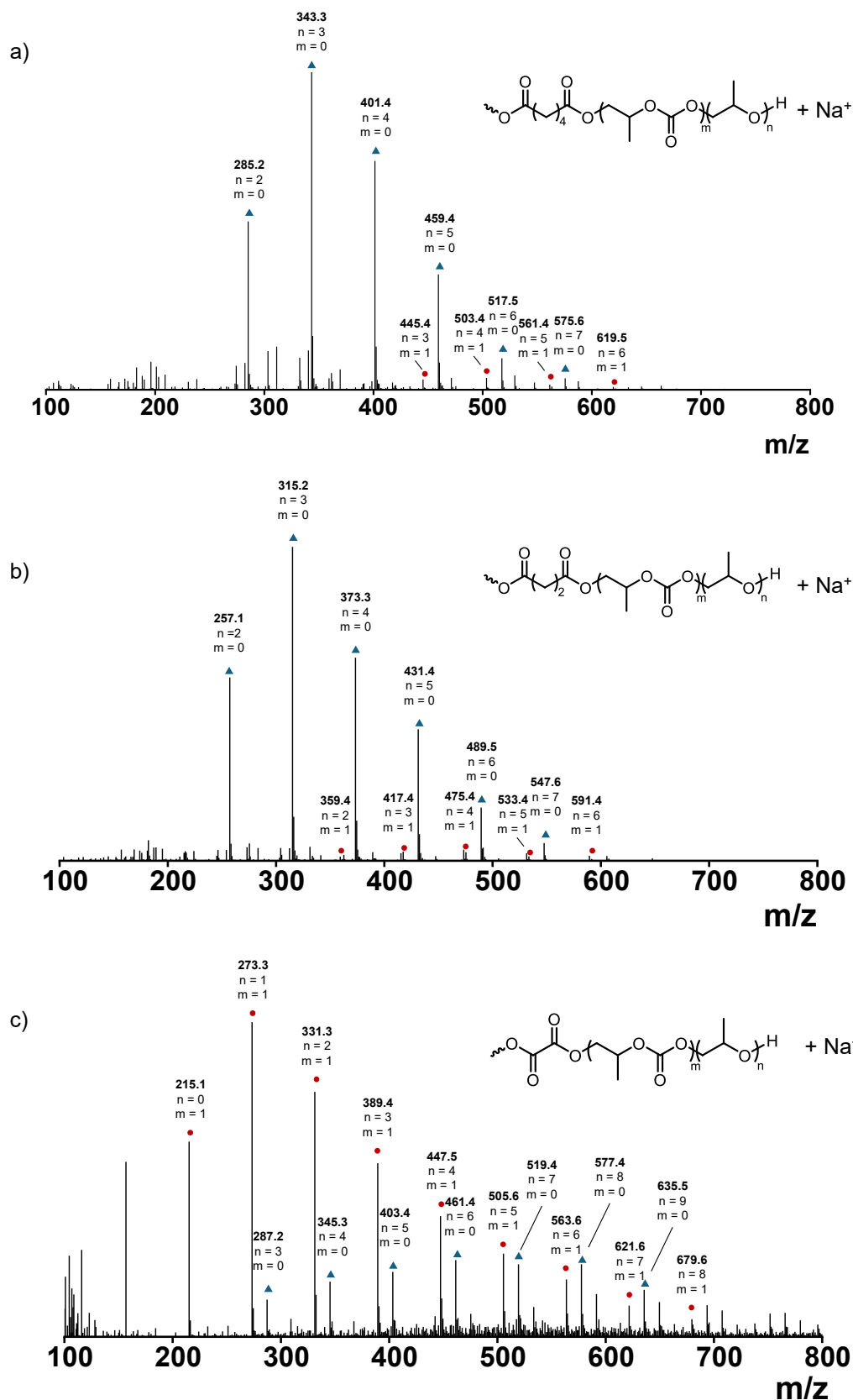
MS spectrums of polyols
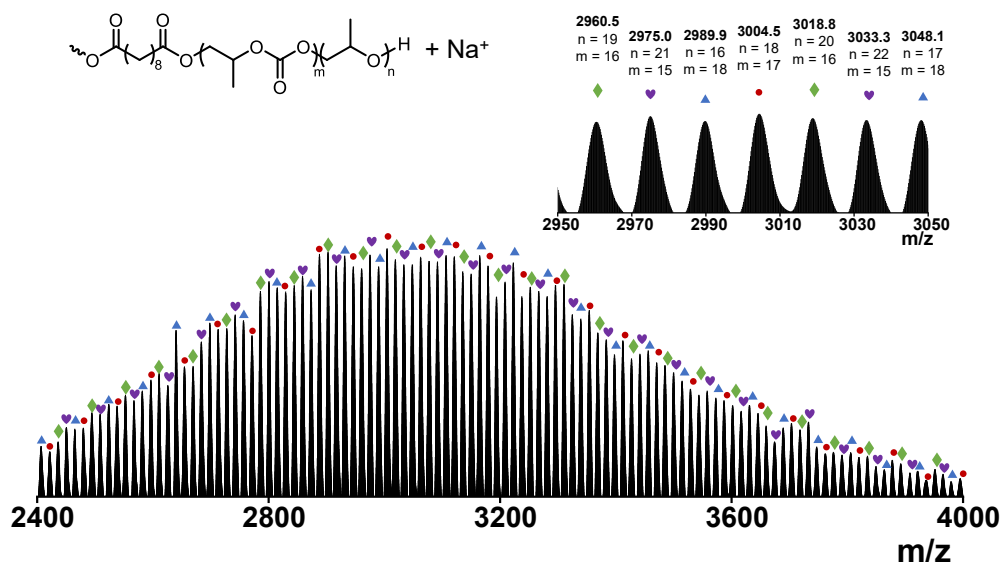
Supplementary Figure 70. MALDI-TOF-MS spectrum of CO_2-polyol using sebacic acid as chain transfer agent (entry 1, Supplementary Table 5).
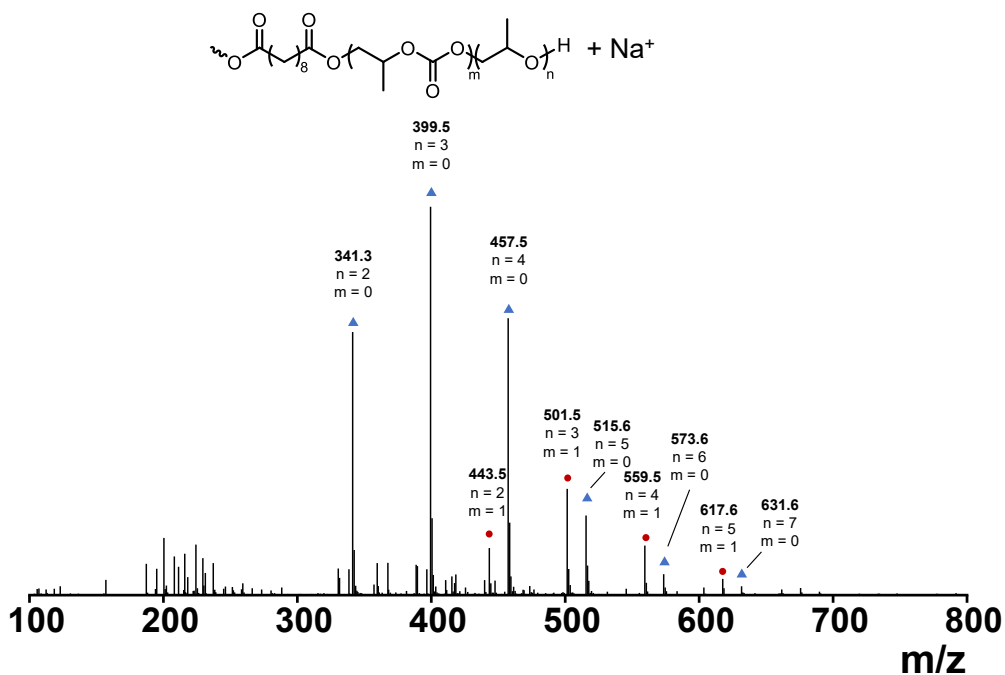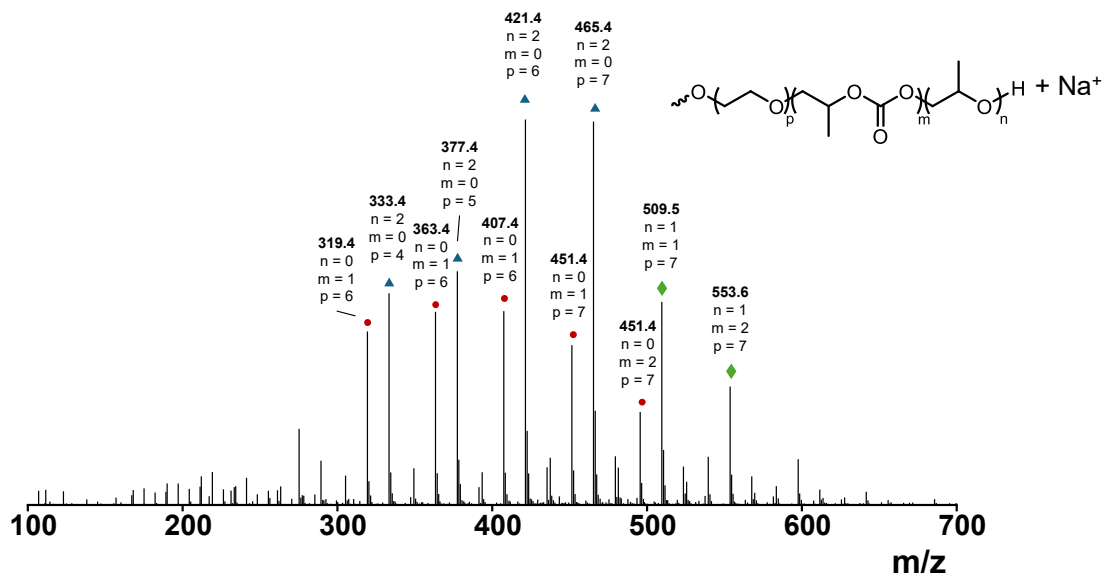

Supplementary Figure 71. ESI-MS of CO_2-polyol using sebacic acid as chain transfer agent (entry 1, Supplementary Table 8).
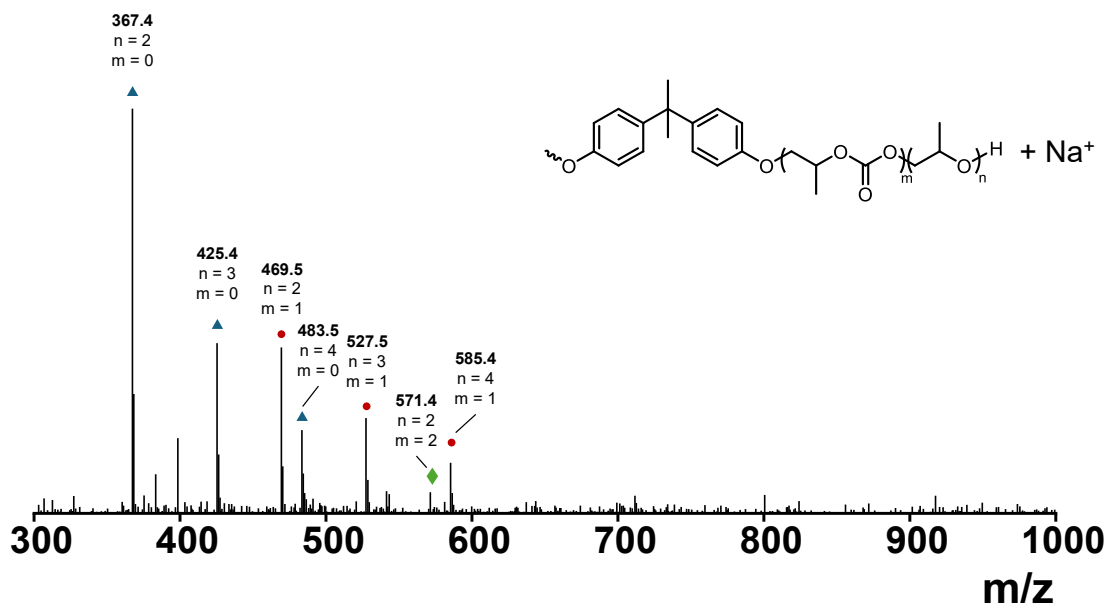
Supplementary Figure 72. ESI-MS of CO_2-polyol using a) adipic acid, b) succinic acid and c) oxalic acid as chain transfer agent (entries 2-4, Supplementary Table 8).
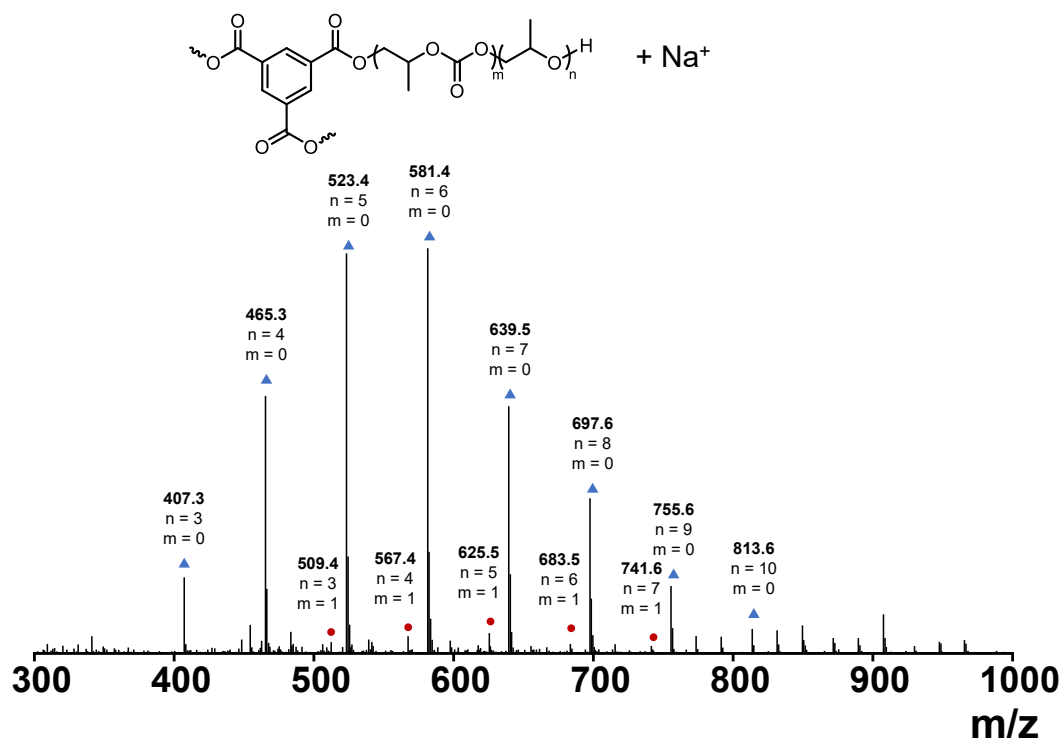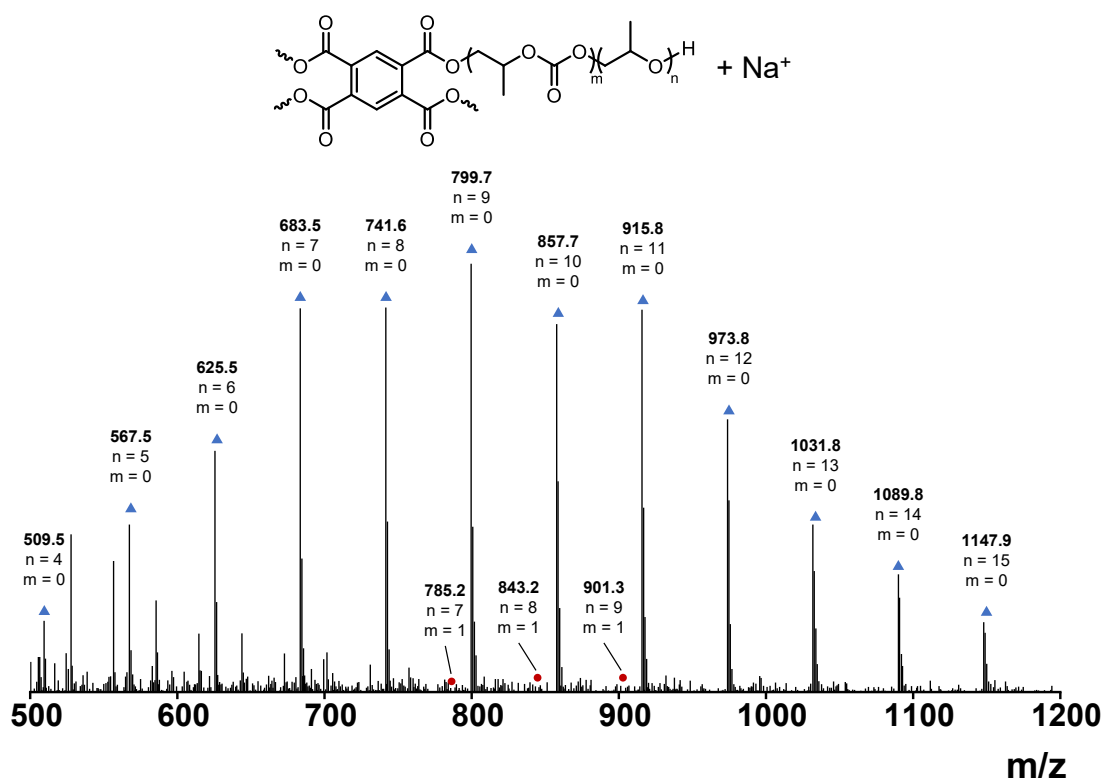
Supplementary Figure 73. ESI-MS of CO_2-polyol using polyethylene glycol (PEG, M_n = 300 g/mol) as chain transfer agent (entry 5, Supplementary Table 8).
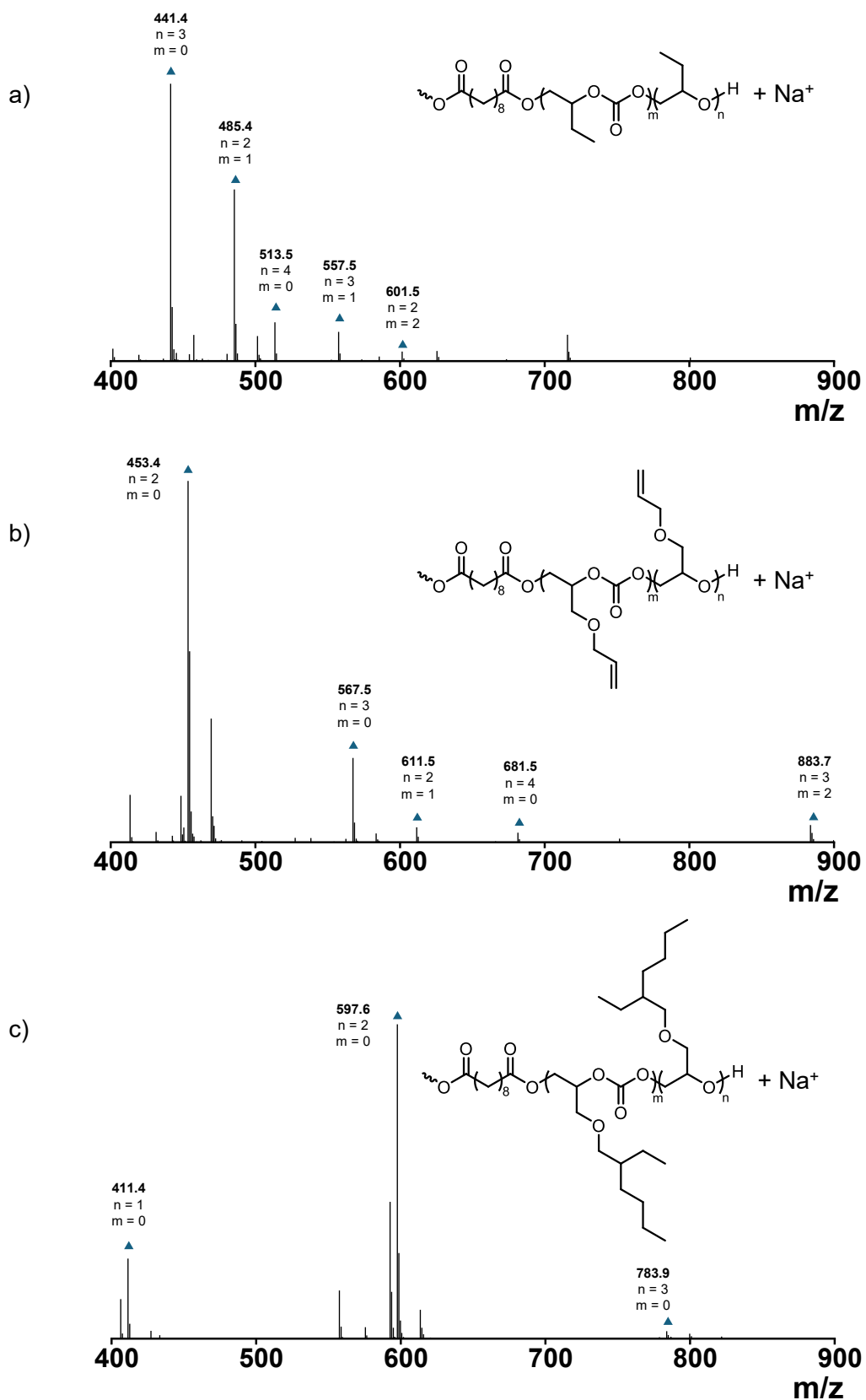

Supplementary Figure 74. ESI-MS of CO_2-polyol using bisphenol A as chain transfer agent (entry 6, Supplementary Table 8).

Supplementary Figure 75. ESI-MS of CO_2-polyol using trimesic acid as chain transfer agent (entry 7, Supplementary Table 8).

Supplementary Figure 76. ESI-MS of CO_2-polyol using 1,2,4,5-benzenetetracarboxylic acid as chain transfer agent (entry 8, Supplementary Table 8).
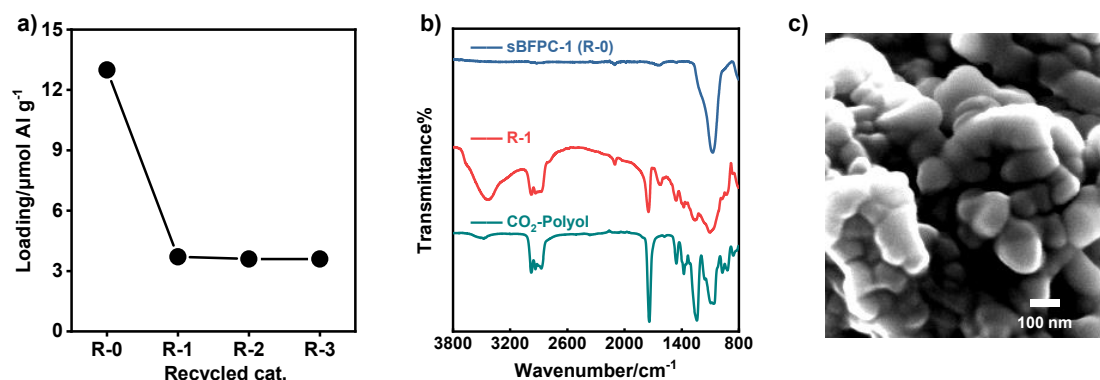
Supplementary Figure 77. ESI-MS of CO_2-polyol using a) BO, b) AGE and c) EHGE as monomer (entries 1-3, Supplementary Table 9).

Supplementary Table 10. Performance comparison for multiple uses of **sBFPC-1**. [a]

| Entry	Cat.	[Al]/SA/M_0[b]	p[c]	Conv. (%)[d]	TOF (h^{-1})[e]	Polymer (%)[f]	CU (%)[g]	$M_n^{theo.}$ (kg/mol)[h]	M_n^{GPC} (kg/mol)[i]	$Đ$[i]	Productivity (kg/g)[j]
1	**sBFPC-1**	1/40000/200000	$8*10^4$	67	3722	99	45	0.5	0.6	1.03	19.5
2	**R-1**	1/40000/200000	$8*10^4$	62	3463	99	47	0.5	0.6	1.02	18.8
3	**R-2**	1/40000/200000	$8*10^4$	58	3195	99	45	0.5	0.6	1.03	18.1
4	**R-3**	1/40000/200000	$8*10^4$	59	3277	98	46	0.5	0.6	1.02	18.2

[a] The polymerization reactions were carried out in neat 2 L PO under CO_2 pressure of 3 MPa at 70 °C in the presence of SA for 36 h. [b] The feed molar ratio. [c] p was the molar ratio of active proton to catalyst (p = [H]/[Al]). [d] Conversion of PO, determined by ^1H NMR analysis of crude reaction mixture. [e] Turnover frequency (TOF) = number of moles of PO consumed/(number of moles [Al]*time). [f] Weight percentage of polyols over cPC. [g] The content of carbonate units in polyols determined by ^1H NMR. [h] Theoretical molecular weight of the polyols calculated according to the conversion of PO, selectivity and CU content. [i] The molecular weight and polymer dispersity index determined by gel permeation chromatography (GPC) in THF at 25 °C, calibrated with polystyrene standards. [j] Kilogram polyol per gram Al porphyrin, calculated by $m_{polyol}/m_{Al\ porphyrin}$.

The loadings of recycled catalysts (**R-z**, **z** = **1**, **2**, **3**) significantly decreased from 13.0 μmol/g to 3.7 μmol/g (Supplementary Figure 78a). To investigate the underlying cause, we utilized the ATR-FT-IR spectrum (Supplementary Figure 78b) and SEM image (Supplementary Figure 78c) to characterize **R-1**. These results revealed that residual polyols were attached to the supported catalyst. These findings suggest that the weakly acidic silanol may function as CTA, facilitating the covalent attachment of polyols to the silicon and impeding their removall[47]. In subsequent tests, the loadings of **R-2** and **R-3** remained essentially unchanged, showing 3.6 μmol/g (Supplementary Figure 78a).
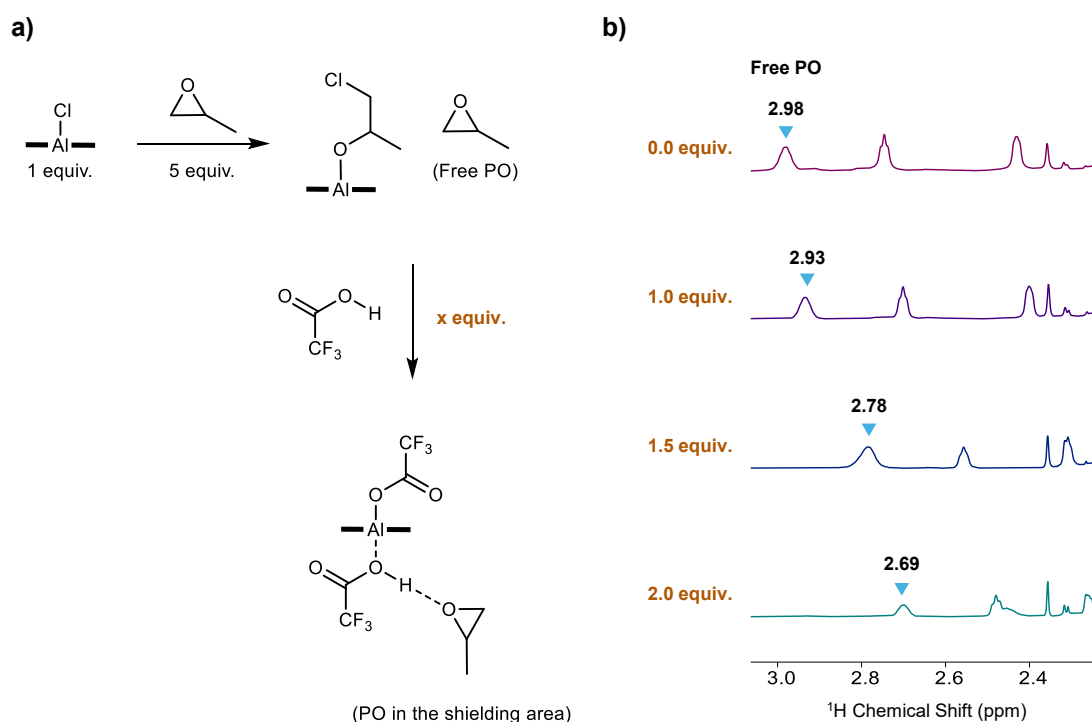

Supplementary Figure 78. a) The catalysts loadings before each cycle. b) ATR-FT-IR spectrums of **sBFPC-1**, **R-1** and CO_2-polyol. c) SEM image of recycled catalyst (**R-1**).
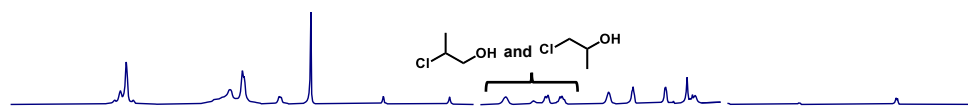
Investigation of interaction between compounds
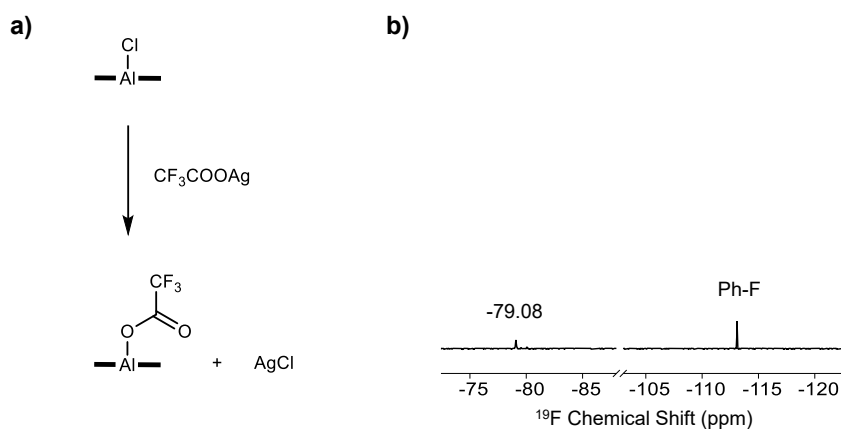
Supplementary Figure 79. The preparation and ^{19}F NMR spectrum of **M-TPPAl** with a TFA axis.

Supplementary Figure 80. a) The reaction between **M-TPPAl** and PO followed by the addition of TFA. b) ^{1}H NMR signal changes (2.4-3.0 ppm from PO) of the mixture of **M-TPPAl**/PO (1/5) titration with TFA in CDCl$_3$.
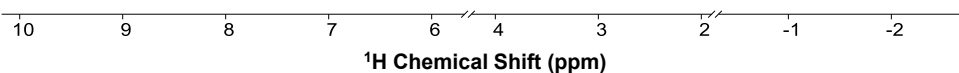
Supplementary Figure 81. ^{1}H NMR spectra of a) **M-TPPAl**/PO = 1/5 and b) **M-TPPAl**/CH$_3$CO$_2$H/PO = 1/2/5 and c) CH$_3$CO$_2$H/PO = 2/5.

Note: The spectra showed signals for 2-chloro-1-propanol and 1-chloro-2-propanol, which resulted from the nucleophilic attack on PO by chloride ions, followed by an exchange with the protic species and detachment from Al porphyrin[48, 49].
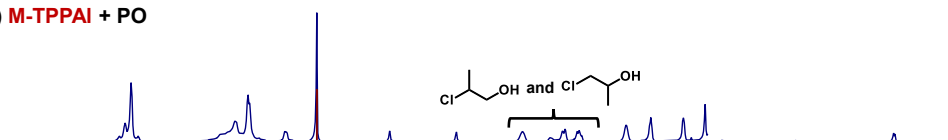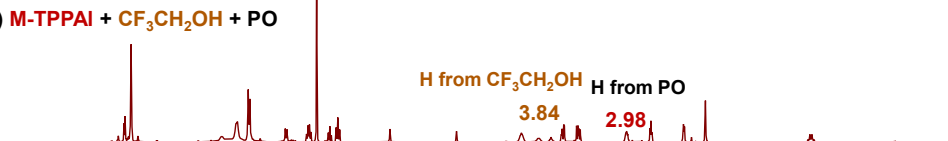
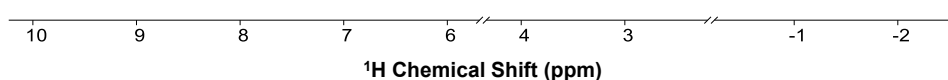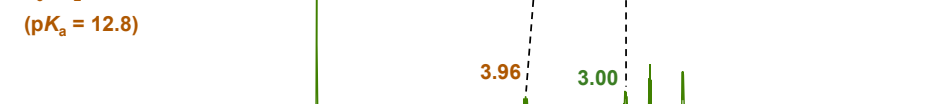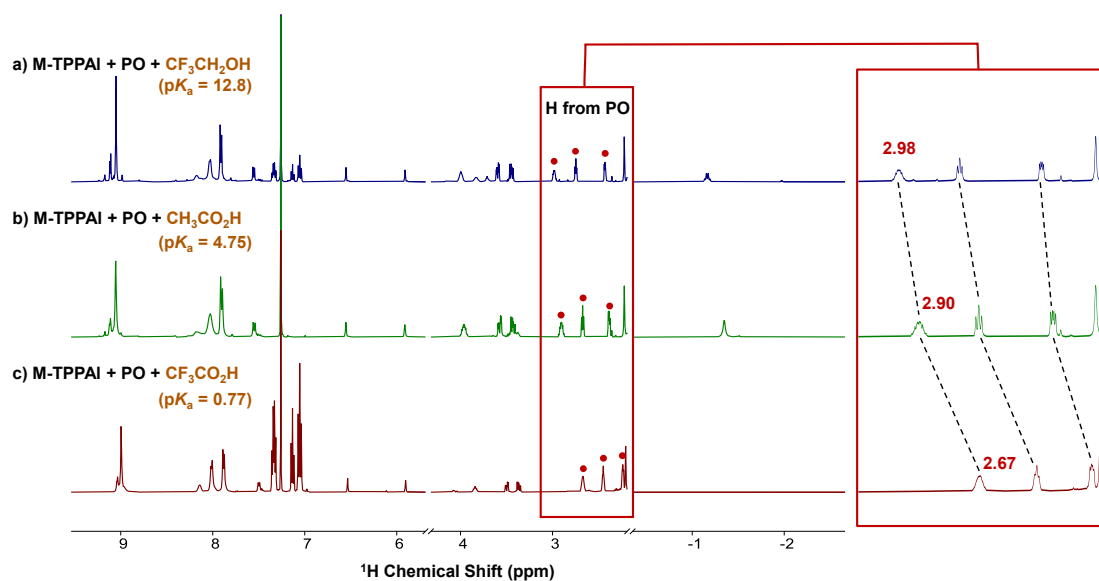**Supplementary Figure 82.** ^{1}H NMR spectra of a) **M-TPPAl**/PO = 1/5 and b) **M-TPPAl**/CF$_3$CH$_2$OH/PO = 1/2/5 and c) CF$_3$CH$_2$OH/PO = 2/5.

Supplementary Figure 83. Comparison of ^{1}H NMR spectra of a) **M-TPPAI**/PO (1/5) with a) CF$_3$CH$_2$OH (pK_a = 12.8), b) CH$_3$CO$_2$H (pK_a = 4.75) and c) CF$_3$CO$_2$H (pK_a = 0.77).
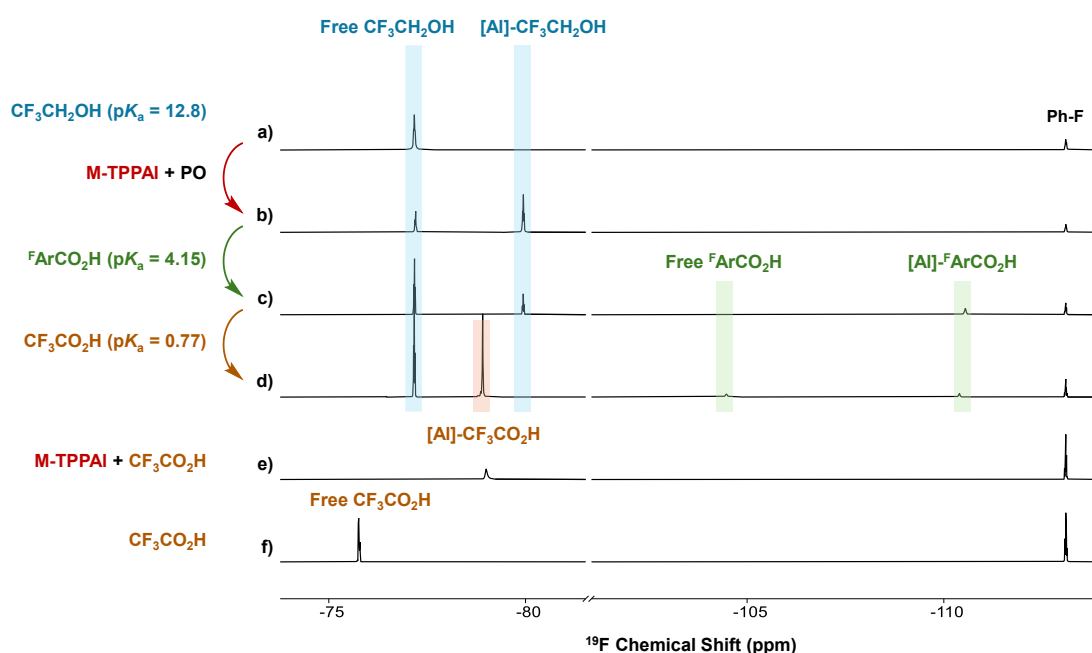
Supplementary Figure 84. ^{19}F NMR spectra of a) CF$_3$CH$_2$OH (pK_a = 12.8, 2 equiv.), e) **M-TPPAI**/CF$_3$CO$_2$H = 1/2 and f) CF$_3$CO$_2$H (pK_a = 0.77). b) Adding **M-TPPAI** (1 equiv.) and PO (5 equiv.) followed by the addition of c) ^{F}ArCO$_2$H (pK_a = 4.15, 2 eqv.) and d) CF$_3$CO$_2$H (pK_a = 0.77, 2 equiv.).

The primary purpose of mixing **M-TPPAI** and PO firstly is to obtain [Al]-alkoxide, which is subsequently replaced by CF$_3$CH$_2$OH to give [Al]-CF$_3$CH$_2$OH. Following the addition of ^{F}ArCO$_2$H, no free ^{F}ArCO$_2$H was detected, and the majority of [Al]-CF$_3$CH$_2$OH was converted to free CF$_3$CH$_2$OH. Upon the addition of CF$_3$CO$_2$H, the remaining [Al]-CF$_3$CH$_2$OH and a portion of [Al]-^{F}ArCO$_2$H were replaced by CF$_3$CO$_2$H. These results indicate that the pK_a governs the chain transfer reaction[25].
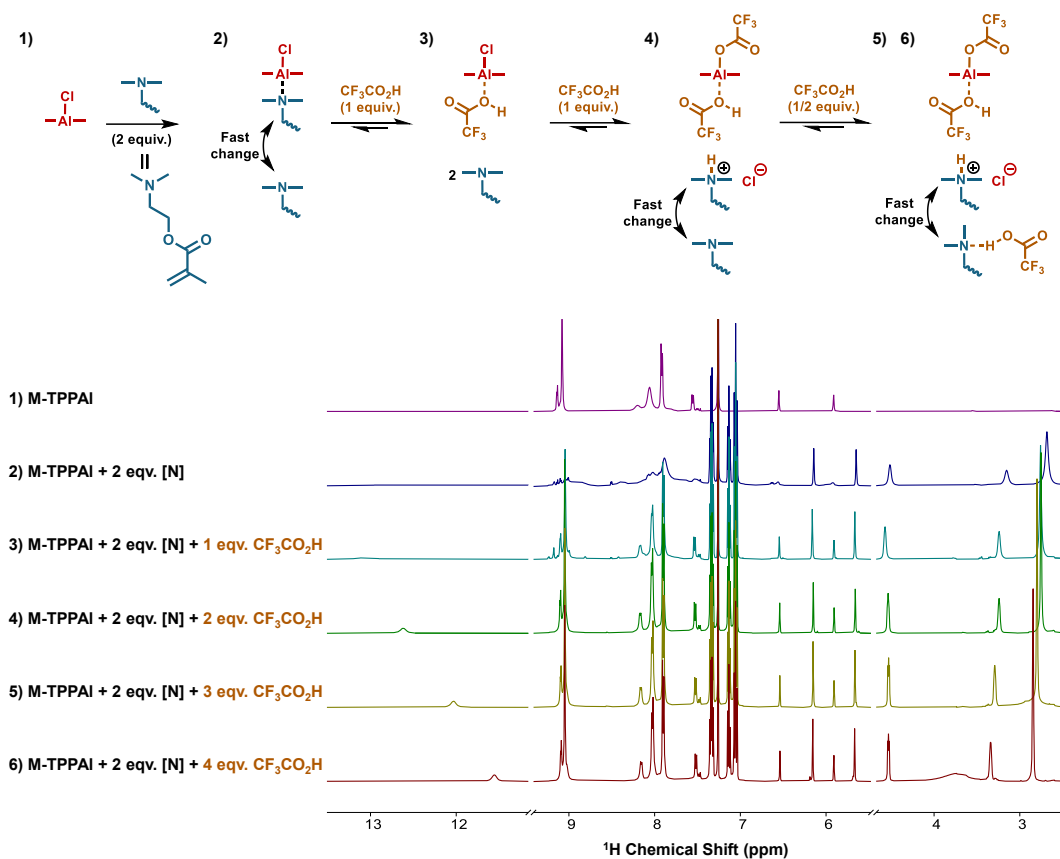
Supplementary Figure 85. ^{1}H NMR spectrums of **M-TPPAl** and the mixture of **M-TPPAl**/DMAEMA (1/2) titrated by CF$_3$CO$_2$H in CDCl$_3$. The signal at 13-11 ppm derives from hydrochloride salt of the tertiary amine (Supplementary Fig. 87).
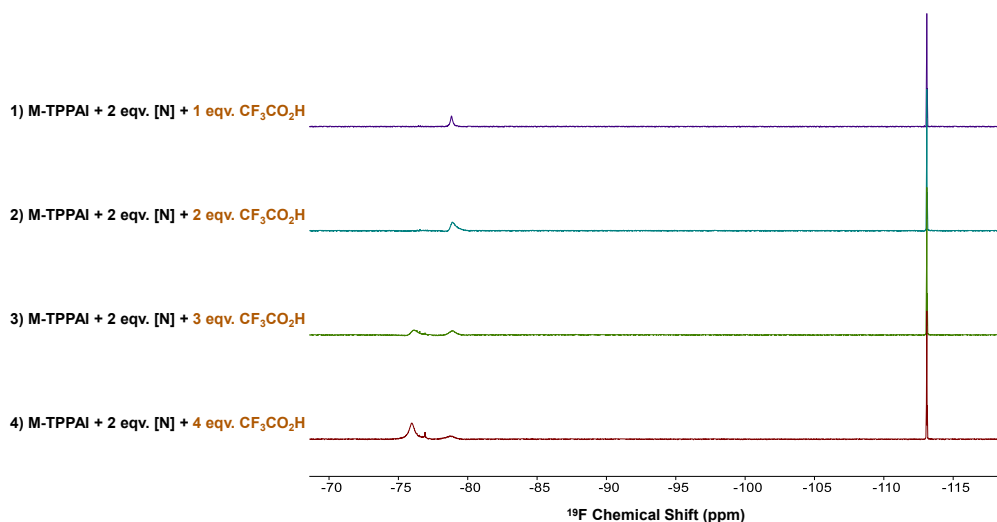
Supplementary Figure 86. ^{19}F NMR spectrums of the mixture of **M-TPPAl**/DMAEMA (1/2) titrated by TFA in CDCl$_3$.

^{19}F NMR spectra indicated that the first two equivalents of CF$_3$CO$_2$H were coordinated to the Al porphyrin, while the remaining equivalents were not bound to Al porphyrin.
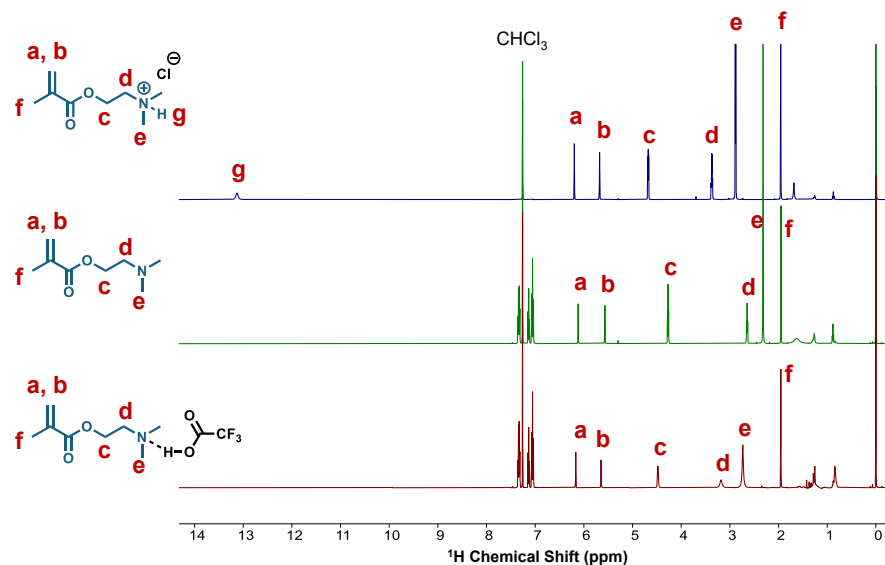
Supplementary Figure 87. Comparison of ^{1}H NMR spectrums of 2-(dimethylamino)ethyl methacrylate hydrochloride (prepared by DMAEMA and HCl), DMAEMA and the mixture of DMAEMA/TFA = 1/1.
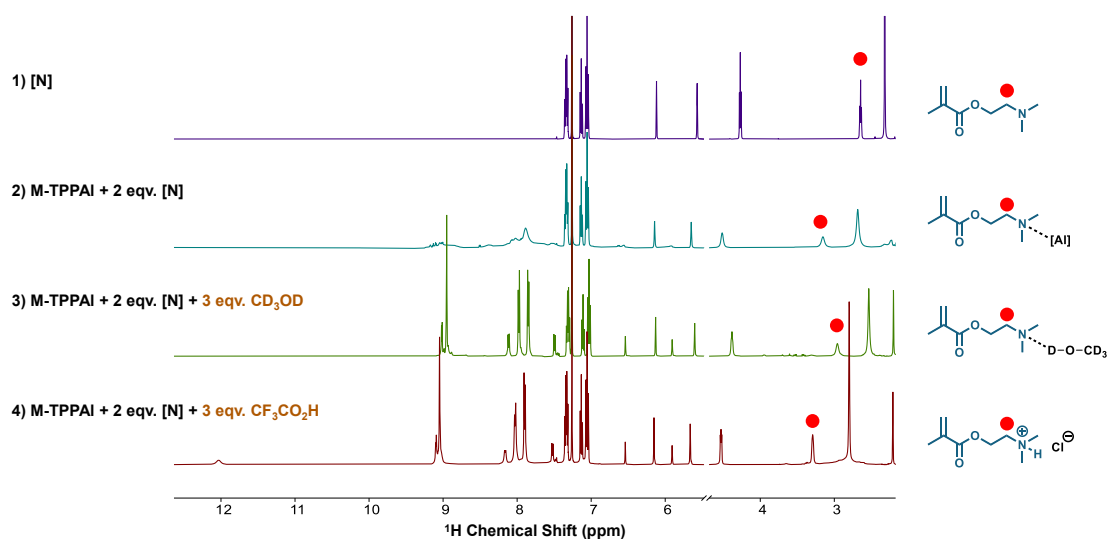
Supplementary Figure 88. Comparison of ^{1}H NMR spectrums of 1) DMAEMA, 2) **M-TPPAI**/DMAEMA = 1/2, 3) **M-TPPAI**/DMAEMA/CD$_3$OD = 1/2/3 and 4) **M-TPPAI**/DMAEMA/CF$_3$CO$_2$H = 1/2/3.

The interaction between Al porphyrin and tertiary amines can also be disrupted by the presence of hydroxyl groups.
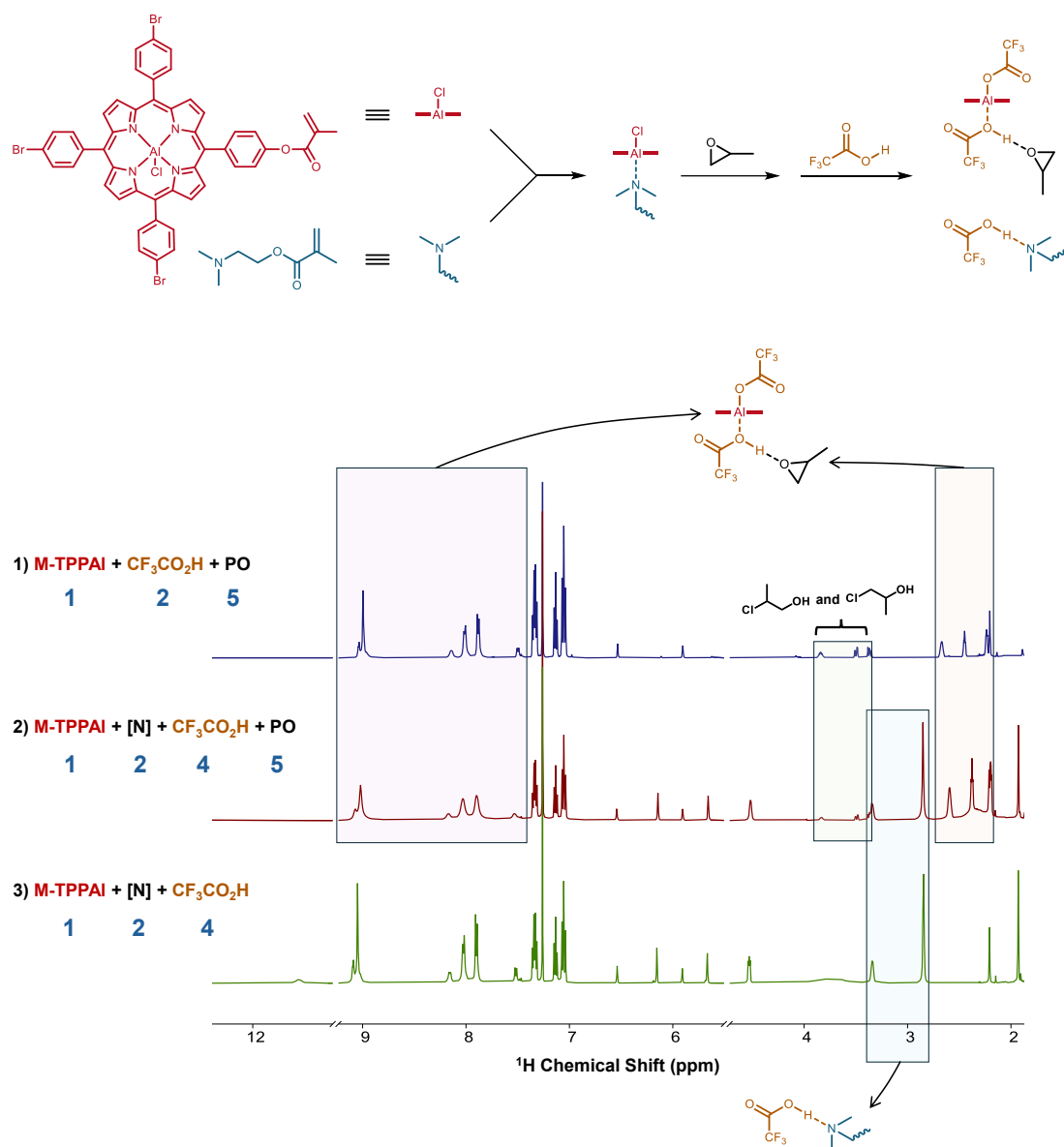
Supplementary Figure 89. Comparison of ^{1}H NMR spectrums of 1) **M-TPPAI**/CF$_3$CO$_2$H/PO = 1/2/5, 2) **M-TPPAI**/DMAEMA/CF$_3$CO$_2$H/PO = 1/2/4/5 and 3) **M-TPPAI**/DMAEMA/ CF$_3$CO$_2$H = 1/2/4. The analysis of products was in Supplementary Figs. 85-88.

Supplementary Table 11. Comparison of different catalysts in the telomerization of PO/CO_2 in the presence of SA. [a]

Entry	Cat.	[Al]/SA/M_0[b]	p[c]	t (h)	Conv. (%)[d]	TOF (h^{-1})[e]	Polymer (%)[f]	CU (%)[g]	$M_n^{theo.}$ (kg/mol)[h]	M_n^{GPC} (kg/mol)[i]	Đ[i]	Productivity (kg/g)[j]
1	SC	1/100/10000	$2*10^2$	24	4	15	100	82	0.5	0.7	1.04	0.06
2	sSC-1	1/100/10000	$2*10^2$	24	34	140	96	26	2.5	1.8	2.22	0.26
3	PC	1/2000/200000	$4*10^3$	36	16	911	99	34	1.4	1.5	1.08	2.9
4	sPC-1	1/2000/200000	$4*10^3$	36	18	1000	98	24	1.4	1.0	1.62	3.0
5	BFPC	1/2000/200000	$4*10^3$	36	50	2789	94	41	3.8	4.5	1.04	8.0
6	sBFPC-1	1/2000/200000	$4*10^3$	36	45	2500	97	35	3.4	2.7	1.06	7.2

[a] The polymerization reactions were carried out in neat PO under CO_2 pressure of 3 MPa at 70 °C in the presence of SA. [b] The feed molar ratio. [c] p was the molar ratio of active proton to catalyst (p = [H]/[Al]). [d] Conversion of PO, determined by ^1H NMR analysis of crude reaction mixture. [e] Turnover frequency (TOF) = number of moles of PO consumed/(number of moles [Al]*time). [f] Weight percentage of polyols over cPC. [g] The content of carbonate units in polyols determined by ^1H NMR. [h] Theoretical molecular weight of the polyols calculated according to the conversion of PO, selectivity and CU content. [i] The molecular weight and polymer dispersity index determined by gel permeation chromatography (GPC) in THF at 25 °C, calibrated with polystyrene standards. [j] Kilogram polyol per gram Al porphyrin, calculated by $m_{polyol}/m_{Al\ porphyrin}$.

Reference

1.   Zhang, R. et al. Unity makes strength: Constructing polymeric catalyst for selective synthesis of CO_2/epoxide copolymer. *CCS Chem.* **5**. 750-760 (2023).

2.   Godula, K., Rabuka, D., Nam, K. T. & Bertozzi, C. R. Synthesis and microcontact printing of dual end-functionalized mucin-like glycopolymers for microarray applications. *Angew. Chem. Int. Ed.* **48**. 4973-4976 (2009).

3.   Lai, J. T., Filla, D. & Shea, R. Functional polymers from novel carboxyl-terminated trithiocarbonates as highly efficient RAFT agents. *Macromolecules*. **35**. 6754-6756 (2002).

4.   Cleveland, J. W. et al. Cooperativity in the aldol condensation using bifunctional mesoporous silica-poly(styrene) MCM-41 organic/inorganic hybrid catalysts. *ACS Appl. Mater. Interfaces*. **14**. 11235-11247 (2022).

5.   Yoon, K. Y. et al. Scalable and continuous access to pure cyclic polymers enabled by 'quarantined' heterogeneous catalysts. *Nat. Chem.* **14**. 1242-1248 (2022).

6.   Cooper, C. L., Cosgrove, T., van Duijneveldt, J. S., Murray, M. & Prescott, S. W. The use of solvent relaxation NMR to study colloidal suspensions. *Soft Matter*. **9**. 7211–7228 (2013).

7.   Yuan, L., Chen, L., Chen, X., Liu, R. & Ge, G. In situ measurement of surface functional groups on silica nanoparticles using solvent relaxation nuclear magnetic resonance. *Langmuir*. **33**. 8724-8729 (2017).

8.   Schlumberger, C., Sandner, L., Michalowski, A. & Thommes, M. Reliable surface area assessment of wet and dry nonporous and nanoporous particles: Nuclear magnetic resonance relaxometry and gas physisorption. *Langmuir*. **39**. 4611-4621 (2023).

9.   Aresta, M., Dibenedetto, A. & Angelini, A. Catalysis for the valorization of exhaust carbon: From CO_2 to chemicals, materials, and fuels. Technological use of CO_2. *Chem. Rev.* **114**. 1709-1742 (2013).

10.   Artz, J. et al. Sustainable conversion of carbon dioxide: An integrated review of catalysis and life cycle assessment. *Chem. Rev.* **118**. 434-504 (2017).

11.   Dabral, S. & Schaub, T. The use of carbon dioxide (CO_2) as a building block in organic synthesis from an industrial perspective. *Adv. Synth. Catal.* **361**. 223-246 (2018).

12.   Liu, Y. & Lu, X.-B. Current challenges and perspectives in CO_2-based polymers. *Macromolecules*. **56**. 1759-1777 (2023).

13.   Darensbourg, D. J. & Wilson, S. J. What's new with CO_2? Recent advances in its copolymerization with oxiranes. *Green Chem.* **14**. 2665-2671 (2012).

14.   Wang, X. Biodegradable polymers, history tells polymer science's fortune. *Chin. J. Polym. Sci.* **40**. 431-432 (2022).

15.   Inoue, S., Koinuma, H. & Tsuruta, T. Copolymerization of carbon dioxide and epoxide. *J. Polym. Sci., Part B: Polym. Lett.* **7**. 287-292 (1969).

16.   Yang, G. W., Zhang, Y. Y. & Wu, G. P. Modular organoboron catalysts enable transformations with unprecedented reactivity. *Acc. Chem. Res.* **54**. 4434-4448 (2021).

17. Lidston, C. A. L., Severson, S. M., Abel, B. A. & Coates, G. W. Multifunctional catalysts for ring-opening copolymerizations. *ACS Catal.* **12**. 11037-11070 (2022).

18. Diment, W. T., Lindeboom, W., Fiorentini, F., Deacy, A. C. & Williams, C. K. Synergic heterodinuclear catalysts for the ring-opening copolymerization (ROCOP) of epoxides, carbon dioxide, and anhydrides. *Acc. Chem. Res.* **55**. 1997-2010 (2022).

19. Fiorentini, F. et al. Understanding catalytic synergy in dinuclear polymerization catalysts for sustainable polymers. *Nat. Commun.* **14**. 4783 (2023).

20. Lu, X.-B. & Ren, B.-H. Partners in epoxide copolymerization catalysis: Approach to high activity and selectivity. *Chin. J. Polym. Sci.* **40**. 1331-1348 (2022).

21. Wang, J. et al. Waterborne polyurethanes from CO_2 based polyols with comprehensive hydrolysis/oxidation resistance. *Green Chem.* **18**. 524-530 (2016).

22. Inoue, S. Immortal polymerization: The outset, development, and application. *J. Polym. Sci., Part A: Polym. Chem.* **38**. 2861-2871 (2000).

23. Darensbourg, D. J. Chain transfer agents utilized in epoxide and CO_2 copolymerization processes. *Green Chem.* **21**. 2214–2223 (2019).

24. Sanford, M. J., Van Zee, N. J. & Coates, G. W. Reversible-deactivation anionic alternating ring-opening copolymerization of epoxides and cyclic anhydrides: Access to orthogonally functionalizable multiblock aliphatic polyesters. *Chem. Sci.* **9**. 134-142 (2018).

25. Lidston, C. A. L., Abel, B. A. & Coates, G. W. Bifunctional catalysis prevents inhibition in reversible-deactivation ring-opening copolymerizations of epoxides and cyclic anhydrides. *J. Am. Chem. Soc.* **142**. 20161-20169 (2020).

26. Dong, J. et al. Construction of ultralow-molecular-weight CO_2–polyols with self-catalytic performance in polyurethane preparation. *Macromolecules*. (2024).

27. Spreitzer, R. J. & Salvucci, M. E. Rubisco: Structure, regulatory interactions, and possibilities for a better enzyme. *Annual Review of Plant Biology*. **53**. 449-475 (2002).

28. Wu, J. et al. Nanomaterials with enzyme-like characteristics (nanozymes): Next-generation artificial enzymes (II). *Chem. Soc. Rev.* **48**. 1004-1076 (2019).

29. Darensbourg, D. J. & Wu, G. P. A one-pot synthesis of a triblock copolymer from propylene oxide/carbon dioxide and lactide: Intermediacy of polyol initiators. *Angew. Chem. Int. Ed.* **52**. 10602-10606 (2013).

30. Patil, N. G. et al. Carboxylate salts as ideal initiators for the metal-free copolymerization of CO_2 with epoxides: Synthesis of well-defined polycarbonates diols and polyols. *Macromolecules*. **52**. 2431-2438 (2019).

31. Nakano, K., Kamada, T. & Nozaki, K. Selective formation of polycarbonate over cyclic carbonate: Copolymerization of epoxides with carbon dioxide catalyzed by a cobalt(III) complex with a piperidinium end-capping arm. *Angew. Chem. Int. Ed.* **45**. 7274-7277 (2006).

32. Lu, X., Ren, W. & Wu, G. CO_2 copolymers from epoxides: Catalyst activity, product selectivity, and stereochemistry control. *Acc. Chem. Res.* **45**. 1721–1735 (2012).

33. Klaus, S., Lehenmeier, M. W., Anderson, C. E. & Rieger, B. Recent advances in CO_2/epoxide copolymerization—new strategies and cooperative mechanisms. *Coord. Chem. Rev.* **255**. 1460-1479 (2011).

34. Cyriac, A. et al. Immortal CO_2/propylene oxide copolymerization: Precise control of

molecular weight and architecture of various block copolymers. *Macromolecules*. **43**. 7398-7401 (2010).

35. Chen, C., Gnanou, Y. & Feng, X. Ultra-productive upcycling CO_2 into polycarbonate polyols via borinane-based bifunctional organocatalysts. *Macromolecules*. **56**. 892-898 (2023).

36. Wang, X.-W., Hui, J.-W., Li, Y.-T., Gu, Y.-R. & Li, Z.-B. Facile synthesis of polycarbonate diol via copolymerization of CO_2 and cyclohexene oxide catalysed by a combination of one-component phosphonium borane lewis pair and water. *Chin. J. Polym. Sci.* **41**. 735-744 (2023).

37. Deacy, A. C., Moreby, E., Phanopoulos, A. & Williams, C. K. Co(III)/alkali-metal(I) heterodinuclear catalysts for the ring-opening copolymerization of CO_2 and propylene oxide. *J. Am. Chem. Soc.* **142**. 19150-19160 (2020).

38. Kember, M. R. & Williams, C. K. Efficient magnesium catalysts for the copolymerization of epoxides and CO_2; using water to synthesize polycarbonate polyols. *J. Am. Chem. Soc.* **134**. 15676-15679 (2012).

39. Chapman, A. M., Keyworth, C., Kember, M. R., Lennox, A. J. J. & Williams, C. K. Adding value to power station captured CO_2: Tolerant Zn and Mg homogeneous catalysts for polycarbonate polyol production. *ACS Catal.* **5**. 1581-1588 (2015).

40. Cao, H., Qin, Y., Zhuo, C., Wang, X. & Wang, F. Homogeneous metallic oligomer catalyst with multisite intramolecular cooperativity for the synthesis of CO_2-based polymers. *ACS Catal.* **9**. 8669-8676 (2019).

41. Zhuo, C., Cao, H., Wang, X., Liu, S. & Wang, X. Polymeric aluminum porphyrin: Controllable synthesis of ultra-low molecular weight CO_2-based polyols. *Chin. Chem. Lett.* **34**. 108011 (2023).

42. Klaus, S. et al. Mechanistic insights into heterogeneous zinc dicarboxylates and theoretical considerations for CO_2 epoxide copolymerization. *J. Am. Chem. Soc.* **133**. 13151–13161 (2011).

43. Liu, S., Qin, Y., Chen, X., Wang, X. & Wang, F. One-pot controllable synthesis of oligo(carbonate-ether) triol using a Zn-Co-DMC catalyst: The special role of trimesic acid as an initiation-transfer agent. *Polym. Chem.* **5**. 6171-6179 (2014).

44. Liu, S. et al. Controllable synthesis of a narrow polydispersity CO_2-based oligo(carbonate-ether) tetraol. *Polym. Chem.* **6**. 7580-7585 (2015).

45. Kuang, Q. et al. Supported catalyst enables synthesis of colorless CO_2-polyols with ultra-low molecular weight. *Angew. Chem. Int. Ed.* **62**. e202305186 (2023).

46. Shellard, E. J. K. et al. Al(III)/K(I) heterodinuclear polymerization catalysts showing fast rates and high selectivity for polyester polyols. *ACS Catal.* **14**. 1363-1374 (2024).

47. Moore, E. et al. Surface-initiated hyperbranched polyglycerol as an ultralow-fouling coating on glass, silicon, and porous silicon substrates. *ACS Appl. Mater. Interfaces*. **6**. 15243-15252 (2014).

48. Fan, P. et al. Rigid-flexible binuclear catalysts: Boosting activity for copolymerization of CO_2 and propylene oxide. *Macromolecules*. **57**. 5702-5711 (2024).

49. Chisholm Concerning the mechanism of the ring opening of propylene oxide in the copolymerization of propylene oxide and carbon dioxide to give poly(propylene carbonate). *J. Am. Chem. Soc.* **126**. 11030-11039 (2004).